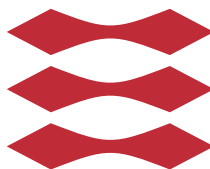


Finger Image Quality Based on Singular Point Localization

Jinghua Wang

DTU



Kongens Lyngby 2013
IMM-M.Sc-2013-52

Technical University of Denmark
Informatics and Mathematical Modelling
Building 321, DK-2800 Kongens Lyngby, Denmark
Phone +45 45253351, Fax +45 45882673
reception@imm.dtu.dk
www.imm.dtu.dk IMM-M.Sc-2013-52

Summary (English)

Finger image quality assessment is a crucial task in the fingerprint-based biometric systems, and plenty of publications state that singular points have the profound influence on the biometric performance. The aim of the thesis is to analyse whether the singular points are significant and what is the degree of importance on the biometric performance.

Existing approaches of orientation field estimation and singular point localization are discussed in this work, and the most accurate and robust of them are applied. Five pattern-based filters are proposed to reduce the detected spurious singular points. One segmentation algorithm is proposed using morphological image processing.

Seven singular point localization-based global Quality Measurement Algorithms are proposed to systematically analyse the effect of singular points on the biometric performance by measuring the finger sample displacement and rotation. Experimental results establish the property of singular points does have influence on biometric performance although not better than the analysis of fine level characteristics. Four local Quality Measurement Algorithms are proposed to give the quality score by analysing the coherence of the ridgeline. Acceptable results are achieved with excellent execution time.

Additionally all the proposed Quality Measurement Algorithms can be potentially incorporated in the ISO/IEC standards or in NIST Finger Image Quality 2.0.

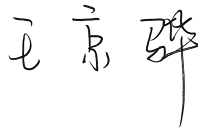
Preface

This thesis was prepared at the department of Informatics and Mathematical Modelling at the Technical University of Denmark in cooperation with Center for Advanced Security Research Darmstadt in fulfilment of the requirements for acquiring an M.Sc. in Informatics.

The thesis deals with the singular point localization and analyse the effect of singular point on the performance of biometric systems.

The thesis consists of an introduction, description of related biometric background, proposed singular point localization algorithm and quality metrics, experimental setup and results, conclusion and appendices.

Lyngby, 07-July-2013

A handwritten signature in black ink, consisting of three stylized Chinese characters: 王 (Wang), 京 (Jing), and 华 (Hua).

Jinghua Wang

Acknowledgements

I would like to express my deepest appreciation to Prof. Dr. Christoph Busch for raising my interest of biometrics and inviting me to conduct my thesis at Center for Advanced Security Research in Darmstadt (CASED) in Germany.

Thanks to MSc. Martin. Aastrup Olsen for supervising. His invaluable ideas and comments helped me to overcome plenty of tricky issues and encourage me to progress throughout this thesis.

I am very grateful to Prof. Dr. Rasmus Larsen for inspiring my work at Technical University of Denmark (DTU).

I would also like to thank my colleagues Elakkiya Ellavarason, Ivan Danov, Marek Dusio, and Vikas Gupta for fruitful discussions. Last but not least, I am indebted to my parents for encouraging and supporting during my master's study.

Contents

Summary (English)	i
Preface	iii
Acknowledgements	v
1 Introduction	1
1.1 Motivation	2
1.2 Goals and methodologies	3
1.3 Thesis overview	3
2 Introduction to Biometrics	5
2.1 Biometric recognition	5
2.2 Biometric systems	6
2.3 Biometric errors	8
2.3.1 System errors	8
2.3.2 Recognition errors	9
2.4 Biometric sample quality	10
2.4.1 Quality components	11
2.4.2 Quality measurement algorithm	11
2.4.3 Utility-based quality computation	13
2.4.4 Quality score fusion	16
2.4.5 Applications of QMA	16
3 Fingerprint Image Quality	19
3.1 Fingerprint analysis	19
3.1.1 Fingerprint feature	20
3.1.2 Fingerprint representation	22
3.1.3 Fingerprint classification	23

3.1.4	Fingerprint comparison	24
3.2	Automatic fingerprint identification systems	26
3.3	Finger image quality assessment	27
3.3.1	Defect factors of fingerprint image	27
3.3.2	Finger image QMAs	28
3.3.3	Approaches to local analysis	29
3.3.4	Approaches to global analysis	33
3.3.5	Foreground area	38
3.4	Aggregation of QMAs	38
3.4.1	Weighted average	38
3.4.2	Pattern classifier	39
3.5	Benchmarking QMAs	40
3.5.1	Error versus reject curves	40
3.5.2	Spearman correlation	41
4	Orientation Field Estimation	45
4.1	Orientation field	45
4.2	Orientation field estimation	46
4.2.1	Previous work	46
4.2.2	Gradient-based approach	47
5	Singular Point Localization	55
5.1	Singular point	55
5.2	Singular point extraction	57
5.2.1	Related work	57
5.2.2	Green's Theorem-based approach	59
5.2.3	Orientation of singular points	61
5.3	Segmentation	63
5.4	Singular point validation	65
6	Proposed Quality Measurement Algorithms	69
6.1	Position-based QMAs	69
6.1.1	Euclidean distance	70
6.1.2	Horizontal and vertical distance	72
6.2	Orientation-based QMA	74
6.3	Coherence	75
7	Experimental Setup	79
7.1	Database selection	79
7.2	Orientation field estimation	82
7.3	Singular point localization	83
7.3.1	Singular point identification	83
7.3.2	Singular point extraction	83
7.4	Proposed QMAs	85

7.4.1	Fingerprint data computation	85
7.4.2	Fingerprint quality estimation	86
7.4.3	Error versus reject curves	87
7.4.4	Spearman correlation tables	88
7.4.5	Utility heatmaps	88
7.5	Computation aspects	89
8	Experimental Results	91
8.1	Orientation field estimation	91
8.1.1	Orientation field estimation assessment	91
8.1.2	Timing	93
8.1.3	Summary	93
8.2	Singular point localization	94
8.2.1	Singular point extraction assessment	94
8.2.2	Timing	96
8.2.3	Summary	96
8.3	Proposed QMAs	97
8.3.1	Error versus reject curves	98
8.3.2	Spearman correlation tables	100
8.3.3	Utility heatmaps	101
8.3.4	Timing	103
8.3.5	Summary	104
9	Conclusion	105
9.1	Future work	106
A	Effect of Displacement to Comparison Scores	109
B	Distance and Orientation Distributions	113
C	Comparison Scores Distribution	119
D	Error versus Reject Curves	123
E	Spearman Correlation Tables	137
F	Utility Heatmaps	143
	Bibliography	149

Introduction

Biometric recognition is widely used for identification and verification because the biometric identifier cannot be easily misplaced, forged or shared unlike traditional token- (e.g., keys or ID cards) or knowledge- (e.g., password or PIN) based methods [MMJP09]. It also possess the excellent property of security, efficiency and ease of use and thus the deployed number of biometric systems is increasing continuously and rapidly.

As one of the biometric characteristics, fingerprints were first proposed as an approach for identification and verification over 100 years ago. Because of the excellent distinctiveness and persistence, as well as the ease of collection, the fingerprint based biometric systems have almost become synonym of biometric systems. Meanwhile, with the relatively low cost and high maturity, fingerprints based products has seen increasing usage over the past decades in a wide range of scenarios, spanning from access control in recreational resorts and fitness centres, to identification of individuals in border control and forensic investigations.

The large-scale fingerprint recognition systems have extensively used by the governments of different countries. U.S.A. has introduced Customs and Border Protection (CBP) management system to collect and analyse the fingerprints by Office of Biometric Identity Management (OBIM) [oHS]. The Schengen States exchanges visa data via Visa Information System which performs primarily fingerprint identification and verification [Com]. Unique Identification Authority

of India (UIDAI) is issuing Unique identification numbers and collecting the fingerprints for more than 1.2 billion citizens of India.

1.1 Motivation

Myriad techniques have been applied in the comparison subsystems, but the performance of biometric systems is suffered from the low quality of samples. Historically, quality measurement algorithm (QMA) have lagged behind recognition algorithm development. As a result, the research attention recently has been shifted from sample comparison to sample quality measurement. High quality of samples can be ensured by analysing the fingerprint using various techniques. For instance, NIST proposed a fingerprint quality measurement tool - NIST Fingerprint Image Quality (NFIQ) in August 2004, and more potential features are being evaluated in NFIQ 2.0 [NIS12]. Meanwhile, with the increasing significance of QMA, ISO/IEC 29749:2009 has defined and specified the methodologies for objective and quantitative quality score expression, interpretation and interchange [ISO12b].

The singular point (SP) of a fingerprint are the most important global feature. Typically SPs, known as core and delta, are located in the regions which possess the higher ridgeline curvature and used as landmarks for classification and alignment of fingerprints in a comparison process. Besides, the position and orientation of SPs indicates the finger displacement and rotation in the sample, and thus the other common use is in registration, i.e., they are used as references to line up two fingerprints in one-to-one comparison [BG02]. Various publications support these view:

“The singular points of fingerprints play an important role in fingerprint recognition and classification systems [WYY11].”

“These singular points are the most important topological features of a fingerprint and are extremely important in biometric identification systems based on fingerprint analysis [fSoP].”

“Singular point, as a global feature, plays an important role in fingerprint recognition [JK10].”

Nevertheless, none of the existing work analyses whether SPs is of importance exactly. It leaves us with the question, do the properties of these landmark points (e.g. position and orientation) have the influence on the finger image

quality? If yes, how significant are SPs and its influence on the biometric performance?

1.2 Goals and methodologies

The research goals of the thesis are:

- Develop an algorithm to localize singular points with high precision and low processing time. The assessment of the algorithm performance is benchmarked against the existing methods using a ground-truth fingerprint database and several public databases.
- Investigate the relationship between biometric performance and properties of SPs. Series of SP localization-based QMAs are required to be proposed, and the assessment is carried out by observing the correlation between the ground-truth comparison scores and computed quality scores.

1.3 Thesis overview

This thesis is divided into four parts. Firstly, chapter 2 and chapter 3 introduces the basic concepts of biometrics. The second part discusses and proposes the algorithm to localize SPs, where chapter 4 and chapter 5 focus on the orientation field estimation and SP localization respectively. Chapter 6 proposes several QMAs using SP localization. Finally the assessments are presented in chapter 7 and chapter 8, and the conclusion and future work are presented in chapter 9.

CHAPTER 2

Introduction to Biometrics

The purpose of this chapter is to introduce the general terminology and overview of biometric systems to those readers who are unfamiliar with this field so that they can follow the following chapters. The terms and definitions in this thesis are based on ISO/IEC 2382-37:2012 [ISO12a] from *International Organization for Standardization/International Electrotechnical Commission (ISO/IEC)*.

2.1 Biometric recognition

The word *biometrics*, also called biometric recognition, refers to the automated recognition of individuals based on their behavioural (e.g., speech, gait) and biological (e.g., fingerprints, face, iris) characteristics [ISO11]. Any characteristic can be used as a biometric identifier to recognize a person as long as it satisfies the following requirements [MMJP09]:

- **Universality:** each person should possess the biometric characteristic.
- **Distinctiveness:** each pair of persons should perform sufficiently difference with regard to the biometric characteristic.
- **Permanence:** the biometric characteristic should be invariant over time.

- **Collectability:** the biometric characteristic can be measured and stored quantitatively.
- **Performance:** the recognition accuracy, speed, and robustness to operational and environmental factors should be accepted.
- **Acceptability:** the measurement and collection of the biometric characteristic should be user-friendly so that each capture subject are willing to accept the biometric identifier.
- **Circumvention:** ease with which the biometric system can be circumvented by fraudulent approaches.

The most widely used biometric characteristics include: face, fingerprint, hand geometry, hand/finger vein, iris, signature, and voice. They are compared in terms of the biometric requirements in table 2.1.

Biometric identifier	Universality	Distinctiveness	Permanence	Collectability	Performance	Acceptability	Circumvention
Face	H	L	M	H	L	H	H
Fingerprint	M	H	H	M	H	M	M
Hand geometry	M	M	M	H	M	M	M
Hand/finger vein	M	M	M	M	M	M	L
Iris	H	H	H	M	H	L	L
Signature	L	L	L	H	L	H	H
Voice	M	L	L	M	L	H	H

Table 2.1: Comparison of commonly used biometric characteristics. High, Medium, and Low are denoted by H, M, and L, respectively. Taken from [MMJP09]

2.2 Biometric systems

Biometric system refers to the system for the purpose of the automated recognition of individuals based on their behavioural and biological characteristics [ISO11]. Depending on how an individual will be recognized, a biometric system can be stated either a *verification* system or an *identification* system [MMJP09]:

- A verification system authenticates an individual's identity by comparing the presently captured biometric characteristic with the person's enrolled biometric reference template which is previously pre-stored in the system. It verifies the identity of the individual by a one-to-one comparison, and then the verification system either accepts or rejects the submitted claim of identity.
- An identification system recognizes an individual by comparing a biometric probe with the entire database of stored the enrolment reference templates. It returns whether the individual is present in the database by a one-to-many comparisons. The identification system verifies whether the individual is enrolled in the system database, without any claim of the identity.

Throughout this thesis, there is no interest in distinguishing the verification and identification so that the generic term *recognition* is used to represent both of them.

Figure 2.1 depicts the overview of a general biometric system which contains several subsystems: data capture, signal processing, data storage, comparison, and decision. It also contains transmission, administration subsystems and interface which are not portrayed. In practice some conceptual components might be absent or not have a direct correspondence with a physical or software entity in the practical biometric systems.

- **Data capture subsystem:** collects the individual's biometric characteristic using capture devices, and outputs an image or signal as a biometric sample.
- **Signal processing subsystem:** performs the processes such as quality control, segmentation, feature extraction and quality enhancement, then generates features which is numbers or labels extracted from biometric samples. In the case of enrolment, the subsystem also creates the reference for the enrolment database.
- **Data storage subsystem:** stores the reference within the enrolment database in order to conduct the verification and identification. The reference can be stored as either sample or features or both.
- **Comparison subsystem:** compares the presently captured features with one or more of the references according to the type of recognition, and outputs a comparison score indicating the degree of the similarity.
- **Decision subsystem:** generates the decision outcome for a verification or identification transaction by the defined threshold and decision policy.

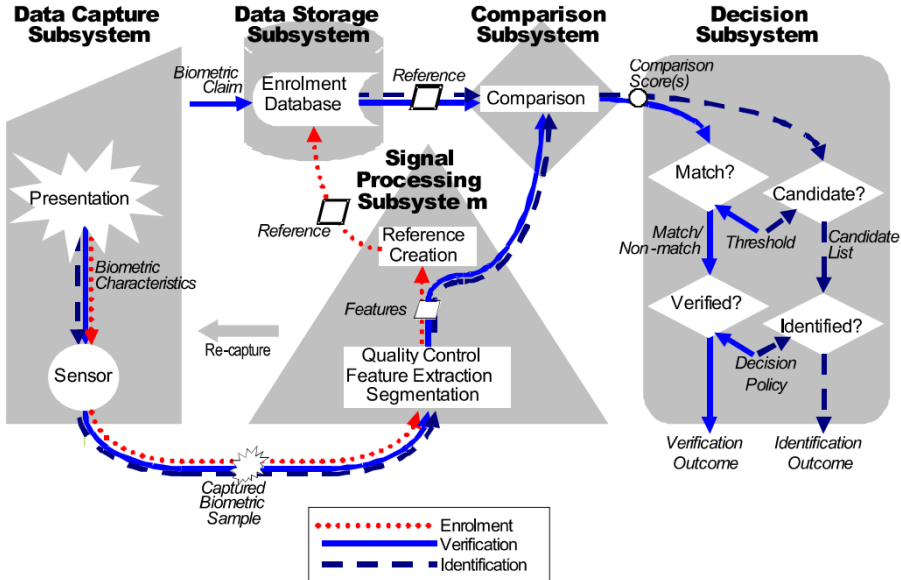


Figure 2.1: Components of a general biometric system. Taken from [ISO11].

- **Transmission subsystem:** connects the entire biometric system and transmits the outputted biometric data to the following subsystem.
- **Administration subsystem:** governs the overall configuration (e.g., threshold and decision policy) and usage of the biometric system.
- **Interface:** performs as an external application or system via an application programming interface, hardware interface or a protocol interface.

2.3 Biometric errors

2.3.1 System errors

Associated with a acquisition of a biometric sample or its image processing, there are multiple system errors a biometric system might be suffered [Bus09]:

- **Failure-to-Capture:** the data capture subsystem is not capable to generate a biometric sample. The reason can be the insufficiency of either the biometric characteristic or sample quality.

- **Failure-to-eXtract**: the signal processing subsystem cannot extract the features of a biometric sample. This can be caused by either the deficiency of the features or the performance of the algorithm.
- **Failure-to-Enrol**: the data storage subsystem is not able to create a biometric reference for the data subject. The failure can be caused by the absent biometric characteristic or the insufficient sample quality.
- **Failure-to-Acquire**: the entire system fails to acquire the features for the decision subsystem, as the biometric sample is not generated (Failure-to-Capture), or the features are failed to extracted (Failure-to-eXtract).

2.3.2 Recognition errors

In contrast to system errors, the recognition errors indicate the errors that are attributed to the decision subsystem.

The decision subsystem will produce the match or non-match decision relying on whether the comparison score exceeds the specific threshold. Figure 2.2 illustrates the probability distribution between the imposter and genuine comparison. In ideal case the imposter and genuine comparison distribution are totally separated with respect to the comparison scores. However, in practice the undesired case is commonly existed which the imposter and genuine distributions are overlapped.

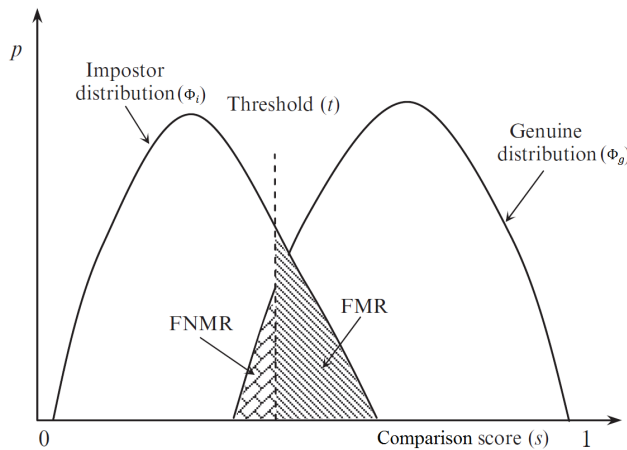


Figure 2.2: FMR and FNMR for a given threshold t are displayed over the genuine and imposter comparison score distribution.

As a result, the *False-Match-Rate* (FMR) and *False-Non-Match-Rate* (FNMR) are constituted [ISO12a]:

- **False-Match-Rate:** proportion of the completed biometric non-match comparison trials that result in a false match. For a specified threshold t , the FMR is computed in eq. (2.1), where s is comparison score, Φ_i is probability distribution function of impostor comparison.

$$FMR(t) = \int_t^1 \Phi_i(s) ds \quad (2.1)$$

- **False-Non-Match-Rate:** proportion of the completed biometric match comparison trials that result in a false non-match. For a specified threshold t , the FNMR is computed in eq. (2.2), where s is comparison score, Φ_g is the probability distribution function of genuine comparison.

$$FNMR(t) = \int_0^t \Phi_g(s) ds \quad (2.2)$$

There is a strict tradeoff between FMR and FNMR in every practical biometric system. For a given threshold t , if t is decreased, then the system is more tolerant regarding input variations and noise and FMR(t) increases. On the other hand, if t is raised, then the system is more secure and FNMR(t) increases.

For a given biometric system, the measurement of FMR and FNMR can be done by plotting a *Detection Error Tradeoff* (DET) [MDK⁺97] curve. For various threshold t , the DET curve plots FMR(t) against FNMR(t) and provides a straight view of the error-vs-error tradeoff, i.e., false (false positive) and missed (false negative) detections. An example is illustrated in fig. 2.3.

Receiver Operating Characteristic (ROC) curve [ZC93] also can depict the performance of biometric systems which is out of the scope of this thesis.

2.4 Biometric sample quality

In biometrics, the term *sample* can be an image, signal, or pattern based interpretation of a physical human feature used for identification or verification using biometric techniques [ISO12b].

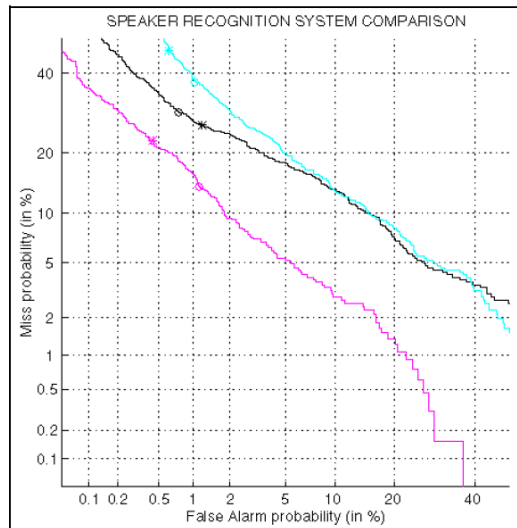


Figure 2.3: DET curves for a speaker recognition evaluation. Taken from [MDK+97].

2.4.1 Quality components

The *quality* refers to the degree to which a biometric sample fulfils specified requirements for a targeted application [ISO12b]. In the area of biometrics, the quality of the sample can be measured in terms of the following aspects:

- **Character:** the inherent features of the source from which the biometric sample is derived.
- **Fidelity:** the degree how a sample is similar with the source.
- **Utility:** the predicted positive or negative contribution of an individual sample to the overall performance of a biometric system.

Utility-based quality depends on both the character and fidelity of the biometric sample shown in table 2.2.

	Fidelity		
		Low	High
Character	Low	Low fidelity and low character results in low utility. Recapture might improve utility. However, if possible use of other biometric characteristics is recommended.	High fidelity and low character results in low utility. Recapture will not improve utility. Use of other biometric characteristics is recommended.
	High	Samples with high character and low fidelity typically will not demonstrate high utility. Utility can be improved upon recapture or image enhancement techniques.	Samples with high character and high fidelity indicate capture of useful sample. High utility is expected.

Table 2.2: Relationship between character, fidelity, and utility. Taken from [ISO12b].

2.4.2 Quality measurement algorithm

Quality measurement naturally lags comparison algorithm development, but has emerged as it is realized that biometric systems fail on certain pathological samples. The main use of a quality measure is an approach to reject a poor quality sample and then initiate another capture attempt [GT07] [YC06] [AFFOG+07] [XYP+11].

Figure 2.4 illustrates the relationship between quality and system performance. The observed utility is the ground-truth quality score as it is derived by the comparison algorithm. The utility-based quality (predicted utility) is used to predict the system performance, instead of the quality based on character or fidelity. Furthermore throughout this thesis, the term *quality* only concentrates on the aspect of the observed utility.

In order to improve the prediction for the observed performance, the *quality measurement algorithm* (QMA) should convey a predicted utility as much as correlated with the observed utility. Many researches have focused on the quality estimation, For instance, *National Institute of Standards and Technology* (NIST) evaluated the performance in accordance with a few quality metrics within NFIQ (NIST Fingerprint Image Quality) [TG09] and more candidate features is assessing in NFIQ 2.0 [NIS12].

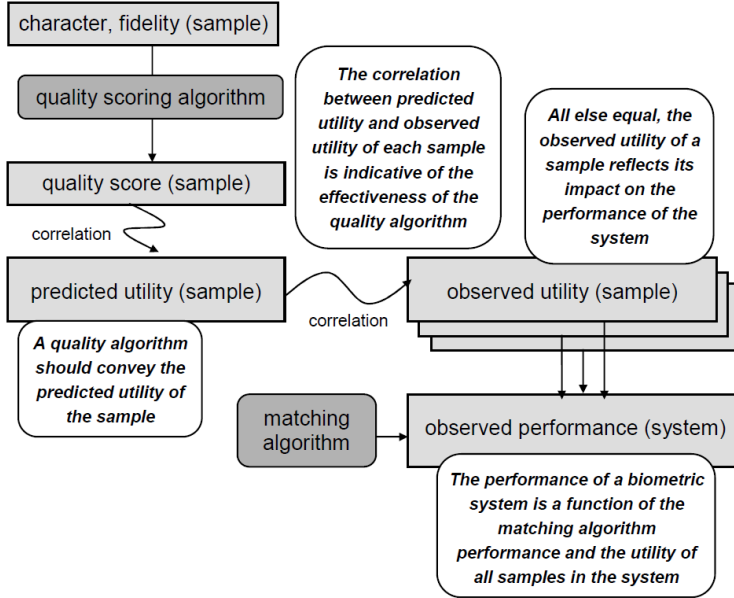


Figure 2.4: Relationship between quality and system performance. Taken from [ISO12b].

2.4.3 Utility-based quality computation

In order to construct the observed quality to predict the performance of a biometric sample regarding character and fidelity, ISO/IEC 29794-1:2009 proposed an approach to quantify the utility scores, and then compute the quality scores by binning the utility scores [ISO12b]. The quality scores are assigned to each sample, i.e., for a biometric dataset containing N_i ($N_i \geq 2$) samples and M subjects, each sample $d_i^{(1)}, d_i^{(2)}, \dots, d_i^{(N_i)}$ is assigned a quality score $q_i^{(1)}, q_i^{(2)}, \dots, q_i^{(N_i)}$, where $i = 1, \dots, M$, note each sample only contains one biometric characteristic.

2.4.3.1 Utility computation

For each comparator V_k , $k = 1, \dots, K$, of K available comparators, a set of utility scores can be computed as:

1. For each instance record $d_i^{(u)}$ (i.e. the u^{th} sample of subject i):

- (a) Generate the set of all possible genuine comparison scores using the k^{th} comparator,

$$S_{ii} = \left\{ s_{i,i}^{u,v} \mid s_{i,i}^{u,v} = V_k(d_i^{(u)}, d_i^{(v)}) \right\} \quad (2.3)$$

$$u = 1, \dots, N_i \text{ and } v = u + 1, \dots, N_i$$

$$i = 1, \dots, M$$

- (b) Generate the set of all impostor comparison scores using the k^{th} comparator,

$$S_{ij} = \left\{ s_{i,j}^{u,v} \mid s_{i,j}^{u,v} = V_k(d_i^{(u)}, d_j^{(v)}) \right\} \quad (2.4)$$

$$u = 1, \dots, N_i \text{ and } v = u + 1, \dots, N_j$$

$$i = 1, \dots, M \text{ and } j = 1, \dots, M \text{ and } i \neq j$$

2. compute the utility for sample $d_i^{(u)}$ as

$$utility_i^u = \frac{m_{i,u}^{\text{genuine}} - m_{i,u}^{\text{imposter}}}{\sigma_{i,u}^{\text{genuine}} + \sigma_{i,u}^{\text{imposter}}} \quad (2.5)$$

where $m_{i,u}^{\text{genuine}}$ is the mean of sample $d_i^{(u)}$'s genuine comparison scores computed as:

$$m_{i,u}^{\text{genuine}} = \frac{\sum_{v=1, v \neq u}^{N_i} s_{i,i}^{u,v}}{N_i - 1} \quad (2.6)$$

and $m_{i,u}^{\text{imposter}}$ is the mean of sample $d_i^{(u)}$'s impostor comparison scores computed as:

$$m_{i,u}^{\text{imposter}} = \frac{\sum_{j=1, j \neq i}^M \sum_{v=1}^{N_j} s_{i,j}^{u,v}}{\sum_{j=1, j \neq i}^M N_j} \quad (2.7)$$

similarly $\sigma_{i,u}^{\text{genuine}}$ is the standard deviation of sample $d_i^{(u)}$'s genuine comparison scores computed as:

$$\sigma_{i,u}^{\text{genuine}} = \sqrt{\frac{\sum_{v=1, v \neq u}^{N_i} (s_{i,i}^{u,v} - m_{i,u}^{\text{genuine}})^2}{N_i - 1}} \quad (2.8)$$

and $\sigma_{i,u}^{\text{imposter}}$ is the standard deviation of sample $d_i^{(u)}$'s impostor comparison scores computed as:

$$\sigma_{i,u}^{\text{imposter}} = \sqrt{\frac{\sum_{j=1, j \neq i}^M \sum_{v=1}^{N_j} (s_{i,j}^{u,v} - m_{i,u}^{\text{imposter}})^2}{\sum_{j=1, j \neq i}^M N_j}} \quad (2.9)$$

2.4.3.2 Quality computation

Once all utility values have been computed, they can be binned into several defined quality classes:

1. Insert (i, u) into set T if its genuine comparison scores is greater than all its impostor comparison scores, i.e. $s_{i,i}^{u,v} > s_{i,j}^{u,v} \forall j \neq i, v \neq u, w$, which can be computed by eq. (2.3) and eq. (2.4).
2. Compute two empirical cumulative distribution functions:

$$C(z) = \frac{|\{utility_i^u : (i, u) \in T, utility_i^u \leq z\}|}{|\{utility_i^u : (i, u) \in T, utility_i^u < \infty\}|} \quad (2.10)$$

and another for those not in that set,

$$W(z) = \frac{|\{utility_i^u : (i, u) \notin T, utility_i^u \leq z\}|}{|\{utility_i^u : (i, u) \notin T, utility_i^u < \infty\}|} \quad (2.11)$$

3. Select quality resolution $L(2 \leq L \leq 100)$, then the quality levels will be $q = 1, \dots, L$ where 1 is the lowest and L is the highest quality score.
4. Bin sample utility scores in to L bins based on quantiles of the target utility distributions $C(\cdot)$ and $W(\cdot)$ in eq. (2.10) and eq. (2.11). One example for $L = 5$ is shown in table 2.3, which $W^{-1}(\cdot)$ and $C^{-1}(\cdot)$ are the quantile functions, and $C^{-1}(0)$ and $C^{-1}(1)$ ($W^{-1}(0)$ and $W^{-1}(1)$) denote the empirical minima and maxima, respectively, x and y are appropriate percentile points selected based on the shape of $C(\cdot)$.

Bin	Range of target utilities
1	$\{z_i : -\infty < z_i < C^{-1}(0.01)\}$
2	$\{z_i : C^{-1}(0.01) \leq z_i < W^{-1}(1)\}$
3	$\{z_i : W^{-1}(1) \leq z_i < C^{-1}(x)\}$
4	$\{z_i : C^{-1}(x) \leq z_i < C^{-1}(y)\}$
5	$\{z_i : C^{-1}(y) \leq z_i\}$

Table 2.3: Binning utility scores. Taken from [ISO12b].

2.4.4 Quality score fusion

In order to evaluate the overall biometric performance of a sample, there are some options to aggregate the K sets of quality scores into quality reference dataset:

1. **Unanimity**: only samples with identical quality assignments from all K comparators are stored in the quality reference dataset, and the rest of them are discarded.
2. **Median or other specified percentile point**: samples with identical quality assignment from more than x percent of K comparators become members of the quality reference dataset. The rest can be discarded.
3. **Arithmetic mean**: quality score of is the arithmetic mean of its quality score from each K comparator.

2.4.5 Applications of QMA

Measuring the quality of biometric samples is a crucial step so the importance of QMA becomes more significant. There has been a variety of applications are applied using QMA [ISO12b]:

- **Real-time quality assessment**: estimated quality data can be used by an operator, automated system or capture subject to help to improve the average quality within biometric systems.
- **Use in different applications**: by means of establishing a set of metrics, quality measurement can evaluate, compare and optimize performances for several biometric systems which might use different capture equipment and comparison algorithm.
- **Use as a survey statistic**: used for operational quality monitoring of the system, e.g., identify anomalous operation according to the quality score.
- **Accumulation of relevant statistics**: by accumulating statistics of capture subjects, informs the system and/or operators of whether a higher quality sample is likely if another capture is attempted.
- **Reference dataset improvement**: improve the quality of reference datasets for the sake of underlying comparisons.

- **Quality-based conditional processing:** evaluates the performances of the existing biometric samples with various metrics, and the poor quality sample can be processed using different algorithm or threshold than normal.
- **Interchange of quality data by disparate systems:** standardized exchange of quality data between disparate systems is used for retaining the modular interchangeability of local or remote system hardware and software components, and the integrity of quality data in the event of such an interchange.

CHAPTER 3

Fingerprint Image Quality

The previous chapter has introduced the concepts of biometrics and biometric sample quality to the reader. In this chapter the discussion will further concentrate on fingerprint analysis, fingerprint image quality as well as give an overview of existing fingerprint QMAs.

3.1 Fingerprint analysis

Human fingerprints have been discovered on a large number of archaeological artefacts and historical items [MMJP09]. In 1788, Mayer thoroughly described the anatomical formation of fingerprint [Moe71] in which several fingerprint characteristics were identified and characterized. Henry Fauld, in 1880, first scientifically indicated the individuality of fingerprints based on empirical observations. At the same period, Herschel stated that he had researched on fingerprint recognition for about 20 years [LG10] [Moe71]. The above mentioned research established the foundation of modern fingerprint recognition.

3.1.1 Fingerprint feature

A *fingerprint* refers to the unique pattern of friction ridge and valley information commonly, depicted in fig. 3.1. Furthermore, the term *friction ridge*, also called ridge, presents on the skin of the fingers and toes, the palms and soles of the feet, which makes contact with an incident surface under normal touch, and *valley* refers to the area between two friction ridges that does not make contact with an incident surface under normal touch [ISO11].

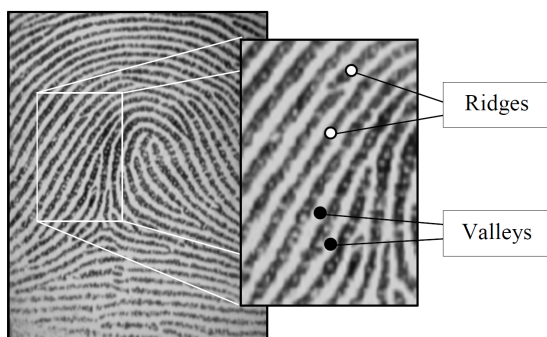


Figure 3.1: Ridges and valleys in a fingerprint image. Taken from [MMJP09].

The *orientation* at a pixel of the fingerprint image is defined by ridge structure. The overall orientation pattern is called *orientation field*. Chapter 4 will further discuss the detailed issues with regard to orientation field estimation.

In the major part of the fingerprint area, ridges run smoothly in parallel but particularly some regions perform higher curvature, called *singular region*, which contains one of the singular points: *core* or *delta*, respectively depicted in fig. 3.2. Chapter 5 will cover the further discussion within this field.

Ridge also results in another commonly used features, called *minutia* which refers the friction ridge characteristics that are used to individualize a fingerprint illustrated in fig. 3.3. The minutiae occur at points where a single friction ridge deviates from an uninterrupted flow. Deviation might cause the form of ending, bifurcation, or a combined type [ISO11]. This term is proposed by Galton [Gal92], as well as he construct a statistical proof of the individuality of fingerprints, which lays the foundation for meaningful comparison among different fingerprints.



Figure 3.2: Singular points within a fingerprint. The sample is taken from FVC2002DB1 [MMC+02].

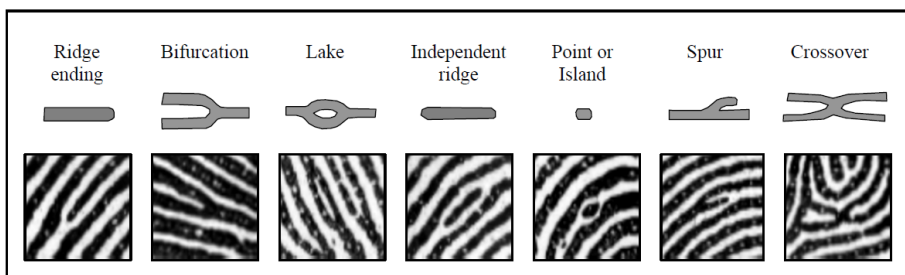


Figure 3.4. Seven most common minutiae types.

Figure 3.3: Seven most common minutia types. Taken from [MMJP09].

3.1.2 Fingerprint representation

The fingerprint representation is an important issue for the comparison sub-systems in fingerprint recognition systems. A effective representation should possess *saliency* and *suitability* [MMJP09], which refer to the distinctness and ease of use respectively.

Image sample is an natural and simple option to represent fingerprints, however, the image-based representation does not perform fair due to different environments (e.g., brightness variations and image quality variations) and sample quality (e.g., scars and large global distortions). Furthermore the image-based representation requires a large amount of storage. An feasible alternative is a feature-based representation by analysing the image at different scales and extracting unique numbers and labels:

- **Level 1:** at the global level, the ridge line delineates a pattern so that fingerprint shape, orientation field and frequency can be extracted. Singular points, core and delta act as control points around which the ridge lines are “wrapped” [LS72]. Singular points and coarse ridge line shape are useful for fingerprint classification, but their distinctiveness is not sufficient for accurate recognition.
- **Level 2:** at the local level, a total number of 150 different local ridge characteristics, called *minute details*, have been identified [Moe71]. The two most significant ridge characteristics, also are most common minutiae: ridge endings and ridge bifurcations, i.e., a ridge point where a ridge ends abruptly and a ridge point where ridge forks or diverges into branch ridges. Although minutiae performs a high saliency, automatic minutiae extraction can be problematic in extremely low-quality fingerprints without clear ridge structure.
- **Level 3:** at the very-fine level, permanent intra-ridge details can be extracted, which contain width, shape, curvature, edge contours of ridges, dots and incipient ridges. One of the most important fine-level details is the finger sweat pores, whose positions and shapes are considered highly distinctive. However, extracting very-fine details including pores is feasible only in high-resolution (e.g., 1,000 dpi) fingerprint images with good quality. With cost and benefit analysis, therefore this level is not practical for non-forensic applications.

3.1.3 Fingerprint classification

In order to reduce the search time and computation complexity in one-to-many comparisons, usually fingerprints are classified and then stored in enrolment dataset. Purkinje, in 1823, proposed the first fingerprint classification scheme, which classified fingerprints into nine categories according to the ridge configurations [Moe71]. Unfortunately it is not an feasible classification due to the ambiguous pattern, such as No. 5, 7 and 8 in fig. 3.4.

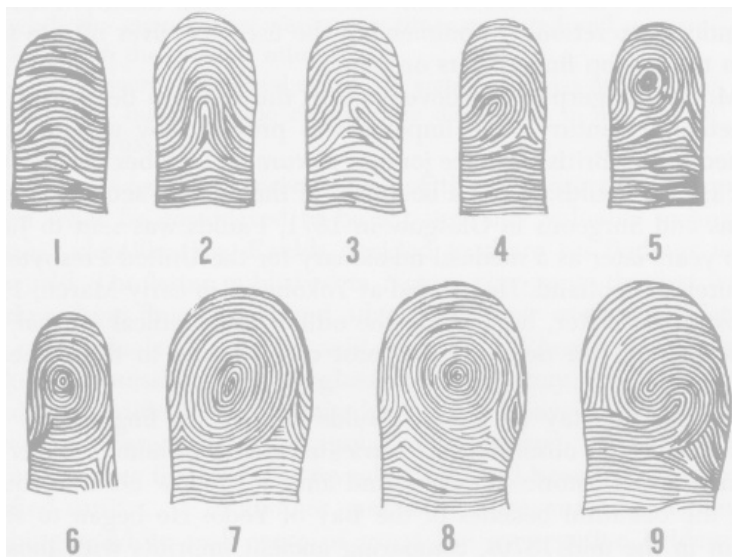


Figure 3.4: The nine patterns illustrated in Purkinjes's thesis. Taken from [Moe71]

In order to establish a reasonable formation of fingerprints, the biological principles of fingerprint patterns are summarized below [Moe71]:

- Individual epidermal ridges and furrows have different characteristics for different fingerprints.
- The configuration types are individually variable, but they vary within limits that allow for a systematic classification.
- The configurations and minute details of individual ridges and furrows are permanent and unchanging.

Based on the above factors, an prominent milestone in fingerprint classification

was made in 1899 by Edward Henry, who introduced the famous *Henry system* to classify the fingerprint as five classes: left loop, right loop, whorl, arch, tented arch depicted in fig. 3.5 [LG10].

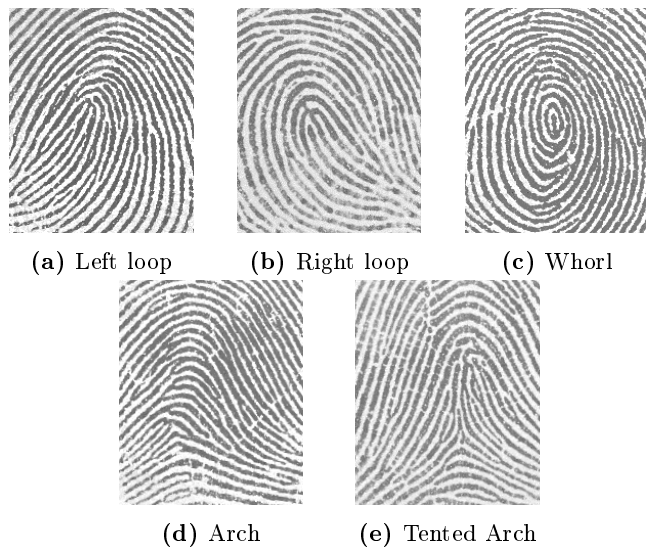


Figure 3.5: Fingerprints are classified in five major classes by Henry classification system. The samples are taken from FVC2000DB2 [MMWJ02].

The five classes are non-uniformly distributed in Henry system, the natural proportion of fingerprints in left loop, right loop, whorl, arch, tented arch is 33.8%, 31.7%, 27.9%, 3.7% and 2.9% respectively from a classification summary of 222 million prints [WCW94].

Because of the small inter-class variability and large intra-class variability within the classification, fingerprint classification is a difficult pattern recognition issue. For instance, in the top row in fig. 3.6, the three fingerprints belong to different classes but have the similar appearance. On the other hand, the three fingerprints in the bottom row belongs to the same class but have different characteristics.

3.1.4 Fingerprint comparison

Fingerprint comparison is an extremely challenging issue in recognition, because each impression for capturing the same finger might be different. The

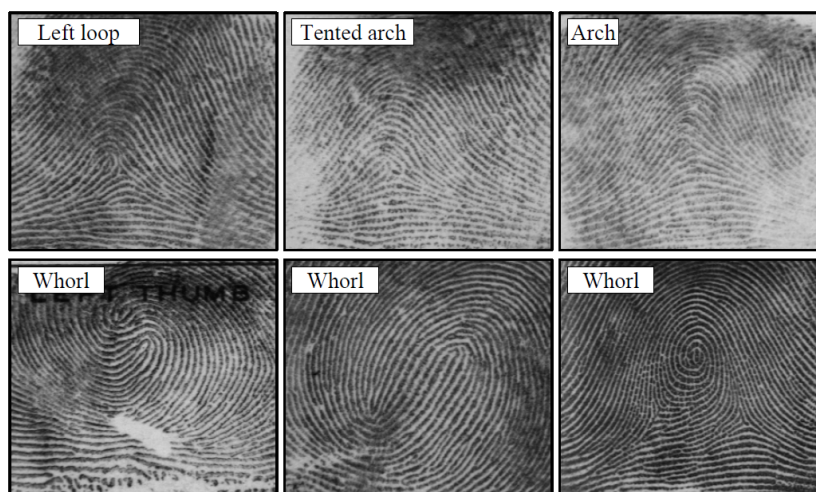


Figure 3.6: Fingerprint classification problem: small inter-class variability and large intra-class variability. Taken from [MMJP09]

main factors can be displacement, rotation, partial overlap, non-linear distortion, variable pressure, changing skin condition, noise, and feature extraction errors. As a result, fingerprints from the same finger may be different and vice versa. A large number of approaches have been proposed which can be classified as follows [MMJP09]:

- **Correlation-based comparison:** a pair of fingerprint samples are superimposed and the correlation between related pixels is computed for different alignments (e.g., various displacements and rotations).
- **Minutiae-based comparison:** minutiae are extracted from the two fingerprints and stored as sets of points in the two-dimensional plane. Minutiae comparison aligns the template and the input minutiae set resulting in the number of matched minutiae.
- **Non-minutiae feature-based comparison:** minutiae are difficult to be extracted in low-quality fingerprint images, whereas other features of the fingerprint ridge pattern (e.g., local ridge orientation and frequency, ridge shape) may be extracted more reliably than minutiae, even though they perform lower distinctiveness generally.

3.2 Automatic fingerprint identification systems

With the rapid expansion of fingerprint recognition, the number of samples in fingerprint databases became large so that manual fingerprint identification became infeasible. *Automated Fingerprint Identification System* (AFIS) is invented and have been widely used in law enforcement and security applications to identify individuals depending on fingerprints [Yam98]. Automatic fingerprint recognition technology has now dramatically grown beyond forensic applications into civilian and commercial applications. Figure 3.7 illustrates the procedure of AFIS.

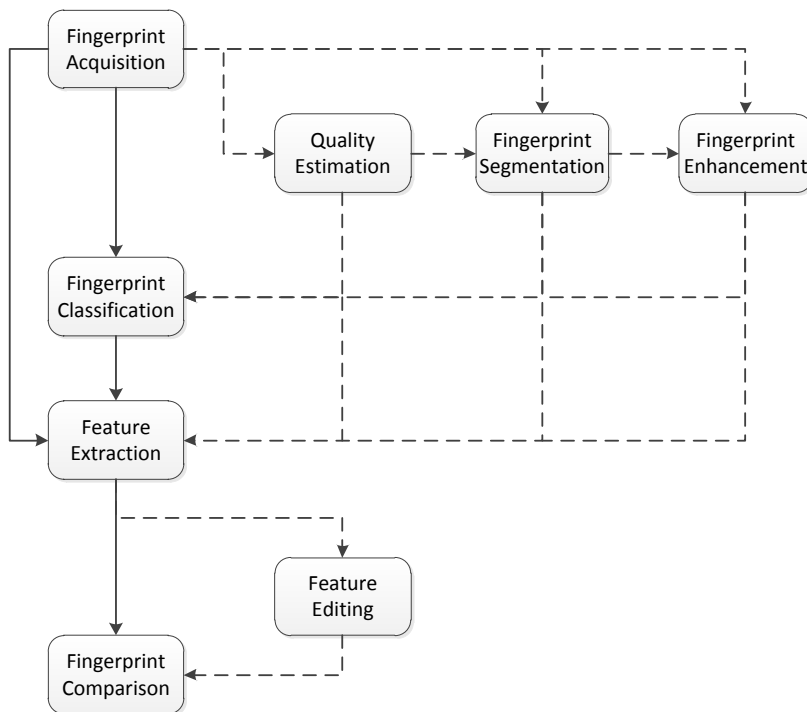


Figure 3.7: Flow chart of a general automatic fingerprint identification system, the dashed lines are the optional paths

However, sample quality often lacks the biometric performance of AFIS and thus quality estimation becomes mandatory recently. It is a criteria to decide whether a poor quality finger sample is submitted to the AFIS for automated processing in the first place. If the quality is assessed as poor, then the AFIS is not considered to be capable of this challenging fingerprint sample and the

sample is thus rather investigated manually.

3.3 Finger image quality assessment

The quality of fingerprint image data, same as mentioned in section 2.4, is can be used as a predictor to improve the biometric performance in fingerprint recognition.

3.3.1 Defect factors of fingerprint image

A captured fingerprint image could have various quality. In general, the low-quality might be caused by the following factors [ISO12c] [XYP⁺11] [UPPJ04]:

- **Acquisition device:** the type (e.g., optical and capacitive sensor, synthetic generator [MMWJ02]) and quality (e.g., resolution depicted in fig. 3.8 and area) of external capture device.

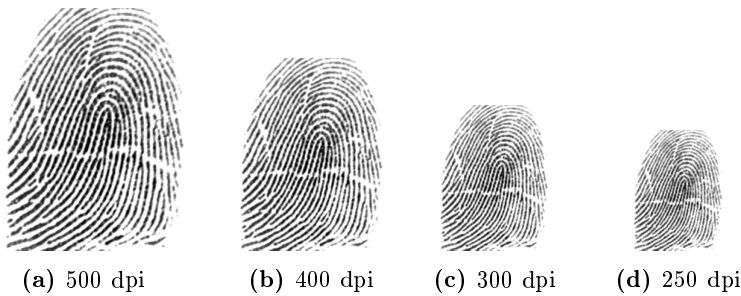


Figure 3.8: The same fingerprint sample with different resolution. Taken from [MMJP09].

- **Capture subject character:** finger condition (e.g., extremely dry and wet depicted in fig. 3.9), character (e.g., scars, wrinkles), disease (e.g., blisters, eczema) and impurities (e.g., dirt latent print).
- **Capture subject behaviour:** improper behaviour when capture the fingerprint image, such as elastic deformation, improper finger placement and insufficient area of finger image.



Figure 3.9: Three fingerprint images of the same finger with different skin conditions. Taken from [MMJP09].

- **Imaging:** imperfection or quality control of in capture subsystem, such as sampling error, low contrast or signal-to-noise ratio, distortion, erroneous or streak lines, uneven background, insufficient dynamic range, non-linear or non-uniform grey scale output, pixels not available due to hardware failure, aliasing problems.
- **Environment:** environmental factors, such as humidity, light, impurities on the scanner surface.

Based on the above factors, Young and Elliott stated the result of a survey that on the average, fingerprint images from index and middle fingers performs better quality, and whorl is the fingerprint class containing the largest proportion of high quality fingerprint image, where arch is at the opposite side of quality scale [YE07].

3.3.2 Finger image QMAs

Finger image QMAs have attached lots of attention due to the requirement of biometric systems, resulting in fruitful publications [ISO12c] [LJY02] [LTS⁺04] [HUW⁺98] [OXB12] [SKK01]. The approaches can be classified as local and global methods, which measure the image quality in block-wise and as a whole respectively.

3.3.3 Approaches to local analysis

Local QMAs partition the fingerprint image into blocks and let each block contains sufficient ridge-valley information. The size of block is setted empirically due to the image resolution. Usually for a 500 ppi fingerprint image, the ridge separation usually varies between 8 to 12 pixels [MMJP09], 32×32 pixels are selected because there are at least two ridges existed. Note other sizes also could be selected due to the requirement of approaches.

3.3.3.1 Orientation certainty level

Orientation certainty level (OCL) analyses the orientation certainty of each block depicted in fig. 3.10. The grey level gradient (dx, dy) along x and y direction exhibits the orientation and the orientation strength at this pixel. Using Principal Component Analysis [Pea01] on the gradients in each block, an orthogonal basis for the block can be obtained by computing its eigenvalues and eigenvectors. The ratio between the two eigenvalues indicates how strong the energy is concentrated along the dominant direction with two vectors pointing to the normal and tangential direction of the average ridge flow respectively [LJY02].

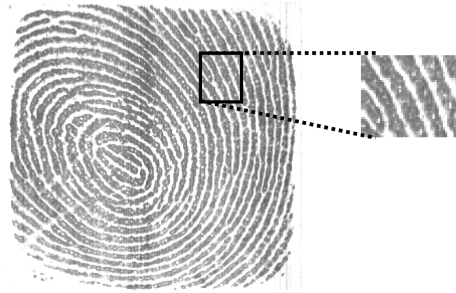


Figure 3.10: A typical texture-like ridge block. Taken from [LJY02].

The covariance matrix C of the gradient vector for a N pixels block is given by:

$$C = \frac{1}{N} \sum_N \left\{ \begin{bmatrix} dx \\ dy \end{bmatrix} \begin{bmatrix} dx & dy \end{bmatrix} \right\} = \begin{bmatrix} a & c \\ c & b \end{bmatrix} \quad (3.1)$$

Based on the covariance matrix, eigenvalues λ are given:

$$\lambda_{max} = \frac{(a+b) + \sqrt{(a-b)^2 + 4c^2}}{2} \quad (3.2)$$

$$\lambda_{min} = \frac{(a+b) - \sqrt{(a-b)^2 + 4c^2}}{2} \quad (3.3)$$

For each block the ocl_i can be computed indicating the orientation certainty level:

$$ocl_i = \frac{\lambda_{min}}{\lambda_{max}} = \frac{(a+b) + \sqrt{(a-b)^2 + 4c^2}}{(a+b) - \sqrt{(a-b)^2 + 4c^2}} \quad (3.4)$$

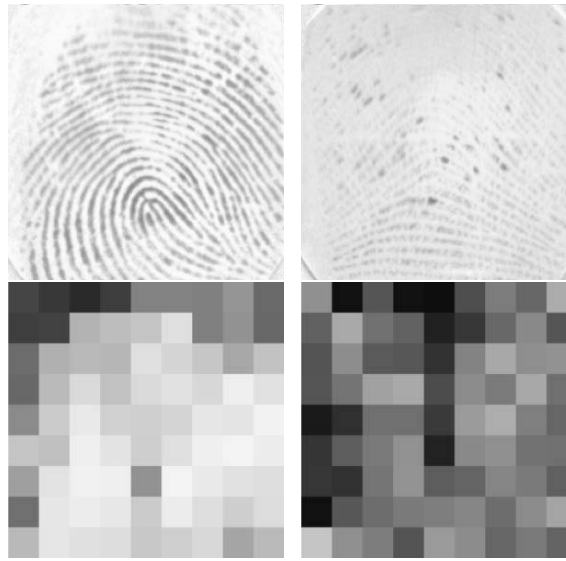
The value of ocl_i is in $[0, 1]$ as $a, b > 0$ and the lower value represents the high orientation certainty level which the stronger energy concentrates along the ridge-valley orientation. However, the low orientation certainty level will be obtained in singular region due to the high curvature, i.e., the ridge orientation performs the opposite orientation.

Finally the quality score Q_{OCL} is computed by the mean of ocl values. An example is illustrated in fig. 3.11, where blocks with high and low quality are mapped to white and black intensity respectively.

3.3.3.2 Frequency domain analysis

Frequency domain analysis (FDA) evaluates each block if the ridge possess a periodic pattern using either a square wave or sinusoidal wave[LTS⁺04]. A signature along ridge-valley direction, centred at the centre of each block is used as illustrated in fig. 3.12. In the frequency domain, an ideal block wave exhibits a dominant frequency with sideband frequency components by *sinc* function [OLBC10]. A sinusoidal wave contains both dominant frequency and minimum component at non-dominant frequencies. Therefore the existences of one dominant frequency and the frequency of such dominant component are two elements can be used to measure the quality of each block.

In the coordinate system, the signature is given by:



(a) High quality sample (b) Low quality sample

Figure 3.11: Orientation certainty level in each block for high and low quality sample. High intensity corresponds to high level of certainty. The samples are taken from FVC2000DB1 [MMWJ02].

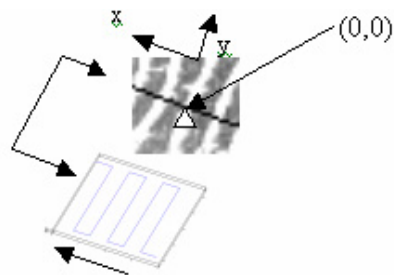


Figure 3.12: Signature along x direction. Taken from [LTS⁺04].

$$T(x) = \frac{1}{2r+1} \sum_{y=-r}^r I(x, y) \quad (3.5)$$

where $I(x, y)$ is the intensity at point (x, y) ; x is the index along x axis and the range $-25 \leq x \leq 26$ is sufficient to cover two ridge separations [MMJP09]; r is the width along y axis and $-10 < r < 10$ is sufficient to obtain the average intensity along y axis.

For N segmented blocks, Discrete Fourier Transform (DFT) [Smi97] can transform each signature $T(x)$ to spacial frequency domain:

$$F(u) = \frac{1}{N} \sum_{n=0}^{N-1} T(x) e^{-2\pi i (\frac{nx}{N})}, \quad i = \sqrt{-1} \quad (3.6)$$

Figure 3.13 illustrates DFTs for the blocks with different quality. Bad quality block, such as fig. 3.13c and fig. 3.13d, can be identified because of the very low frequency and lack of obvious dominant frequency respectively.

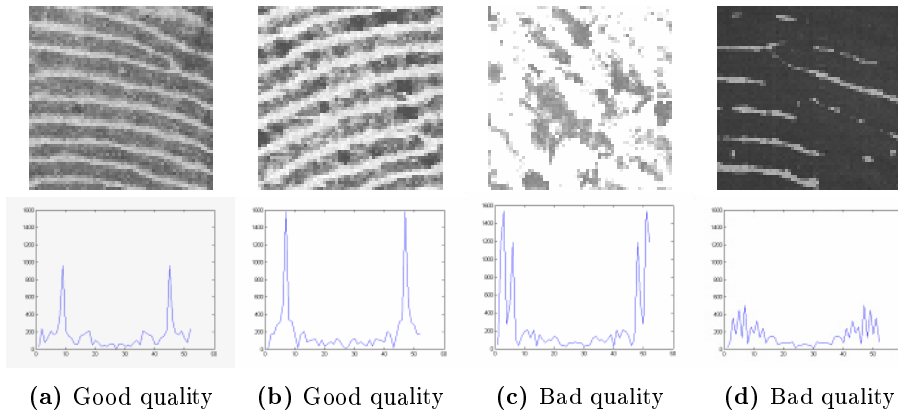


Figure 3.13: Different blocks with DFTs of the signatures along x . Taken from [LTS⁺04].

The quality score fda_i of block i is given by:

$$fda_i = \frac{A(F_{max} + 0.3[A(F_{max} - 1) + A(F_{max} + 1)])}{\sum_{F=1}^{NF/2} A(F)} \quad (3.7)$$

where $A(x)$ is the amplitude at frequency domain and F is the DFT frequency index. The final quality score Q_{FDA} is the mean of scores assigned to foreground blocks.

Due to the averaging process in eq. (3.5), the noises along the ridges and valley flow might be cancelled out or provide a better modelling of smoothing signal if they are perpendicular to ridge flow. Moreover, the pixel level noise along the ridges and valleys are neglected. Figure 3.14 depicts the FDA result in terms of high and low quality fingerprint image

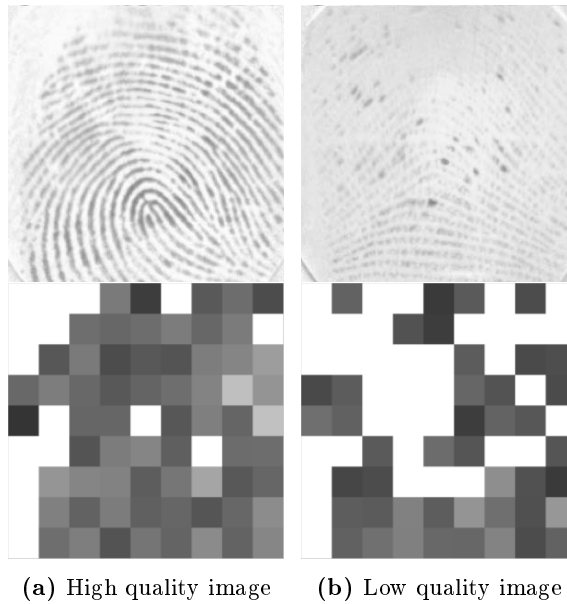


Figure 3.14: Frequency domain analysis in each block. High intensity corresponds to low quality block. The samples are taken from FVC2002DB1.

3.3.4 Approaches to global analysis

Different with local analysis, the global analysis takes the entire fingerprint image into consideration. These global features, such as ridge continuity and ridge-valley uniformity, are used to give the quality score.

3.3.4.1 Gabor

Gabor quality measurement method performs on a pixel-wise evaluation by calculating the standard deviation of the Gabor filter bank responses. The strength of the response at a given location corresponds agreement between filter orientation and frequency in the location neighbourhood. For areas in the fingerprint image with a clear ridge-valley pattern there will be a high response from one or a few filter orientations. In areas containing background or unclear ridge-valley structure the Gabor response of all orientations will be low and constant [OXB12].

The general form of the complex 2D Gabor filter h_{cx} in the spatial domain is given by [HUW⁺98]:

$$h_{cx}(x, y; f, \theta, \sigma_x, \sigma_y) = \exp\left(-\frac{1}{2}\left(\frac{x_\theta^2}{\sigma_x^2} + \frac{y_\theta^2}{\sigma_y^2}\right)\right) \exp(i2\pi f x_\theta), \quad i = \sqrt{-1} \quad (3.8)$$

where

$$\begin{aligned} x_\theta &= x \sin\theta + y \cos\theta \\ y_\theta &= x \cos\theta - y \sin\theta \end{aligned}$$

and f is gabor filter frequency of the sinusoidal plane wave along the orientation θ , and σ_x, σ_y are Gaussian window.

The filter bank size with regard to the orientation θ in dependence on the input value n :

$$\theta = \frac{k-1}{n\pi}, \quad k = 1, \dots, n \quad (3.9)$$

Empirically the parameters are recommended for 500 ppi images [NIS12]:

$$\sigma_x = \sigma_y = 6, \quad f = 0.1, \quad n = 4$$

Consequently a image possesses n Gabor filter responses, fig. 3.15 depicts the response for each orientation, $0, \pi/4, \pi/2, 3\pi/4$.

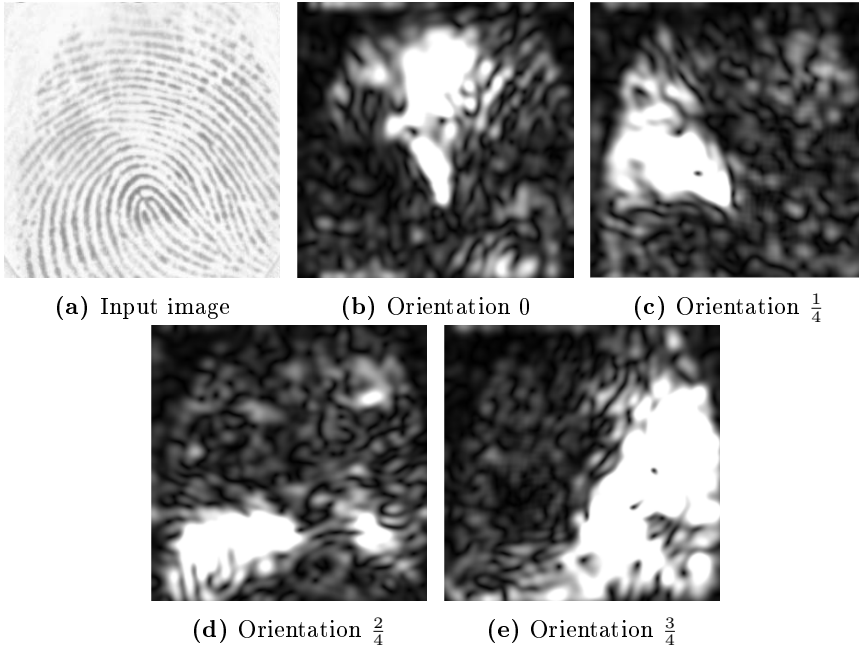


Figure 3.15: Garbor response for filtered image at different orientation. The samples are taken from FVC2002DB1.

Compute the standard deviation of the Gabor magnitude response values G_{std} among all orientations depicted in fig. 3.16, The final quality score Q_{Gabor} is produced by the mean of the G_{std} . The background which performs the orientation, such as latent fingerprint, might have influence of this metric.

3.3.4.2 Radial Power Spectrum

The Radial Power Spectrum (RPS) is a metric to measure the maximal power in a given frequency band of the global Radial Fourier spectrum. Ridges can be locally approximated by means of a single sine wave, hence high energy concentration a narrow frequency band corresponds to consistent ridge structures [NIS12] [CDJ05].

The two-dimensional Radial Fourier transform $f(u, v)$ of image intensity $I(x, y)$ is given by:

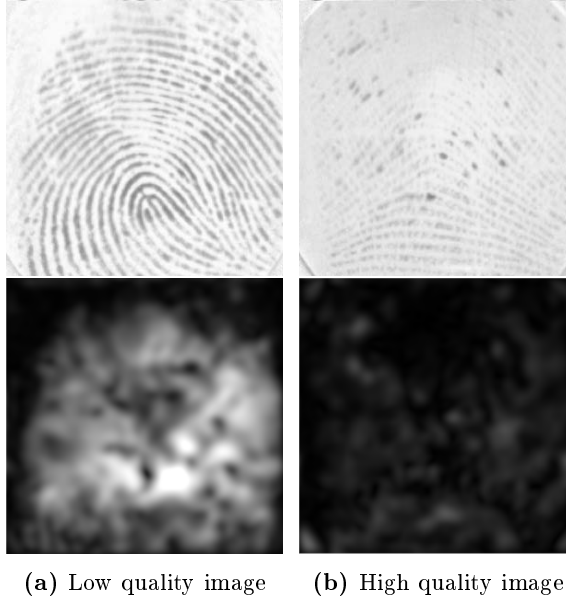


Figure 3.16: Standard deviation of Gabor filtered responses. The samples are taken from FVC2000DB1.

$$f(u, v) = \frac{1}{MN} \sum_{m=0}^{M-1} \sum_{n=0}^{N-1} I(x, y) e^{-i2\pi(\frac{mx}{M} + \frac{ny}{N})}, \quad i = \sqrt{-1} \quad (3.10)$$

The Fourier spectrum $J(r)$ is computed as:

$$J(r) = \frac{\sum_{\alpha=0}^{\pi} \sum_r^{r+\Delta r} |f(\alpha, r)|}{\sum_{\alpha=0}^{\pi} \sum_{r_{min}}^{r_{max}} |f(\alpha, r)|} \quad (3.11)$$

where $f(\alpha, r)$ is the spectrum $f(u, v)$ representation in polar coordinate system (α, r) , r_{min} , r_{max} is the lowest and highest frequency in the reasonable Fourier domain and Δr is sampling step. Note reasonable domain is also called region of interest (ROI) which is determined by the ridge frequency in a fingerprint image [HJ04].

The quality score Q_{RPS} is the maximum value of $J(r)$ in the ROI. Figure 3.17 illustrates the Radial Fourier spectrum for good and bad images.

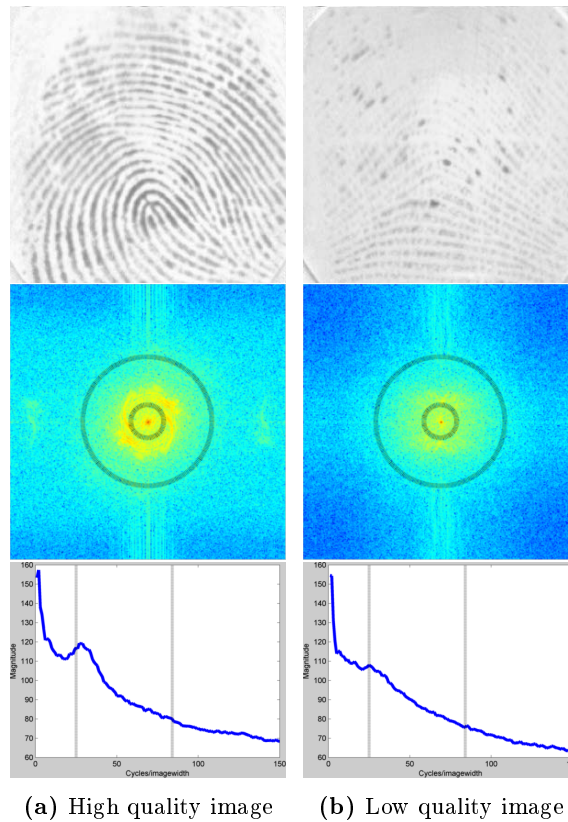


Figure 3.17: Radial Power Spectrum of images. The first row presents the original fingerprint images, the second row is the spectrum where ROI is inside the ring pattern. The third row is the magnitude spectrum where ROI is the region between two lines. The samples are taken from FVC2000DB1.

3.3.5 Foreground area

The fingerprint foreground refers to fingerprint area in a image with recognized ridge-valley structures. It is also should be taken into consideration, as it is likely that a fingerprint image possesses a small ridge-valley area with good quality. As a result, the acceptable quality score is given to the entire image, however, a low comparison score might be obtained for this image. Figure 3.18 depicts the different foreground areas. Fingerprint segmentation is further discussed in section 5.3.

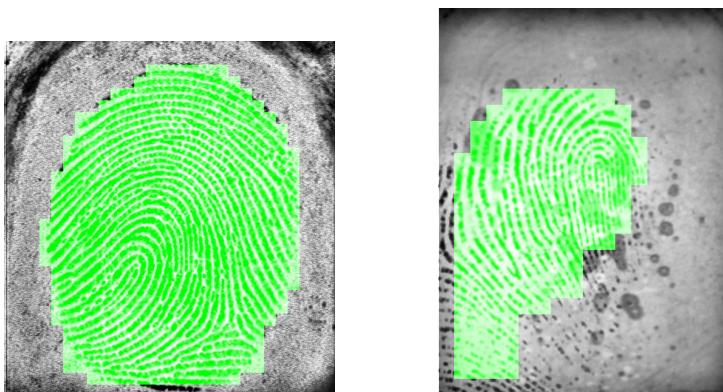


Figure 3.18: Fingerprint ridge-valley region, the valid ridge-valley area is marked by green block. Taken from [ISO12c] [MMC⁺04].

3.4 Aggregation of QMAs

In order to measure the quality of a fingerprint image comprehensively, plenty of metrics should be combined to measure the quality in both local and global levels.

3.4.1 Weighted average

An approach to combine the M local, N global metrics QL_i and QG_j with valid area VA , is to compute their weighted average as the final unified quality score[ISO12c]:

$$QS = \sigma_1 \sum_{i=1}^M \alpha_i QL_i + \sigma_2 \sum_{j=1}^N \beta_j QG_j + \sigma_3 VA \quad (3.12)$$

where

$$\sum_{i=1}^M \alpha_i = 1, \sum_{j=1}^N \beta_j = 1, \sum_{k=1}^3 \sigma_k = 1 \quad (3.13)$$

and σ, α, β are the weights. Note the input scores are unified, i.e., $0 \leq QL_i \leq 1$, $0 \leq QG_j \leq 1$ and $0 \leq VA \leq 1$, resulting in $0 \leq QS \leq 1$.

3.4.2 Pattern classifier

Beside the above approach, the issue can be formulated as a classification problem. *Pattern classifier* refers to a mathematical model that can intelligently predict an output for same sort of sample based on the learned concept after well-formed training. Training a pattern classifier could be performed using utility or utility-based quality scores which generated by the ground-truth comparison scores as described in section 2.4.

A neural network pattern classifier is trained to classify fingerprint quality is quantified into 5 values [TG09] [TW05] within NFIQ according to the feature vector in the table 3.1.

Similarly a new feature vector can be established depending on M local, N global QMA quality scores and valid area:

$$f = (QL_1, \dots, QL_M, QG_1, \dots, QG_N, VA)^T \quad (3.14)$$

Once the pattern classifier is well-formed trained with a feature, the pattern classifier will be able to produce the resultant overall quality score or quality category.

Number	Description
1	number of blocks that are quality 1 or better
2	number of total minutiae found in the fingerprint
3	number of minutiae that have quality 0.5 or better
4	number of minutiae that have quality 0.6 or better
5	number of minutiae that have quality 0.75 or better
6	number of minutiae that have quality 0.8 or better
7	number of minutiae that have quality 0.9 or better
8	percentage of the foreground blocks of quality map with quality = 1
9	percentage of the foreground blocks of quality map with quality = 2
10	percentage of the foreground blocks of quality map with quality = 3
11	percentage of the foreground blocks of quality map with quality = 4

Table 3.1: Features used in NFIQ. Taken from [TG09].

3.5 Benchmarking QMAs

Massive publications state that QMAs should provide acute prediction of the comparison, however, it is difficult to assert whether these approaches are viable and appropriate due to lack of formal specification. This section will discuss the approaches to compare the performance of proposed QMAs.

3.5.1 Error versus reject curves

Error versus reject curves (ERC) are proposed as an visually approach to evaluate how efficiently rejection of low quality samples results in improved performance [TG09].

From the same subject i , there is a pair of samples $q_i^{(1)}, q_i^{(2)}$ are compared to generate a comparison score $s_{ii}^{(k)}$ by a comparator. Two sample's quality in biometric comparison can be combined as:

$$q_i = H(q_i^{(1)}, q_i^{(2)}) \quad (3.15)$$

where $H(x, y) = \sqrt{xy} + N(0, 0.01)$, N is Gaussian noise which serves to randomly reject samples within a quality level and produces an approximation of the lower convex hull of the geometric mean curve [PR96].

For a level of acceptable quality threshold u , the set of low quality entries $R(u)$ is given by:

$$R(u) = \{i : q_i < u\} \quad (3.16)$$

The FNMR is the fraction of genuine comparison scores below a given threshold t computed for those samples not in the set $R(u)$.

$$FNMR(u) = \frac{|\{s_{ii} : s_{ii} \leq t, i \notin R(u)\}|}{|\{s_{ii} : s_{ii} \leq \infty, i \notin R(u)\}|} \quad (3.17)$$

Note the value of t is fixed and set empirically, in practice it will be set to give some reasonable non-match rate r , i.e. $t = M^{-1}(r)$ where M is the comparison algorithm from one of the comparators.

With the different quantile of acceptable quality threshold u , the performance among with mentioned QMAs in section 3.3.2 are depicted in fig. 3.19, where NFIQ is the resultant algorithm of NFIQ project. In practice it is not realistic higher than $\frac{1}{3}$ samples could be rejected, so at most 35% rejection is presented. If the computed quality values are perfectly correlated with the genuine scores, then FNMR should decrease quickly with the fraction rejected. Visually a good QMA should approach to the ideal case which means all the low comparison scores are caused by the low quality sample.

3.5.2 Spearman correlation

An alternative method is to present the correlation between QMAs and ground-truth scores (e.g., utility or utility-based quality scores) using *Spearman correlation*. In statistics, Spearman correlation, fully called *Spearman's rank correlation coefficient*, named after Charles Spearman who first proposed this method in [Spe87] and often denoted by ρ . Different with *Pearson correlation* [RN88], it is a non-parametric measure the degree of association between two variables using a monotonic function. The Spearman correlation ρ is given by:

$$\rho = \frac{\sum_i (x_i - \bar{x})(y_i - \bar{y})}{\sqrt{\sum_i (x_i - \bar{x})^2 (y_i - \bar{y})^2}} \quad (3.18)$$

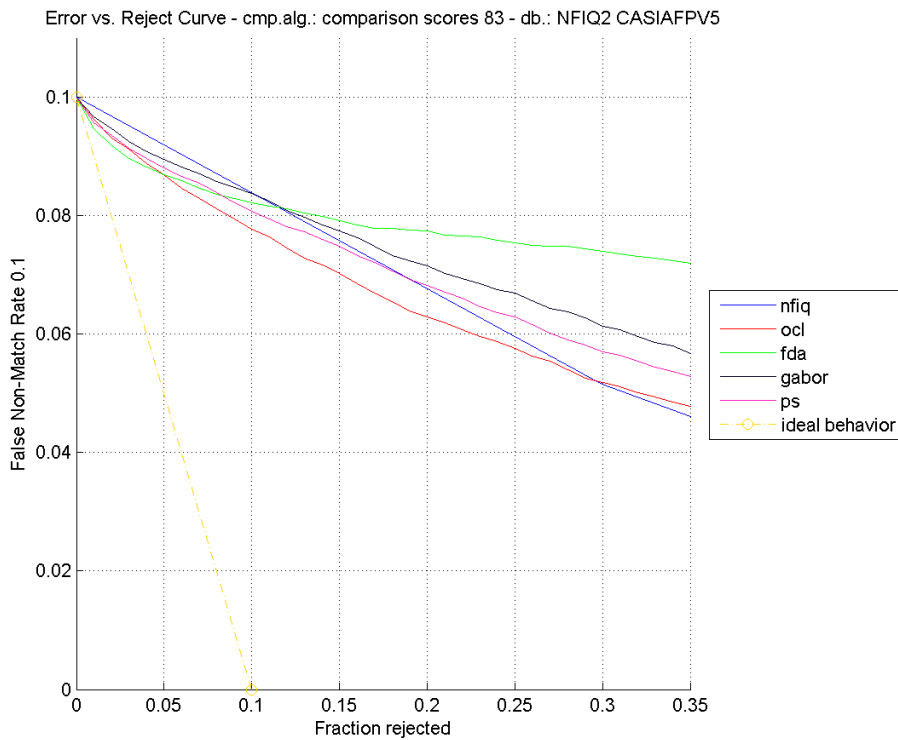


Figure 3.19: ERC for database CASIAFPV5-FULL [oSIoA] using a black-box comparator. FNMR is set as 0.1 and at most 35% samples are rejected.

Consequently $-1 \leq r \leq 1$, +1 or -1 is obtained if relation between two variables can be described by a perfect monotone function. Table 3.2 illustrates the correlation among QMAs and utility scores.

	FDA_1	gabor_0	GS_5	GS_9	GSh_10	LCS_1	LCS_7	miL_0	MMB_0	MMSB_0	MSB_0	OCL_0	OF_2	PS_0	RVU_0	RVU_1	sigma_0	SSB_1	util26	util63	util83
FDA_1	100	-32	24	-35	-6	-36	45	42	69	13	-41	17	81	23	-38	-32	-25	40	1	1	4
gabor_0	-32	100	19	66	89	86	61	-77	-4	13	64	73	-8	66	-38	-37	78	-43	31	22	24
GS_5	24	19	100	12	20	11	32	-22	14	21	20	27	28	14	-22	-20	16	-18	2	2	2
GS_9	-35	66	12	100	47	70	35	-73	0	24	70	37	-27	33	-8	-9	62	-51	2	0	-1
GSh_10	-6	89	20	47	100	66	72	-57	19	6	37	84	24	76	-55	-52	70	-26	41	30	34
LCS_1	-36	86	11	70	66	100	57	-79	-12	14	72	63	-23	43	-25	-27	77	-47	14	12	11
LCS_7	45	61	32	35	72	57	100	-41	56	13	23	88	58	70	-64	-57	57	-16	29	22	25
miL_0	42	-77	-22	-73	-57	-79	-41	100	5	16	-52	-52	24	-37	-6	-7	-93	85	-2	-1	-2
MMB_0	69	-4	14	0	19	-12	56	5	100	0	-28	36	70	35	-31	-24	12	4	10	7	11
MMSB_0	13	13	21	24	6	14	13	16	0	100	65	0	-3	13	-42	-47	-27	49	1	-2	-4
MSB_0	-41	64	20	70	37	72	23	-52	-28	65	100	24	-43	25	-19	-23	33	-18	3	0	-2
OCL_0	17	73	27	37	84	63	88	-52	36	0	24	100	49	65	-59	-55	69	-25	34	27	30
OF_2	81	-8	28	-27	24	-23	58	24	70	-3	-43	49	100	34	-51	-44	-3	25	19	15	18
PS_0	23	66	14	33	76	43	70	-37	35	13	25	65	34	100	-48	-39	49	-11	36	24	28
RVU_0	-38	-38	-22	-8	-55	-25	-64	-6	-31	-42	-19	-59	-51	-48	100	86	-7	-35	-39	-28	-31
RVU_1	-32	-37	-20	-9	-52	-27	-57	-7	-24	-47	-23	-55	-44	-39	86	100	-5	-40	-34	-26	-27
sigma_0	-25	78	16	62	70	77	57	-93	12	-27	33	69	-3	49	-7	-5	100	-76	9	8	10
SSB_1	40	-43	-18	-51	-26	-47	-16	85	4	49	-18	-25	25	-11	-35	-40	-76	100	8	6	5
util26	1	31	2	2	41	14	29	-2	10	1	3	34	19	36	-39	-34	9	8	100	80	83
util63	1	22	2	0	30	12	22	-1	7	-2	0	27	15	24	-28	-26	8	6	80	100	82
util83	4	24	2	-1	34	11	25	-2	11	-4	-2	30	18	28	-31	-27	10	5	83	82	100

Table 3.2: Spearman correlation coefficients among QMAs and utility scores within NFIQ 2.0. Taken from [NIS12]

Beside the correlation between the ground-truth and QMA scores, the correlation between QMAs is more important, which is used to analyse whether the two QMAs give the similar indication or the scores are complementary.

Orientation Field Estimation

Based on the previous chapters with the concepts of biometrics and fingerprints, this chapter will discuss techniques to estimate orientation fields of fingerprints, which can be used as a foundation of singular point localization in 5.

4.1 Orientation field

The term *local ridge orientation* was firstly proposed in 1969 [Gra69], which represents the ridge-valley structure of a fingerprint. With regard to the orientation in a fingerprint image, it is an cyclic and unoriented direction ranging from $(-\frac{\pi}{2}, \frac{\pi}{2}]$, or $(0, \pi]$ depending on the representation. The angle θ_{ij} at the pixel (i, j) is depicted in 4.1, where an additional value r_{ij} is often obtained with each orientation θ_{ij} to denote the reliability of the orientation. In the other words, the value r_{ij} is high for good quality regions in the fingerprint image and low for noisy and seriously corrupted regions. Furthermore, *Orientation field* (OF), also called directional field, refers to the overall orientation patten in a fingerprint.

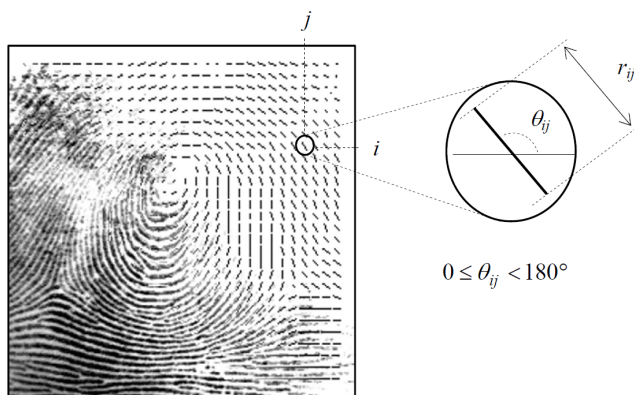


Figure 4.1: A fingerprint image faded into the corresponding orientation image computed over a square-meshed grid of size 16×16 . Each element denoted the local orientation of the fingerprint ridges; the element length is proportional to its reliability. Taken from [MMJP09].

4.2 Orientation field estimation

4.2.1 Previous work

OF estimation is an essential step of fingerprint recognition, especially in fingerprint classification and singular point localization. In order to estimate an accurate OF, plenty of approaches have been proposed and they can be classified as [JK10] [MMJP09] [GMM09] [ZG04]:

- **Gradient-based:** it is proposed by Kass and Witkin in 1987 [KW87]. This approach is the simplest and most natural approach based on computation of gradients of pixels or blocks. Nevertheless, it is susceptible to interference by scars, dirt, moisture of the finger with interrupted, thick or grainy ridge structures in the acquired image.
- **Filterbank-based:** also called slit-based approach, orientation is determined according to highest filter response based on a fixed number of reference orientations [JPH99] [JPHP00]. It is resistant to noises but not accurate due to the limited number of pre-defined orientations. Furthermore, moderately high computation cost is required.
- **Model-based:** Sherlock and Monroe introduced a zero-pole model using rational complex functions [SM93], and some variants have been proposed

[VG96] [ZG04]. It has the disadvantage of requiring the prior knowledge of the singular regions which is violate the motivation of this thesis.

4.2.2 Gradient-based approach

Compared with the other approaches, gradient-based approach is reported as the most accurate estimation with lowest computation complexity [BG02] [GMM09] [WHH07] [ZYHZ06]. Hence OFs are estimated using gradient-based approach. The proposed gradient-based approach can perform both in pixel- and block-wise, so the term *element* is used to represent the both cases in the following.

The pixel-wise gradient vectors $[G_x \ G_y]^T$ whose phase angle denoted the direction of the maximum intensity change are given by:

$$\begin{bmatrix} G_x \\ G_y \end{bmatrix} = \nabla I(x, y) = \begin{bmatrix} \frac{\partial I(x, y)}{\partial x} \\ \frac{\partial I(x, y)}{\partial y} \end{bmatrix} \quad (4.1)$$

where $I(x, y)$ is the intensity at pixel (x, y) . An example finger sample and its Region of Interest (ROI) is depicted in fig. 4.2, of which the gradients are depicted in fig. 4.2.

The ridge orientation is orthogonal to the gradient phase angle at each pixel, however, the gradient vector cannot directly be used to compute because opposite gradient vectors will be cancelled out with each other although they represents the same orientations. Furthermore the orientation obtained from the gradient vectors should be cyclically in $(-\frac{\pi}{2}, \frac{\pi}{2}]$, for instance, the value $\frac{3\pi}{4}$ should be treated as $\frac{\pi}{4}$. A feasible representation is proposed by doubling the angles of the gradients so that opposite gradient vectors will point in the same direction [KW87].

Gradient vectors can be converted to polar coordinates from Cartesian coordinates:

$$\begin{bmatrix} G_\rho \\ G_\phi \end{bmatrix} = \begin{bmatrix} \sqrt{G_x^2 + G_y^2} \\ \tan^{-1} \frac{G_y}{G_x} \end{bmatrix} \quad (4.2)$$

so that gradient vectors can be represented using polar coordinates:



Figure 4.2: Example finger sample, the ROI is marked in the red square. The sample is taken from FVC2000DB2

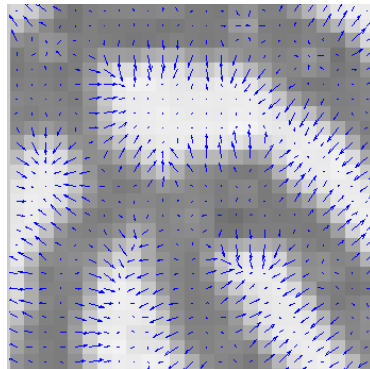


Figure 4.3: Gradients of ROI. The direction of arrow is from the low to high intensity.

$$\begin{bmatrix} G_x \\ G_y \end{bmatrix} = \begin{bmatrix} G_\rho \cos G_\phi \\ G_\rho \sin G_\phi \end{bmatrix} \quad (4.3)$$

With the doubling the angle of gradients, the length of gradient vectors is squared. By computing trigonometric identities, squared gradient vectors $[G_{s,x} \ G_{s,y}]^T$ does not require G_ρ and G_ϕ :

$$\begin{bmatrix} G_{s,x} \\ G_{s,y} \end{bmatrix} = \begin{bmatrix} G_\rho^2 \cos 2G_\phi \\ G_\rho^2 \sin 2G_\phi \end{bmatrix} = \begin{bmatrix} G_\rho^2 (\cos^2 G_\phi - \sin^2 G_\phi) \\ G_\rho^2 (2 \sin G_\phi \cos G_\phi) \end{bmatrix} = \begin{bmatrix} G_x^2 - G_y^2 \\ 2G_x G_y \end{bmatrix} \quad (4.4)$$

Figure 4.4 illustrates the squared gradients of ROI where the length is unified in order to be observed and the one ridge orientation only has a unique squared gradient representation.

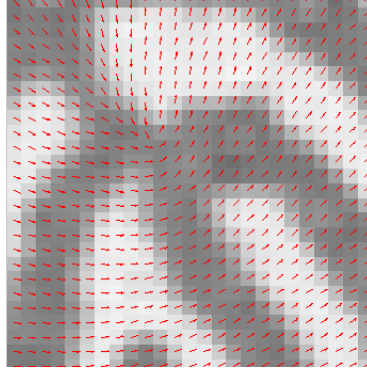


Figure 4.4: Squared gradients of ROI.

An efficient implementation can be achieved if gradient vectors are considered as complex numbers. As a result, “doubling the angle and squaring the length of a vector” is equivalent to “squaring a complex number”:

$$G_{s,x} + jG_{s,y} = (G_x + jG_y)^2 = (G_x^2 - G_y^2) + j(2G_x G_y) \quad (4.5)$$

A single orientation at fine pixel level is sensitive to noises in fingerprints, thus the averaged squared gradient $[\overline{G_{s,x}} \ \overline{G_{s,y}}]^T$ of each element is computed according to squared gradient vectors within a $M \times N$ window W :

$$\begin{bmatrix} \overline{G_{s,x}} \\ \overline{G_{s,y}} \end{bmatrix} = \begin{bmatrix} \sum_W G_{s,x} \\ \sum_W G_{s,y} \end{bmatrix} = \begin{bmatrix} \sum_W G_x^2 - G_y^2 \\ \sum_W 2G_x G_y \end{bmatrix} = \begin{bmatrix} G_{xx} - G_{yy} \\ 2G_{xy} \end{bmatrix} \quad (4.6)$$

where

$$G_{xx} = \sum_W G_x^2 \quad (4.7)$$

$$G_{yy} = \sum_W G_y^2 \quad (4.8)$$

$$G_{xy} = \sum_W G_x G_y \quad (4.9)$$

The edge length M , N is suggested in [15, 35] pixels for a 500 dpi image [BG02] [ZYHZ06], because high curvature property of ridgeline in singular region will be lost with a large size, whereas it is noise-sensitive with a small one. Furthermore, the averaging of squared vectors leads to a consequence that the stronger intensity have a higher vote in the average orientation than weaker one.

The average gradient direction Φ is given by:

$$\phi = \frac{1}{2} \angle(G_{xx} - G_{yy}, 2G_{xy}) \quad (4.10)$$

where the function $\angle(x, y)$ is computed by

$$\angle(x, y) = \begin{cases} \tan^{-1}(y/x), & x \geq 0 \\ \tan^{-1}(y/x) + \pi, & x < 0 \wedge y \geq 0 \\ \tan^{-1}(y/x) - \pi, & x < 0 \wedge y < 0 \end{cases} \quad (4.11)$$

Subsequently Φ lies in $(\frac{1}{2}\pi, \frac{1}{2}\pi]$

$$\theta = \begin{cases} \phi + \frac{1}{2}\pi, & \phi \leq 0 \\ \phi - \frac{1}{2}\pi, & \phi > 0 \end{cases} \quad (4.12)$$

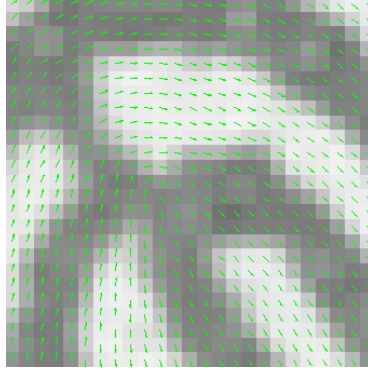


Figure 4.5: OF of ROI.

Figure 4.5 depicted the ridge OF within ROI.

A approach is proposed to measure *coherence* at each element how well all the squared gradient vectors $[G_{s,x} \ G_{s,y}]^T$ in the averaging window W have the same orientation [KW87]:

$$Coh = \frac{|\sum_W (G_{s,x}, G_{s,y})|}{\sum_W |(G_{s,x}, G_{s,y})|} \quad (4.13)$$

As a result, coherence lies in $[0, 1]$, where the minimum coherence 0 indicates the gradient vectors are distributed over all directions and all parallel to each other for maximum coherence 1, receptively. The coherence of the sample in fig. 4.2 is depicted in fig. 4.6.

The gradient-based approach is mathematically proofed that is equal to the *Principal Component Analysis* of the autocorrelation matrix of the gradient vectors [BG02]. Furthermore, the major flaw of this approach is the unreliable orientation might be computed due the to small denominator in eq. (4.11). Secondly the discontinuous orientation may be obtained especially for the block-wise estimation.

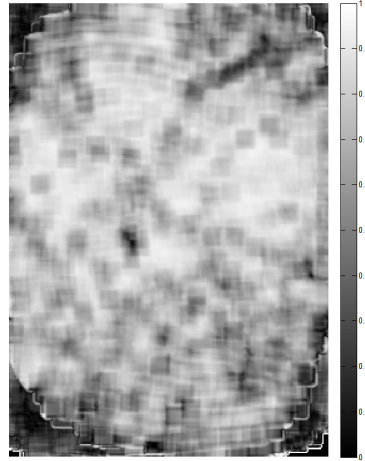


Figure 4.6: Coherence of the sample in pixel level, 0 and 1 are respectively mapped to black and white.

4.2.2.1 Redundant Estimation

In order to address the mentioned problem, hierarchical [USKV07] and weighted averaging scheme [WHS05] are proposed to guarantee the continuous and smooth OF. The basic idea behind the approaches is to establish a redundant estimation for each target element and the latter possesses the better improvement in terms of the accurateness and computation complexity.

The approach initially groups every $K \times K$ adjoining elements into a composite block, in which every $J \times J$ ($J < K$) adjoining elements is grouped into a neighbourhood D . For instance in fig. 4.7, the elements $\{I, II, IV, V\}$ are D_1 , and similarly $\{II, III, V, VI\}$ are D_2 , $\{IV, V, VII, VIII\}$ are D_3 , $\{V, VI, VIII, IX\}$ are D_4 . In each computation the averaged squared gradients in eq. (4.6) of centrally targeted element is re-estimated in accordance with the averaged squared gradients and coherence of it and its neighbourhoods:

$$\begin{bmatrix} \overline{G_{s,x}} \\ \overline{G_{s,y}} \end{bmatrix} = \begin{bmatrix} \sum \omega \cdot G_{s,x} \\ \sum \omega \cdot G_{s,y} \end{bmatrix} \quad (4.14)$$

where ω is the elementary weight in the K element composite block which is given by:

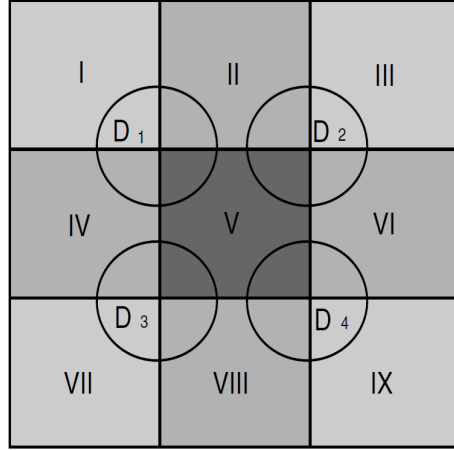


Figure 4.7: A composite block consists of 3×3 elements for the target element V in the centre and four overlapping neighbourhoods D_1 , D_2 , D_3 , D_4 . Taken from [WHS05].

$$\sum_I \omega = \sum_I \frac{r}{K} = 1 \quad (4.15)$$

r is the constant counting the times of element involving in the estimation, i.e., how strong is the correlation between the element and target element in terms of the neighbourhood D . For the case in fig. 4.7, r is $\frac{4}{16}$ for element V , $\frac{2}{16}$ for element II , IV , VI , VII , and $\frac{1}{16}$ for element I , III , $VIII$, IX .

Singular Point Localization

The previous chapter discusses approaches to estimate the orientation field of fingerprint image. Depending on an accurate orientation field, singular points can be extracted as a landmark of the fingerprint. This chapter discusses related techniques for singular point localization, and proposes several pattern-based filters to improve detection correctness.

5.1 Singular point

Singular point (SP), also called singularity, consists of *core* and *delta* which is usually associated with the point of higher ridge line curvature [MMJP09]. The region around SP is called singular region which is commonly used for fingerprint alignment and classification.

There are a few of definitions for SP, leading to a contradiction whether there is a core in arch fingerprints, because highest curvature ridgeline is not as prominent as the other types depicted in fig. 5.1. Some publications state that there is no SP in arch fingerprint [MMJP09] [BG02], while core is detected as a reference point [WBS12]. Therefore the most authoritative definitions in ISO/IEC 19794-1:2011 are adopted [ISO11]:

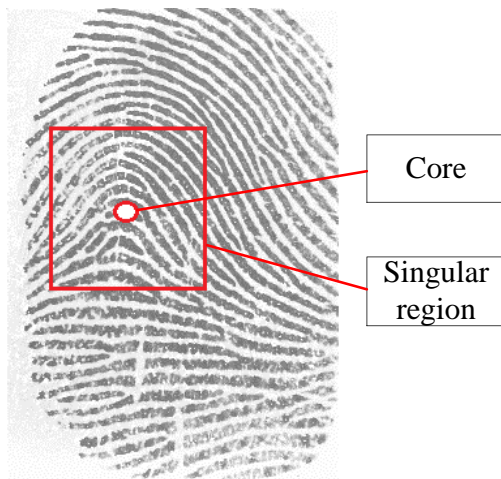


Figure 5.1: Arch fingerprint where the singular region and core is marked by square and circle respectively. The sample is taken from FVC2000DB2.

- **Core:** topmost point on the innermost recurving ridgeline of a fingerprint. Generally, the core is placed upon or within the innermost recurve of a loop.
- **Delta:** point on a ridge at or nearest to the point of divergence of two *typelines* and located at or directly in front of the point of divergence. The *typeline* refers to one of the two innermost friction ridges that start parallel, diverge, and surround or tend to surround the pattern area.

In terms of the mentioned definition, there is a core point presented in the arch fingerprints, because it does present a “recurving” pattern in singular region where ridges are curved backward. However, it is unnatural to claim the core is on the innermost recurving ridgeline, as it does not perform the highest curvature. Hence, the core point is defined on the ridge with highest curvature for the arch fingerprints in this thesis.

As a result, the analysis of the different fingerprint classes with regards to the number of SPs and the relative examples are illustrated in fig. 5.2:

- Arch fingerprints consist of one core point.

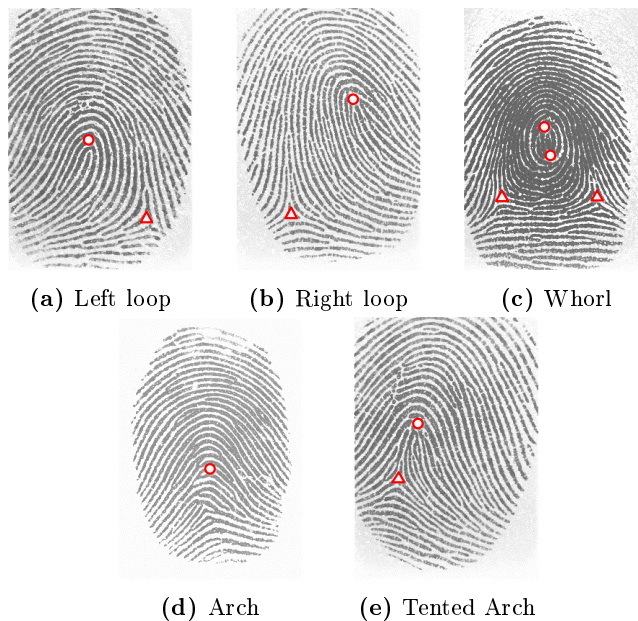


Figure 5.2: SPs for different type of fingerprints, where cores and deltas are marked by circles and triangles respectively. The samples are taken from FVC2000DB2.

- Left loop, right loop and tented arch fingerprints all consist of one core and one delta point.
- Whorl fingerprints consist of two core and delta points.

5.2 Singular point extraction

5.2.1 Related work

There are plenty of approaches proposed for SP extraction and most of them are based on the ridge OF. They can be classified as:

- *Poincaré index*: it is a natural and practical method based on Poincaré index and firstly proposed by Kawahgoe and Tojo in 1984 [KT84].

Each element (i, j) is surrounded by an orientation field \mathbf{G} , and then a closed curve C is formed which is immersed in \mathbf{G} . The Poincaré index $P_{\mathbf{G},C}(i, j)$ is defined as the total rotation of the orientations of \mathbf{G} along C at (i, j) . However, it is not resistant with noises and inefficient especially when smaller size of element is adopted in OF estimation.

Figure 5.3 illustrated an example for a 3×3 element length curve C . The path defining C is the ordered sequence of the eight elements \mathbf{d}_K ($k = 0 \dots 7$) surrounding (i, j) . The Poincaré index is then computed as:

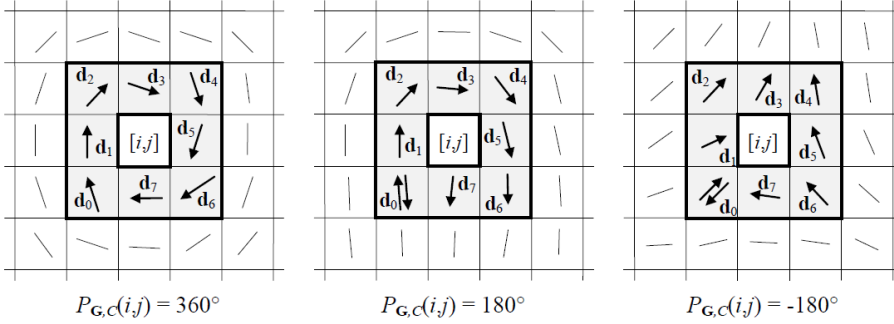


Figure 5.3: Poincaré index computation in the 8-neighbourhood of points belonging to a whorl, core, and delta (from left to right), respectively. Note that, for the core and delta points, the direction of d_0 is first chosen upward (to compute the angle between d_0 and d_1) and then successively downward (when computing the angle between d_7 and d_0). Taken from [MMJP09]

$$P_{\mathbf{G},C}(i, j) = \begin{cases} 0^\circ, & (i, j) \text{ does not belong to any SP} \\ 360^\circ, & (i, j) \text{ belongs to two core points} \\ 180^\circ, & (i, j) \text{ belongs to core point} \\ 180^\circ, & (i, j) \text{ belongs to delta point} \end{cases} \quad (5.1)$$

Note when OFs are estimated in a fine level using a smaller element, the whorl type is detected as two core points.

- **Local characteristics-based:** this series of approaches analyses the orientation so that the SP is characterized by high irregularity, curvature, or symmetry [CLMM99] [SM92] [LZH06]. However, these methods cannot provide an high accuracy.
- **Partitioning-based:** the orientation is only coarsely discretized by a limited number of orientation values and each orientation value determines

a region. SPs are detected on the crossing point of borderlines which are formed between two adjacent orientations. Wang, Bhattacharjee and Srinivasan reported an excellent result but it requires the pre-alignment [WBS12].

5.2.2 Green's Theorem-based approach

In order to address the problems of noise-sensitivity and low computation efficiency of Poincaré index, an discrete line integral is applied using Green's Theorem [BG02]. The algorithm doubles the orientation field resulting in an interval $(-\pi, \pi]$, and then compute gradients of the doubled orientation field, that the gradient vectors around SPs is depicted in fig. 5.4. Because of the doubling and integral, the Poincaré index values for non-SP, core and delta points becomes approximated values which are approaching to 0, 2π , -2π respectively.

$$\begin{bmatrix} Jx(x, y) \\ Jy(x, y) \end{bmatrix} = \nabla 2\theta(x, y) = \begin{bmatrix} \frac{\partial 2\theta(x, y)}{\partial x} \\ \frac{\partial 2\theta(x, y)}{\partial y} \end{bmatrix} \quad (5.2)$$

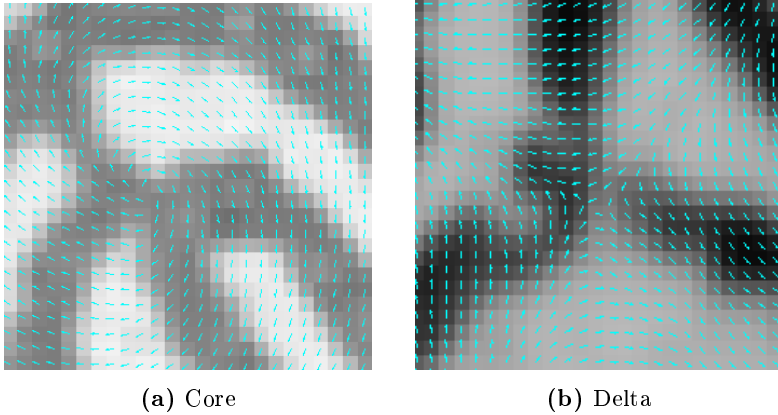


Figure 5.4: Gradients of doubled OFs. The core and delta possess particular patterns respectively.

Due to the periodicity of ridge orientation, the gradients of doubled orientation field should be computed cyclically, i.e., the transition of doubled orientation from $-\pi$ to π is continuous. For instance, there is only $\frac{\pi}{4}$ difference between $-\frac{3\pi}{4}$ and π , instead of their absolute difference. An alternative approach is proposed

to address this issue depending on the periodicity of trigonometric functions [Has08]:

$$Jx = \frac{\partial 2\theta}{\partial x} \quad (5.3)$$

$$= (\sin^2 2\theta + \cos^2 2\theta) \cdot \frac{\partial 2\theta}{\partial x} \quad (5.4)$$

$$= \cos 2\theta \cdot \frac{\partial \sin 2\theta}{\partial x} - \sin 2\theta \cdot \frac{\partial \cos 2\theta}{\partial x} \quad (5.5)$$

and similarly along the y direction:

$$Jy = \frac{\partial 2\theta}{\partial y} \quad (5.6)$$

$$= (\sin^2 2\theta + \cos^2 2\theta) \cdot \frac{\partial 2\theta}{\partial y} \quad (5.7)$$

$$= \cos 2\theta \cdot \frac{\partial \sin 2\theta}{\partial y} - \sin 2\theta \cdot \frac{\partial \cos 2\theta}{\partial y} \quad (5.8)$$

Green's Theorem can be applied instead of using the conventional Poincaré index method, whereas a closed line-integral over a vector field can be computed as the surface integral over the rotation of this vector field [Nyk]:

$$\oint \omega_x dx + \omega_y dy = \iint_A \text{rot}[\omega_x \ \omega_y]^T dx dy = \iint_A \left(\frac{\partial \omega_y}{\partial x} - \frac{\partial \omega_x}{\partial y} \right) dx dy \quad (5.9)$$

where A is the surface area for the vector field $[\omega_x \ \omega_y]^T$, and ∂A is the contour around this area.

The discrete Green's Theorem can be applied by summing the gradients of the doubled orientation $[Jx \ Jy]^T$ over the contour [YA06]:

$$\text{Index} = \sum_{\Delta x, \Delta y \text{ along } \partial A} (Jx \cdot \Delta x + Jy \cdot \Delta y) = \sum_A \text{rot}[Jx \ Jy]^T = \sum_A \left(\frac{\partial \omega_y}{\partial x} - \frac{\partial \omega_x}{\partial y} \right) \quad (5.10)$$

In practice because of the summing used in the computation, results in the non-zero Poincaré index values being spread over a small cluster of pixels around the

SPs rather than being isolated at one pixel. Depending on the definition of SP, one of the pixels performing the strongest rotation is identified as the detected SPs.

Compared with the conventional Poincaré index approach, this method is more robust against noises, because obtained values are various instead of limited candidates 0° , 180° , -180° . As a result, noisy points without enough rotation can be eliminated by setting a proper threshold while they might be detected as SPs by conventional Poincaré index. Moreover, a typically spurious core-delta pair being appeared nearby can be easily cancelled out using a proper size of window.

Nevertheless, this method cannot detect core points in arch fingerprints, as it does not perform a strong rotation degree as the others although it possesses the strongest rotation in the whole sample. As a solution, the fingerprint is considered as a arch type if there is no SP detected, and then the threshold is lowered so that the point with the highest curvature in a arch fingerprint is extracted as core point.

5.2.3 Orientation of singular points

Furthermore, orientations of extracted SPs can be estimated by comparing the doubled OF with precomputed reference models that representing prototypes for both core and delta. The orientation of core is the direction where the core points to, and for delta is the direction where one of the three vertexes points to the top of the image, depicted in fig. 5.5

The effectiveness of this method is proofed [BG02], and the basic idea is that all the components of doubled orientation field rotate the same angle when they image rotates around the SP.

The reference models of doubled orientation fields around core and delta can be established by:

$$DOF_{core,ref} = \frac{(y, -x)}{\sqrt{x^2 + y^2}} \quad (5.11)$$

$$DOF_{delta,ref} = \frac{(-y, -x)}{\sqrt{x^2 + y^2}} \quad (5.12)$$



Figure 5.5: Orientations of SPs, the orientation of core and delta is represented by the red and green arrows.

Note $|DOF_{core,ref}| = |DOF_{delta,ref}| = 1$ for all pixels. Example precomputed reference models are illustrated in fig. 5.6.

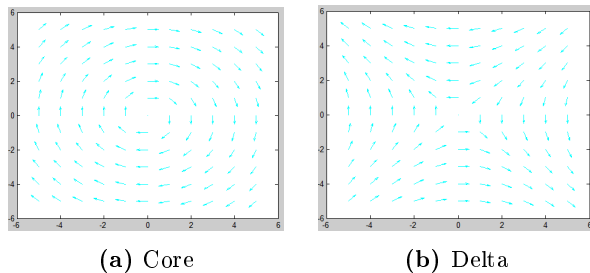


Figure 5.6: Reference models of core and delta with the size of 11×11 pixel.

The orientation of core is given by taking the element-by-element product of the estimated doubled gradient vectors $DOF_{core,obs}$ and the complex conjugated of the reference model $DOF_{core,ref}$:

$$\hat{\alpha}_C = \angle \frac{1}{N} \sum_{x,y} DOF_{core,ref}^* \cdot DOF_{core,obs} \quad (5.13)$$

Similarly with delta, but the value is divided by three due the the definition:

$$\hat{\alpha}_D = \frac{1}{3} \angle \frac{1}{N} \sum_{x,y} DOF_{delta,ref}^* \cdot DOF_{delta,obs} \quad (5.14)$$

5.3 Segmentation

Gaussian filter is usually applied to smooth the fingerprints and reduce the effects of noisy areas on fingerprint images [HA91], however, the strength of the smoothing filter is difficult to determined because the foreground and background of fingerprint suffers from noises with different degrees, i.e., SPs might be missed with stronger Gaussian filter and the slight smoothing filter may not remove the influence of noises.

One of the good choice is to segment the background and apply the Gaussian filter to the foreground. At first a simple and rough method is used by thresholding the variance of each $M \times N$ block [Meh93][Kov]:

$$Var = \frac{1}{MN} \sum_{i=0}^{M-1} \sum_{j=0}^{N-1} (I(x,y) - Mean)^2 \quad (5.15)$$

where I is the intensity at pixel (x,y) and $Mean$ is the mean of the intensity in each block.

Consequently the fingerprint segmentation might suffer from the following problems:

- Singular region as part of foreground might be eliminated exactly, illustrated in fig. 5.7.
- More than one fragments are detected due to latent fingerprint or noises, which might cause spurious SPs, illustrated in fig. 5.8.
- The foreground edgeline shows blocking artefacts so that part of background is still remained, illustrated in fig. 5.9.

It is valuable to apply the mathematical morphology to images [Jai89]. Empirically a fingerprint image always possesses a unique connected area with round

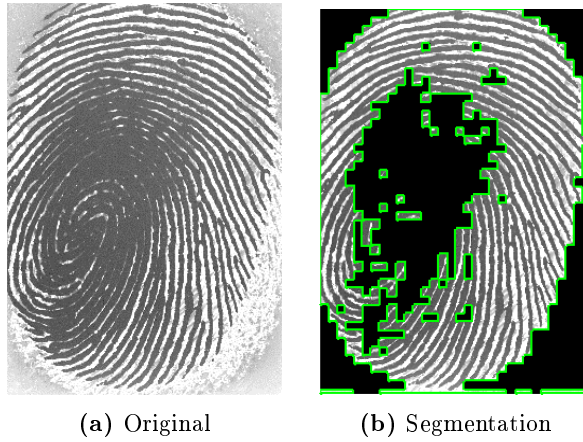


Figure 5.7: The singular region is eliminated because of the low variance, and the boundaries of foreground is surrounded by green lines. The sample is taken from FVC2000DB2.

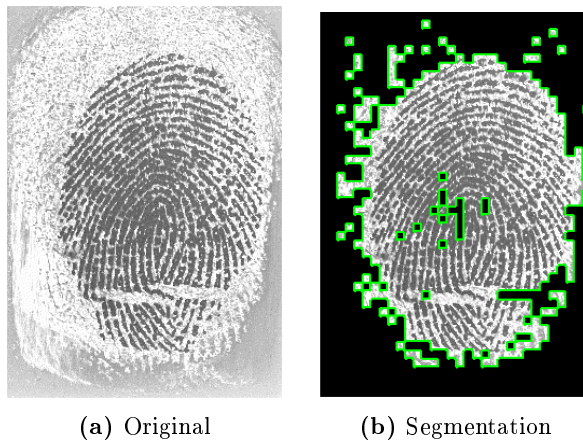


Figure 5.8: More than one fragments are remained due to the latent fingerprint, and the boundaries of foreground is surrounded by green lines. The sample is taken from FVC2000DB2.

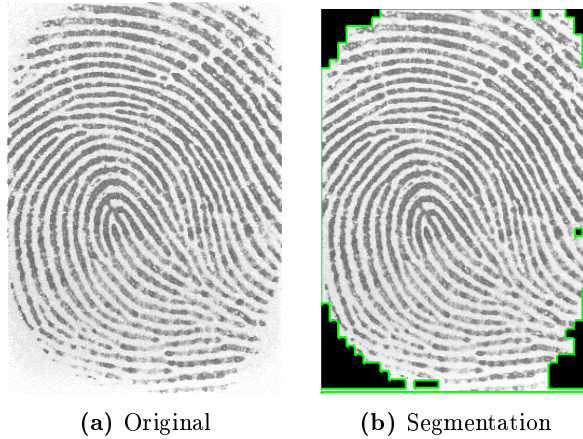


Figure 5.9: The edge of foreground presents a square shape, and the boundaries of foreground is surrounded by green lines. The sample is taken from FVC2000DB2.

edge. Hence after the rough segmentation, a couple of morphological methods is applied as a post-processing:

- Select the largest area as the underlying fingerprint foreground.
- Fill all the holes in the selected area.
- Morphologically open the selected area using disk shape to erode the square shape edge.

The same fingerprints are segmented with post-processing, where the mentioned issues are resolved, depicted in fig. 5.10.

5.4 Singular point validation

After the segmentation, there still might be some spurious SPs remained on the foreground due to noises. Filters are required to proposed in order to eliminate false detections from a set of candidate SPs. Simple idea takes the mean and standard variance as the filters, but it does not provide fair performance because OF for the areas with low mean and variance might be estimated accurately resulting in correct SPs detections, depicted in fig. 5.11.

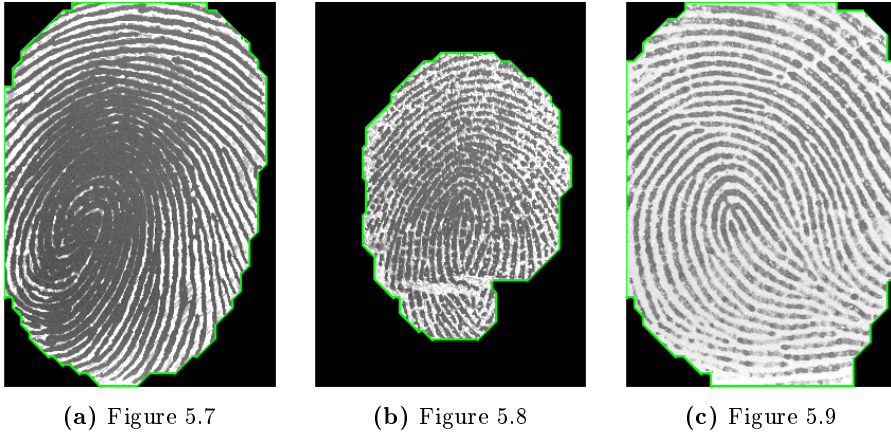


Figure 5.10: The results of segmentation and the boundaries of foregrounds are surrounded by green lines. The samples are taken from FVC2000DB2.

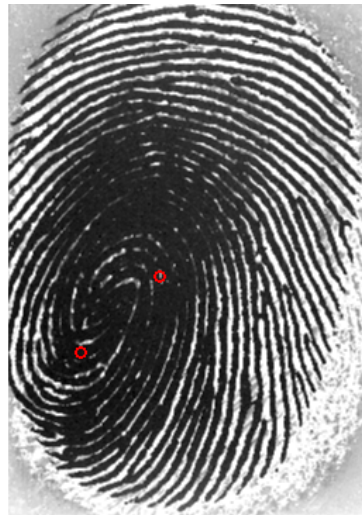


Figure 5.11: Correct SPs detection with low mean and variance area. The cores is marked by the circles. The sample is taken from FVC2000DB2.

A series of semantic filters is proposed, which are based on the assumption that the core is in the centre of the fingerprint area and further that the fingerprint area provides higher signal quality if around the core. Therefore, if SPs does not satisfy the filters then part of them which are near to the edge will be removed.

In any fingerprint image, the following conditions should be satisfied:

- **C2D2**: There are at most two cores and two deltas.
- **CCDIS**: If there are two cores, then they are not far from each other.
- **CCORIDIFF**: If there are two cores, then they possess the approximately opposite orientations.
- **DDORIDIFF**: If there are two deltas, then they possess the similar orientations.
- **DCDANGLE**: If there are two deltas and at least one core, then angle $\text{delta1} - \text{core} - \text{delta2}$ lies in a certain interval depicted in fig. 5.12.

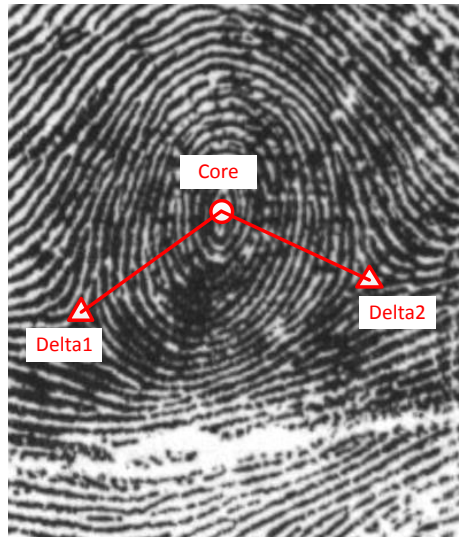


Figure 5.12: Angle $\text{delta1} - \text{core} - \text{delta2}$ of a image, the midpoint is used as the position of core if there are more than one core points.

CHAPTER 6

Proposed Quality Measurement Algorithms

The previous chapters discuss the approaches to conduct OF estimation and SP localization respectively. Based on the mentioned methods, this chapter proposes several QMAs to measure fingerprint image quality.

The international standard ISO/IEC 29794-1:2009 defines that a quality score lies in $[0, 100]$ with ascending order in terms of the quality, i.e. high score refers to a high quality and vice versa [ISO12b]. Hence eventually all the scores of proposed QMAs are normalized and inverted if they are descending.

6.1 Position-based QMAs

Core points are located in the centre of fingers so that the position of core is commonly used to obtain displacement of finger sample. Plenty of publications suggest to use these centre points as registration points to line up a pair of fingerprint in comparison process, because the displacement or presence of core point is one of the criterion to register a fingerprint for measuring whether the finger is placed properly [Weg82] [Lin98]. The error or warning can be reported if its fingerprint performs a large displacement because a poor comparison score

might be obtained between two fingerprint images if they shift to the opposite direction.

Depending on the position of core, metrics can be established to measure the displacement of fingerprint image, i.e., whether the core is located around the centre of fingerprint foreground. Given a foreground of a fingerprint, the coordinate of centre (C_x, C_y) of N pixels foreground is computed as:

$$C_x = \frac{1}{N} \sum_{i=0}^{N-1} M_x \quad (6.1)$$

$$C_y = \frac{1}{N} \sum_{i=0}^{N-1} M_y \quad (6.2)$$

where $[M_x, M_y]$ is the index of foreground mask along x and y direction. It is fair that the centre of foreground is computed without the consideration of the image intensity, as there is no interest to find the centre of gravity of a fingerprint image.

6.1.1 Euclidean distance

- **Distance:** the quality score is given by the distance from the centre to the core, depicted in fig. 6.1a. For a given finger sample, the algorithm performs as follows:
 1. Obtain the fingerprint foreground by the segmentation algorithm in section 5.3.
 2. Localize the position of core point by the algorithm in section 5.2.2 and apply the core-related filters in section 5.4. If there are two cores detected, the midpoint is used as the core position.
 3. The quality score is given by Euclidean distance from the centre of the foreground to the point of core.
 4. Invert the order of the quality scores and normalize to $[0, 100]$.
- **Distance ratio:** The quality score is given by the ratio of the distance from the centre to the core, to the maximum distance from the centre to the edge of the foreground, illustrated in fig. 6.1b. For a given finger sample, the algorithm performs as follows:

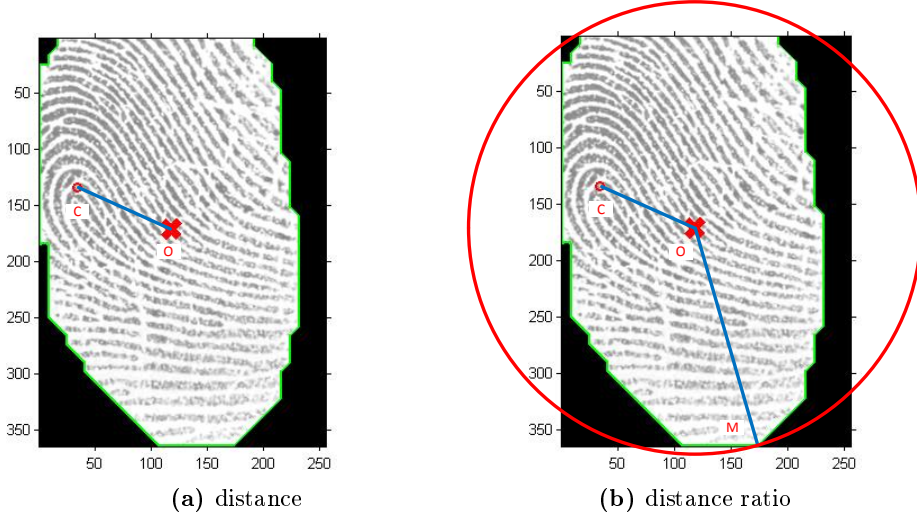


Figure 6.1: Example of distance and distance ratio, where O is the centre of the foreground, C is the position of the core point, and M is the farthest point from the centre to the boundary. The sample is taken from FVC2002DB2 [MMC+02].

1. Obtain the fingerprint foreground by the segmentation algorithm in section 5.3.
2. Localize the position of core point by the algorithm in section 5.2.2 and apply the core-related filters in section 5.4. If there are two cores detected, the midpoint is used as the position of core.
3. The quality score is given by the ratio:

$$Q = 1 - \frac{OC}{OM} \quad (6.3)$$

where OC is the distance from the centre to core, and OM is the maximum distance from the centre to the edge of the foreground.

4. Normalize the quality scores to $[0, 100]$.

The proposed distance and distance ratio are based on the conclusion that the displacements in x and y have the same effect to the comparison score, so the weights for different directions are not required. The conclusion is obtained with prototype databases FVC2000DB2 and FVC2002DB2 [MMWJ02] [MMC+02], which both consist of 880 images and the core points are marked manually.

The similar effect is made although there are different size of height and width, 256 by 364 and 396 by 560 pixels respectively. Figure 6.2 illustrates the effects of displacements both in x and y direction to one of the comparators. The complete observation for three comparators can be found in the appendix A.

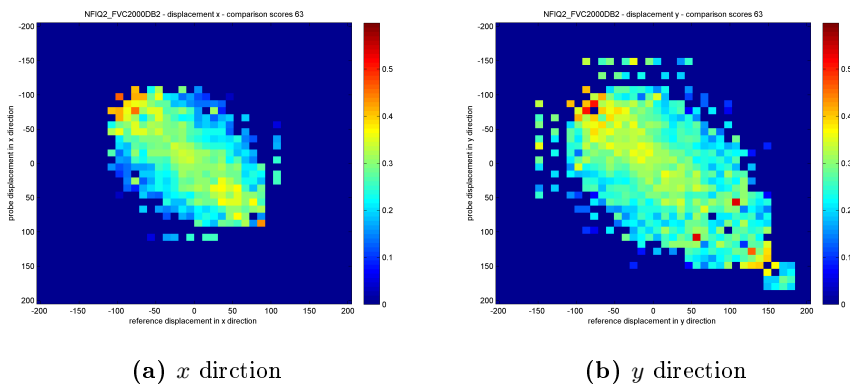


Figure 6.2: The effects of displacements to the genuine comparison scores for FVC2000DB2 using one of the comparators. The value of each block is the mean of the comparison scores within 10 pixels.

The distance ratio consider the area of the foreground, because a high score might be obtained in a large area foreground although the core is far away from the centre. By contrast, the dis only consider the absolute distance. Both two core points might be absent in a fingerprint image, so workaround in this case is to give a low value 0.

6.1.2 Horizontal and vertical distance

Besides Euclidean distance, It is also interesting to observe the effect of displacement in either horizontal or vertical direction, i.e., the length of projection onto x or y axis. For instance, there is a possibility that the second phalanx of finger is also captured in a sample, and thus the vertical dislocation is larger and core points cannot be in the centre of the fingerprint area. As a result, the measurement of displacement in x direction is significant because more fingerprint area is lost with displacement in x direction. Vice versa the same scenario might be existed in the vertical direction. For a given finger sample, quality scores are given given by :

- **Horizontal distance:** the horizontal distance from the centre to the core, depicted in fig. 6.3a.

- **Horizontal distance ratio:** the ratio of the horizontal distance from the centre to the core, to the maximum horizontal distance from the centre to the edge of the foreground, depicted in fig. 6.3b.
- **Vertical distance:** the vertical distance from the centre to the core, depicted in fig. 6.3a.
- **Vertical distance ratio:** the ratio of the vertical distance from the centre to the core, to the maximum vertical distance from the centre to the edge of the foreground, depicted in fig. 6.3b.

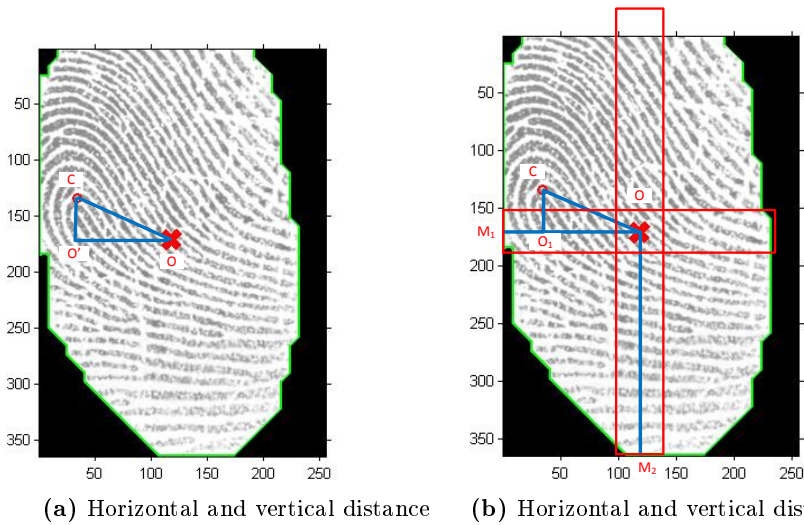


Figure 6.3: Example of horizontal, vertical distance and horizontal, vertical distance ratio, where O is the centre of the foreground, C is the position of core point, OO_1 and CO_1 are the horizontal and vertical distance of OC respectively; M_1 and M_2 is the farthest point from the centre to the edge on horizontal and vertical direction respectively. The sample is taken from FVC2002DB2.

The proposed algorithms perform similarly with distance and distance ratio in section 6.1.1. The position of core point is detected, and the horizontal and vertical distances and ratios are computed, the scores computed by ratios are inverted, and all the scores are normalised to be in $[0, 100]$.

6.2 Orientation-based QMA

The comparison algorithms high likely suffer from the not only displacement but also rotation of the finger sample, i.e., strong rotation might degenerate the biometric performance. ISO/IEC 19794-4:2011 proposes the finger orientation is measured as angle with respect to the horizontal axis from right to the left [ISO12c], depicted in fig. 6.4. The finger orientation generally can be represented by the orientation of core point (one of the cores for whorl type) although there exists minor difference for left and right loop. Therefore, the orientation of core can be proposed as a metric to check if the finger is placed properly without significant rotation.

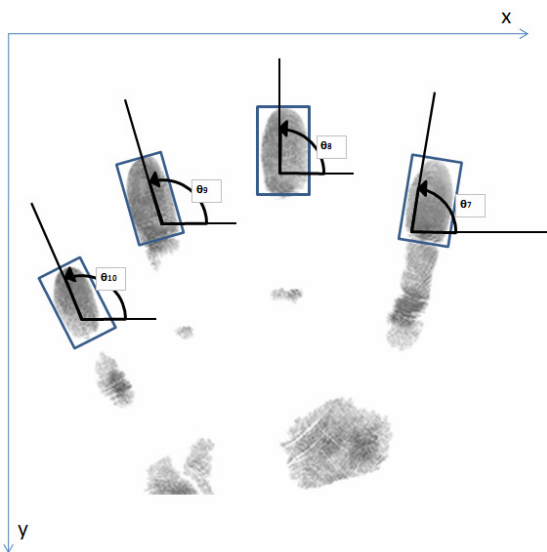


Figure 6.4: Finger orientation, the orientations of fingers (from left to right) are θ_{10} , θ_9 , θ_8 , θ_7 respectively. Taken from [ISO12c].

- **Orientation:** the quality score is given by the rotation of the finger sample. In practice the ideal fingerprints are captured with the orientation $\frac{\pi}{2}$ (fingertip points to the upward). Hence the quality score is highest at $\frac{\pi}{2}$ and decreased along the angle of rotation in fig. 6.5a. The algorithm performs as follows:

1. Obtain the fingerprint foreground by the segmentation algorithm in section 5.3.

2. Localize the position of core point by the algorithm in section 5.2.2 and apply the core-related filters in section 5.4. If there are two cores detected, the core near to the foreground centre is selected to compute the orientation using the method in section 5.2.3.
3. The quality score is given by the orientation, highest score is obtain when fingertip points to the top of image, and scores are decreased symmetrically along with the rotation from left and right side. An example is illustrated in fig. 6.5b:

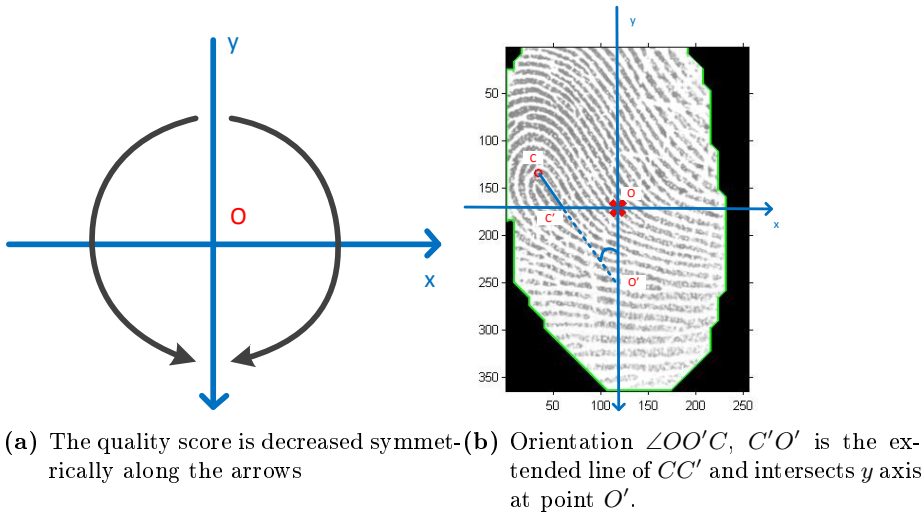


Figure 6.5: Orientation of the fingerprint, the x and y axes are shifted to the centre of foreground O and C is the position of core point, and. The sample is taken from FVC2002DB2.

4. Normalize the quality scores to $[0, 100]$.

The highest value of this metric is selected by the empirical observation that most of the sample is captured upside down (fingertip points to the top of the image). Moreover the ideal orientation can be adjusted according to the database.

6.3 Coherence

Due to the continuity and smoothness of fingerprint ridges, the ridges in a small area usually provide a similar shape so that the sharp orientation changes often

denote low-quality area. The squared gradient can uniquely represent each ridge orientation as the discussion in chapter 4, therefore the coherence as the norm of the sum of orientation vectors divided by the sum of their individual norms can be used to measure the quality of each block [MMJP09].

- **Coherence:** the quality score is given by the mean of the coherence values of all blocks. The algorithm performs as follows:

1. Compute the coherence of each block using eq. (4.13). The example is depicted in fig. 6.6.

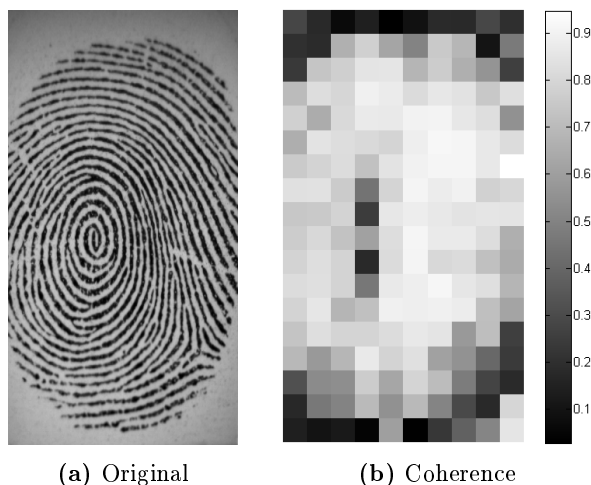


Figure 6.6: Coherence of each 32×32 block, high and low values are map to white and black receptively. The sample is taken from FVC2002DB2.

2. The quality score is given by the mean of the coherence values of all blocks.
 3. Normalize the quality scores to $[0, 100]$.
- **Coherence Segment:** using segmentation, the quality score is given by the mean of the coherence values of foreground blocks. The foreground is segmented by thresholding the variance in 4.13, because the each whole block is required to be maintained, i.e., mathematical morphology might break the desired blocks.
 1. Obtain the fingerprint foreground by the segmentation algorithm in eq. (5.15).

2. Compute the coherence of each block on the foreground using eq. (4.13), the block size is selected as same in segmentation. An example is depicted in fig. 6.7.

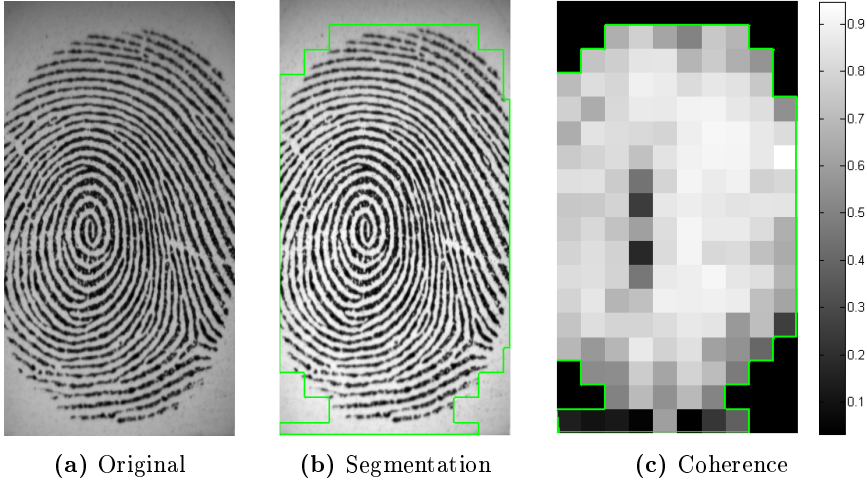


Figure 6.7: Coherence of each 32×32 foreground block which is surrounded by the green lines, and the high and low values are map to white and black receptively. The sample is taken from FVC2002DB2.

3. The quality score is given by the mean of the coherence values of all foreground blocks.
4. Normalize the quality scores to $[0, 100]$.

As for computation, for block i , the coh_i in eq. (4.13) can be computed further by eq. (4.9):

$$coh_i = \frac{|\sum_W (G_{s,x}, G_{s,y})|}{\sum_W |(G_{s,x}, G_{s,y})|} \quad (6.4)$$

where the numerator is given by:

$$\begin{aligned}
\left| \sum_W (G_{s,x}, G_{s,y}) \right| &= \sqrt{\left(\sum_W (G_{s,x}) \right)^2 + \left(\sum_W (G_{s,y}) \right)^2} \\
&= \sqrt{\left(\sum_W (G_x^2 - G_y^2) \right)^2 + \left(\sum_W (2G_x G_y) \right)^2} \quad (6.5) \\
&= \sqrt{(G_{xx} - G_{yy})^2 + 4G_{xy}^2}
\end{aligned}$$

and the denominator is given by:

$$\begin{aligned}
\sum_W |(G_{s,x}, G_{s,y})| &= \sum_W \sqrt{\left(\sum_W (G_{s,x}) \right)^2 + \left(\sum_W (G_{s,y}) \right)^2} \\
&= \sum_W \sqrt{(G_x^2 - G_y^2)^2 + (2G_x G_y)^2} \\
&= \sum_W \sqrt{G_x^4 + 2G_x^2 G_y^2 + G_y^4} \quad (6.6) \\
&= \sum_W \sqrt{(G_x^2 + G_y^2)^2} \\
&= \sum_W G_x^2 + G_y^2 \\
&= G_{xx} + G_{yy}
\end{aligned}$$

In the computation the denominator might be equal to 0 so that the workaround is to ignore the these blocks for computing the mean value. Similarly with orientation certainty level as discussed in section 3.3.3.1, a low value of singular region is given because of the high curvature.

Experimental Setup

This chapter describes the experiment preparations in this thesis. Foremost, the fingerprint sample databases are selected. Furthermore all the empirical parameters of proposed algorithm in chapter 4, chapter 5 and chapter 6 are specified.

7.1 Database selection

In order to conduct the experiments, the databases of fingerprints samples are required.

- **FVC2000DB2:** *Fingerprint Verification Competition* (FVC) 2000 database 2 was collected using low-cost capacitive sensor “TouchChip” by ST Microelectronics [MMWJ02] with 500 dpi resolution. There are 110 fingers and 8 impressions per finger resulting in 880 256 × 364 fingerprints. The examples are illustrated in fig. 7.1.
- **FVC2002DB1:** FVC 2002 database 1 was collected by optical sensor "TouchView II" by Identix with 500 dpi resolution. The 880 388 × 374



Figure 7.1: Example fingerprint images in FVC2000DB2.



Figure 7.2: Example fingerprint images in FVC2002DB1.

pixels images in the same file structure are acquired [MMC⁺02]. The example fingerprint images are depicted in fig. 7.2

- **FVC2002DB2:** FVC 2002 Database 2 was collected by optical sensor “FX2000” by Biometrika with 569 dpi resolution. The 880 296 × 560 pixels images in the same file structure are acquired [MMC⁺02]. The example fingerprint images are depicted in fig. 7.3



Figure 7.3: Example fingerprint images in FVC2000DB2.

- **SD14-BKA-GTD:** ground-truth database of which foregrounds, minutiae, and SPs are identified by the forensic experts in *Federal Criminal Police Office* (BKA) and *CrimeTrac*, based on the *NIST Special Database 14* including 486 832 × 768 pixels off-line inked impression images. All the fingerprints are scanned at 19.7 pixels per mm and examples are depicted in fig. 7.4.
- **MCYT330PB:** a subset of *Ministerio de Ciencia y Tecnología* (MCYT) 330 biomodal Fingerprint subcorpus [OGFAS⁺03]. 330 individuals has

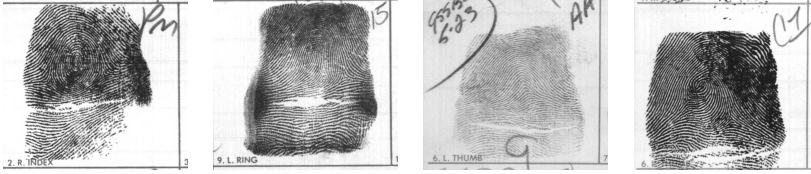


Figure 7.4: Example fingerprint images in SD14-BKA-GTD.

been acquired by a CMOS-based capacitive capture device, model 100SC from Precise Biometrics, with a resolution of 500 dpi. Each individual provides 10 fingers and 12 acquisitions resulting 39600 300×300 pixels fingerprints ¹.

- **MCYT330DP:** the other subset of MCYT 330 biomodal Fingerprint subcorpus [OGFAS+03]. Same file structure are collected with an optical capture device, model UareU from Digital Persona, also with a resolution of 500 dpi. The resolution of images are 296×400 pixels.
- **CASIAFPV5-FULL:** *CASIA Fingerprint Image Database Version 5.0* consist of 20,000 fingerprint images of 500 subjects [oSIoA]. Each finger is captured for 5 acquisitions by URU4000 optical fingerprint sensor with 500 dpi, so that the image resolution is 328×356 . The examples are depicted in fig. 7.5.



Figure 7.5: Example fingerprint images in CASIAFPV5-FULL.

- **CASIAFPV5-SUB:** there is large-scale systematic rotations in CASIA5-FULL where the orientation distribution of finger sample is illustrated fig. 7.6. It is also interesting only to analyse the performance of samples which the finger points to top of the image and thus the samples whose rotation is greater than $\frac{\pi}{4}$ are filtered out. As a result 6603 samples are select in this subset. The full version of distance and orientation distribution for databases can be observed in appendix B.

The small-scale databases FVC2000DB2, FVC2002DB1, FVC2002DB2, SD14-BKA-GTD are used to evaluate the performance of the fist experiment - SP

¹MCYT bimodal database is confidential according to the MCTY-license.

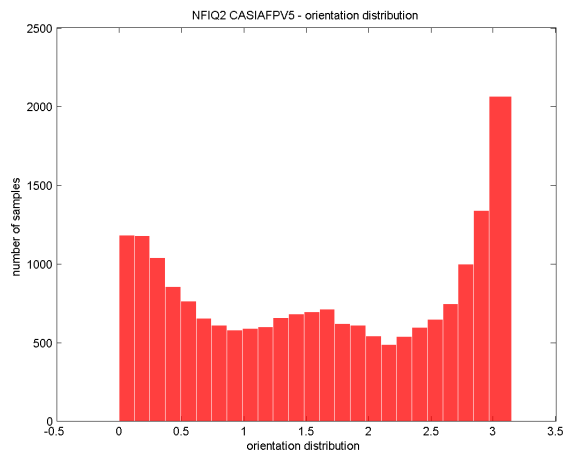


Figure 7.6: Orientation distribution for CASIA-FULL. The orientation is estimated using the Orientation metric in section 6.2. The x coordination refers to the orientation values, i.e., value π and 0 refers to non-rotation and full-rotation.

localization. On the other hand, it make more sense to observe the performance of QMAs for large databases, so MCYT330PB, MCYT330DP, CASIAFPV5-FULL and CASIAFPV5-SUB are adopted.

7.2 Orientation field estimation

This section describes the experiment perpetration for OF estimation, which all the related parameters are specified. The database FVC2000DB2, FVC2002DB1, FVC2002DB2, and SD14-BKA-GTD are used in this part of experiment.

Initially the Gaussian window is adopted to smooth the finger images in order to reduce the influence of the noises [Lin93]. For a 500 dpi image, 2×2 window and $\sigma = 6$ is taken. Then the segmentation and morphological processing described in section 5.3 is applied with 8×8 window and threshold 0.2.

Based on the obtained foreground, the OF is estimated as the foundation of SP extraction. In order to maintain the SP information and reduce the interference of noises, the fingerprint samples can be downsized. Good results are achieved for the 500 dpi images by resizing to the quarter of the original image. Meanwhile

much less computation is requested due to the processing of smaller images.

As mentioned in section 4.2.2, the orientation estimation can be carried out both in pixel and block level. As for the resized images, the pixel-wise computation is selected, as in section 5.2.2 the computation of Poincaré index values requires a cluster of elements to approach 2π and -2π for core and delta respectively, i.e., pixel-wise element can provide more values involved in the computation. As for averaging the orientation for each pixel, the window size 15×15 is empirically selected for 500 dpi image. For SD14-BKA-GTD 25×25 pixels window is taken because of the different resolution and serious noises.

The redundant OF estimation in section 4.2.2.1 can improve the accurateness for larger size element. However, for pixel-wise OF estimation it does not offer dramatical improvement and spend more time. As a result, redundant OF estimation is not applied for pixel-wise element in the experiment.

7.3 Singular point localization

This section describes the experiment perpetration for SP localization, and all the related parameters are specified.

7.3.1 Singular point identification

The fingerprint samples captured by various sensors are intended to be observed. Therefore, SD14-BKA-GTD are selected for inked samples of which the SPs are marked by the fingerprint specialists. FVC2000DB2 is used for capacitive sensors, FVC2002DB1, FVC2002DB2 are used for optical sensors, and the SPs in those databases are identified manually according to the definition in 5.1.

7.3.2 Singular point extraction

Based on the estimated OF, three approaches of SP extraction - conventional Poincaré index, Green's Theorem-based approach and Green's Theorem-based approach and proposed filters are tested to compare the performance.

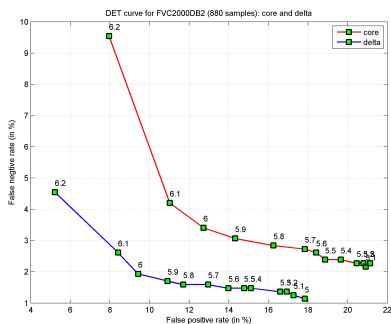
7.3.2.1 Poincaré index

Using the algorithm in section 5.2.1, each 3×3 pixels curve is used to compute the Poincaré index around the central pixel.

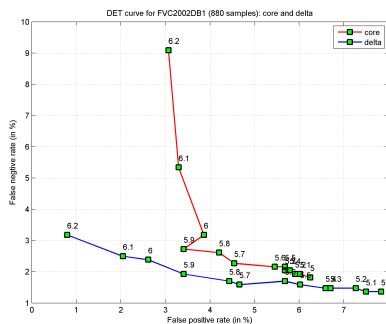
7.3.2.2 Green's Theorem-based approach

As for the Green's Theorem-based approach, a relatively large 23×23 window are applied in the computation of Poincaré index values, so that the commonly spurious core-delta pair can be cancelled out itself by the summation.

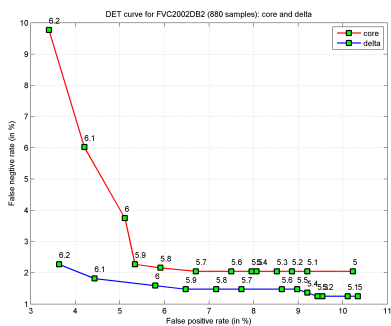
The thresholds are selected by the DET curves in fig. 7.7, which plots the false (false positive) and missed (false negative) detection rate for various thresholds.



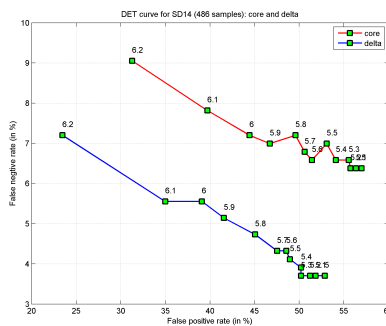
(a) FVC2000DB2



(b) FVC2002DB1



(c) FVC2002DB2



(d) SD14-BKA-GTD

Figure 7.7: DET curves for databases where the thresholds are from 5.0 to 6.2 (step is 0.1).

The principle for selecting is to choose the threshold resulting in the least number of errors (sum of false and missed detection), as a result the thresholds for core and delta are specified in table 7.1.

Database	Core	Delta
FVC2000DB2	6.1	-6.2
FVC2002DB1	5.8	-6.2
FVC2002DB2	5.9	-6.2
SD14-BKA-GTD	6.2	-6.2

Table 7.1: The thresholds of core and delta for each databases

7.3.2.3 Green's Theorem-based approach with proposed filters

As for SP validation, the parameters of proposed filters in section 5.4 are applied to eliminate the spurious SPs. The parameters in each filter are specified in table 7.2.

Database	CCDIS	CCORIDIFF	DDORIDIFF	DCDANGLE
FVC2000DB2	[0, 101]	[0, 1.6]	[0, 0.2]	[1.2, 1.5]
FVC2002DB1	[0, 107]	[0, 1.4]	-	-
FVC2002DB2	[0, 115]	[0, 1]	-	-
SD14-BKA-GTD	[0, 112]	[0, 1.6]	[0, 0.8]	[0.8, 2.6]

Table 7.2: The values of parameters used in proposed pattern-based filter. The DDORIDIFF and DCDANGLE is not required for FVC2002DB1 and FVC2002DB2 because they already possess low false detection rate.

7.4 Proposed QMAs

This section describes the preparation for the second part, QMAs assessment. The computation for the comparison scores, utility scores, and quality scores are explained, as well as the empirical parameters used in the proposed QMAs are specified. In this part, large-scale database MCYT330PB, MCYT330DP, CASIAFPV5-FULL and MCYT330FPV5-SUB are used.

7.4.1 Fingerprint data computation

Three commercial comparison algorithms are used for research purposes which are provided by the industrial vendors. The source of these comparators is confidential so that they are used as black-box to produce the comparison scores in terms of a pair of fingerprint samples. The codenames for these anonymous comparator are called 28, 63 83 which are used in this thesis.

7.4.1.1 Comparison score calculation

Genuine and imposter comparison scores are computed in each database by the three comparators:

- **Genuine comparison scores:** all the genuine comparison (same finger from the different acquisition) are computed.
- **Imposter comparison scores:** 25 imposter comparison scores (different finger) are computed for the large-scale database MCYTPB, MCYTDP, CASIAFPV5-FULL and CASIAFPV5-SUB. All the imposter combinations are selected by random seeds.

7.4.1.2 Utility score calculation

The utility values are computed using comparator 28, 63 and 83, in accordance with ISO/IEC TR 29794-4 [ISO12b] as describe in section 2.4.3.1. They are used as “ground truth” metric for quality, i.e. the correlation coefficients of the quality values with utility are supposed to indicate their dependency on quality and vice versa.

7.4.2 Fingerprint quality estimation

For each finger sample, the quality scores are computed by the reference and proposed QMAs.

7.4.2.1 Reference QMAs

The resultant algorithm of NFIQ introduced in section 3.4.2:

- NIST Finger Image Quality (NFIQ)

Several NFIQ 2.0 candidate quality features introduced in section 3.3.2 :

- Orientation Certainty Level (OCL)
- Frequency Domain Analysis (FDA)
- Gabor (GABOR)
- Radical Power Spectrum (PS)

7.4.2.2 Proposed QMAs

The global SP localization-based approaches proposed in section 6.1 and section 6.2:

- Distance (DIS)
- Distance ratio (DISR)
- Horizontal distance (HDIS)
- Horizontal distance ratio (HDISR)
- Vertical distance (VDIS)
- Vertical distance ratio (VDISR)
- Orientation (ORI)

The local method by measuring the coherence of ridgeline proposed in section 6.3:

- Coherence (COH_x): $x = 16, 32$, i.e., this QMA is assessed with the two size of block, $16 \times 16, 32 \times 32$ pixels.
- Coherence Segment (CS_x): $x = 16, 32$, similarly the QMA is assessed using the $16 \times 16, 32 \times 32$ pixels blocks.

7.4.3 Error versus reject curves

ERC is a visual approach to evaluate the performance of proposed QMAs as explained in section 3.5.1, and empirically the FNMR is set as 0.1 and at most 35% samples are rejected. There might be a variety of QMAs are presented in the same graph, so that it is difficult to compare if they are seriously multiple intersection. In order to improve the readability, the green area under the curve in fig. 7.8 is used to indicate the performance. Therefore, the QMA possesses better performance if the area is in proximity of 0.



Figure 7.8: Example area of ERC curve. For the ease of reading, the area under the curve is enlarged as 100 times. The area in yellow indicates the area of ideal case, and green indicates the area under the QMA curve subtract the ideal area.

7.4.4 Spearman correlation tables

As mentioned in section 3.5.2, the Spearman correlation is the rank correlation which can be used among the QMAs and “ground-truth” utility scores. Furthermore among the QMAs, correlation coefficients with other feature’s values indicate the potential redundancy among the different features. In order to be readable, the correlation matrices are coloured according to the absolute value of the correlation coefficient (darker colour for higher absolute values) and the coefficients are shown multiplied by 100 and rounded.

7.4.5 Utility heatmaps

In order to investigate the effect of displacement on the biometric performance, utility heatmaps are generated according to the position of core points (middle point is adopted if there are two cores) and utility scores. These utility heatmaps can be plotted for comparator 28, 63 and 83 respectively to observe their performance in terms of the displacement of the finger image using the dislocation of core points. In addition, the number of samples in each area is also plotted in order to comprehensively analyse utility heatmaps, i.e., the utility scores are meaningful only if they are averaged by plenty of samples.

7.5 Computation aspects

All the algorithms are implemented in Matlab, and the execution time is tested based on a 3.0 GHz with duo core computer with 4 GB memory. The execution time is computed by averaging the processing time for 100 samples in FVC2000DB2 (256×364 pixels) and the I/O time is included.

Experimental Results

Associated with the previous chapter 7 the experiment is conducted to evaluate performance of OF estimation, SP localization as well as proposed QMAs.

8.1 Orientation field estimation

The OF estimation approach can be carried out in either pixel- or block-wise, and this section presents resultant OF which is estimated in pixel-wise described in section 7.2.

8.1.1 Orientation field estimation assessment

Since no ground-truth database can be used to benchmark the estimation of OF, so several examples are presented. The OF of region of interest (ROI) suffers from the different noises effects, caused large creases, callus, moist or smudges are illustrated:

In fig. 8.1, for the left original finger sample, the OF estimation for ROI is “correct” locally if only the ROI are observed. However, globally the OF estimation

is incorrect because of the interference of large area noises, resulting in spurious core and delta area. For the right sample, the resizing operation can improve the accurateness of OF estimation because the areas of noises are downsized.

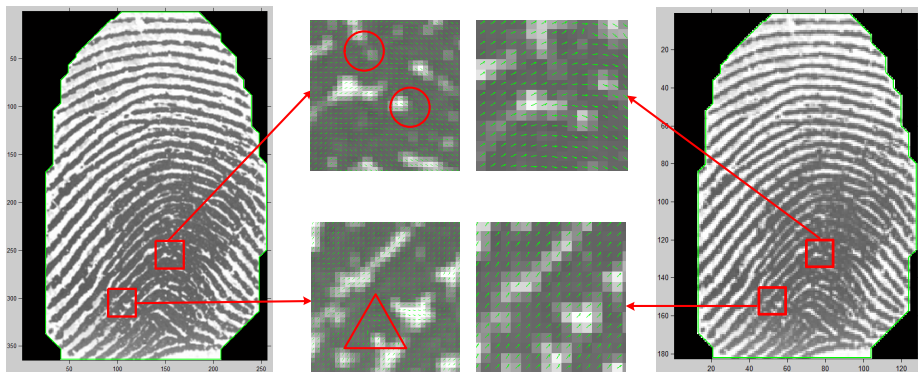


Figure 8.1: Comparison of pixel-wise OF estimation for original (left) and quarter size (right). Squares, circles and triangle refer to ROI, spurious core and delta region. The sample is taken from FVC2000DB2.

Figure 8.2 illustrates the performance of the approach for the detailed area. Although the finger sample is resized as quarter, the approach can still offer accurate OF estimation. The OF of crease of ridgeline is restored by averaging squared gradients, and even though the OF approaching to the boundary can be estimated correctly.

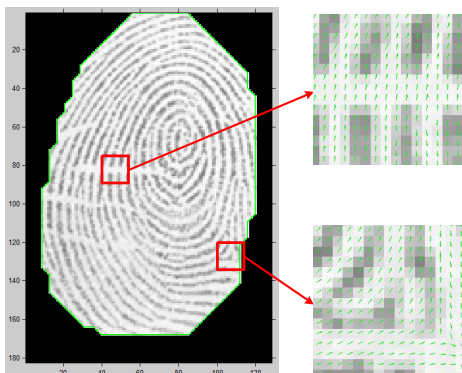


Figure 8.2: Pixel-wise OF for quarter size sample, squares refers to ROI. The sample is taken from FVC2000DB2.

However, the seriously corrupted area cannot be estimated in fig. 8.3 because the ridge-valley structure of ROI and the area around ROI has almost disappeared.

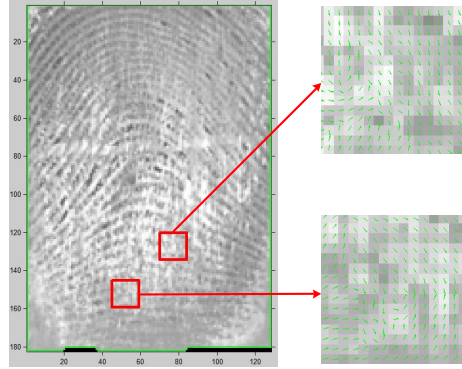


Figure 8.3: Pixel-wise OF for seriously corrupted ridgeline area, the squares refers to ROI. The sample is taken from FVC2000DB2.

8.1.2 Timing

The execution time of OF estimation is tested in pixel-wise for original and quarter size, the execution time is 0.44s and 0.11s respectively. On the other hand, the block-wise estimations with redundant estimation are tested based on the original size, 4×4 , 8×8 and 16×16 pixels take 0.10s, 0.09s, and 0.08s respectively, and. If the redundant estimation is applied with 3×3 pixels window, the execution time are 0.70s, 0.68s, and 0.65s.

Furthermore, the proposed segmentation algorithm requires 0.42s per quarter size sample.

8.1.3 Summary

The approach of OF estimation can provide a accurate OF for the fair quality sample. The resizing operation is applied to resist the interference of large-scale noises, but the OF cannot be estimated for the seriously corrupted area.

As for timing, the approach OF estimation which used in the following SP extraction only takes 0.11s, segmentation takes 0.42 in quarter size.

8.2 Singular point localization

This section presents the result of SP localization based on specified parameters in section 7.3.2.

8.2.1 Singular point extraction assessment

The results of the three approaches, conventional Poincaré index in section 5.2.1, Green's Theorem-based approach in 5.2.2 and Green's Theorem-based approach with proposed filters in section 7.3.2 are presented in following. The performance for core, delta and SP (core and delta) are presently separately. The values of false (false positive) and missed (false negative) detection are computed with regards to the number of samples, i.e., what percent of samples have false or missed detection. For the ease of reading, the percent sign % is omitted in the following tables.

- **FVC2000DB2**

Type	Error	PI	Green	Green & Filters
Core	False	26.7	11.4	6.6
	Missed	7.7	4.8	6.6
Delta	False	29.0	5.3	4.9
	Missed	3.4	4.7	4.8
SP	False	33.5	13.4	9.9
	Missed	11.1	9.0	10.7

Table 8.1: Results of SP localization for FVC2000DB2 (in %).

- **FVC2002DB1**

Type	Error	PI	Green	Green & Filters
Core	False	13.9	6.3	3.0
	Missed	3.4	2.0	3.1
Delta	False	14.6	0.8	0.8
	Missed	3.3	3.2	3.2
SP	PI	24.9	7.0	3.8
	Missed	6.7	5.2	6.3

Table 8.2: Results of SP localization for FVC2002DB1 (in %).

- **FVC2002DB2**

Type	Error	PI	Green	Green & Filters
Core	False	15.9	6.9	3.3
	Missed	4.8	3.0	3.6
Delta	False	18.5	3.5	3.5
	Missed	2.3	2.3	2.3
SP	False	24.6	8.6	5.9
	Missed	7.1	5.3	5.9

Table 8.3: Results of SP localization for FVC2002DB2 (in %).

- **SD14-BKA-GTD:**

Type	Error	PI	Green	Green & Filters
Core	False	58.9	31.3	9.9
	Missed	8.4	9.0	10.5
Delta	False	62.4	23.5	11.3
	Missed	4.7	7.2	9.3
SP	False	66.7	38.5	17.3
	Missed	11.5	14.8	15.0

Table 8.4: Results of SP localization for SD14-BKA-GTD (in %).

The conventional Poincaré index method possesses the worst performance, which in general possesses lower missed rate, but rather higher false detection rate.

In contrast, the Green Theorem-based approach are more robust for the noises, resulting to relatively lower false detection, especially for FVC2002DB1 and FVC2002DB2 (3.8% and 5.9% respectively). The missed detection rate is almost equivalent to conventional Poincaré index method.

By filtering out the spurious SPs by proposed filters, the SPs are validated so that the false detection is further decreased dramatically. Meanwhile the missed detection rate is slightly higher due to the elimination by mistake. A typical case is SD14-BKA-GTD, which the false rate detection is dramatically decreased (from 38.5% to 17.3%), and SPs in only more 0.2% sample are missed.

8.2.2 Timing

The SPs are detected based on the obtained OF (quarter size), and the filters are applied. As a result, Poincaré index and Green's Theorem version takes 1.45s and 0.09s respectively.

8.2.3 Summary

Conventional Poincaré index approach is not noise-resistant, and Green's Theorem-based method is more robust because the spurious core-delta pair can be cancelled out by the summing in the window, depicted in fig. 8.4. To address the high sensitivity and low computation efficiency of conventional Poincaré index approach, the block-wise OF estimation and redundant estimation is suggested to be applied, instead of pixel-wise estimation.

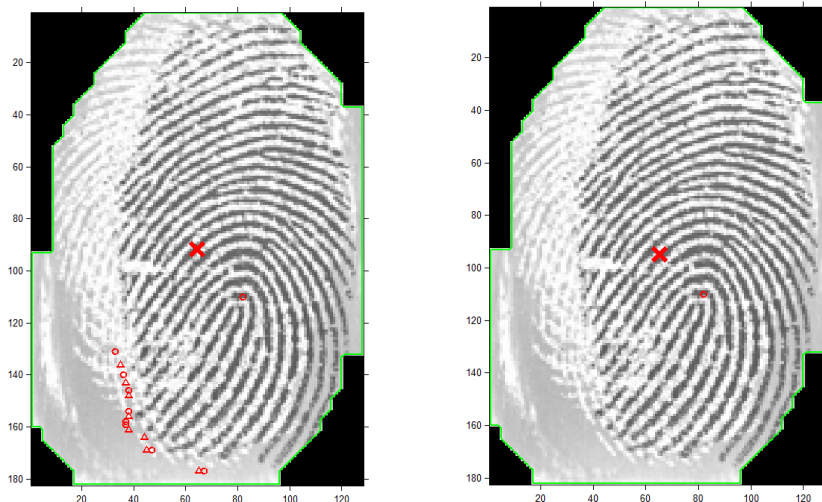


Figure 8.4: Result of SP extraction by conventional Poincaré index (left) and Green's Theorem-based method (right) on the same OF. The circle, triangle and cross refers to the detected core, delta and centre of foreground. A cluster of spurious SPs are detected on the background by conventional Poincaré index method because of the latent fingerprint. The sample is taken from FVC2000DB2.

After applying the proposed pattern-based filters, the performance of SP localization is improved with a beneficial tradeoff, i.e., false detection rate is decreased and missed rate is only slightly higher.

With regards to the existing faults, the type can be classified as follows:

- **Segmentation fault:** The noises (e.g., latent fingerprint and smudge) on the background cannot be eliminated if they have the similar variance with foreground, and thus they might generate false detection.
- **OF estimation fault:** the seriously corrupted ridgeline might leads to the inaccurate OF estimation, which may results in the potential false and missed detection.
- **SP extraction fault:** The structures of SPs are incomplete if they are approaching to the boundary of foreground in fig. 8.5. The squared OF around this type of SP cannot offer the sufficient rotation so that the computed Poincaré index values cannot reach the pre-defined threshold.



Figure 8.5: Incomplete structure of core (left) and delta (right), where the ROI is marked by the squares. The samples are taken from FVC2000DB2.

8.3 Proposed QMAs

The proposed QMAs are analysed by ERC and Spearman correlation and compared with reference methods as described in section 7.4.2.1.

8.3.1 Error versus reject curves

Foremost, ERC visually presents how low quality samples given by proposed QMAs are correlated with ground-truth comparison scores as introduced in 3.5.1. In order to improve readability, the area values under the curves are presented, rather than the various curves, as described in section 7.4.3.

Due to the more than one comparators, the mean of the area vales for the three comparators (28, 62, 83) are given as the results in table 8.5. The full version of ERC can be observed in appendix D.

QMA	MCYT330DP	MCYT330PB	CASIAFPV5 -FULL	CASIAFPV5 -SUB
NFIQ	1.56	1.47	2.26	2.15
OCL	2.58	2.10	2.17	2.00
FDA	1.71	1.91	2.39	2.39
GABOR	2.62	1.99	2.28	2.20
PS	2.14	2.11	2.21	2.00
DIS	2.57	2.41	2.96	2.75
DISR	2.40	2.23	2.95	2.59
HDIS	2.92	2.64	2.89	2.52
HDISR	2.68	2.46	2.87	2.41
VDIS	2.63	2.58	3.03	3.04
VDISR	2.42	2.37	2.98	2.88
ORI	2.81	2.53	2.97	2.71
COH_16	2.58	2.22	2.18	2.01
COH_32	2.52	2.21	2.24	2.07
CS_16	2.47	2.14	2.39	2.34
CS_32	2.47	2.09	2.39	2.36

Table 8.5: The values of area under the ERC curves for large-scale database MCYT330DP, MCTY330PB, CASIAFPV5-FULL and CASIAFPV5-SUB. The values are computed by the mean of the three comparators (28, 63 and 83).

It seems the SP-localization QMAs are not a fair metric for CASIAFPV5-FULL, but the opposite point is obtained for MCYT330DP, MCYT330PB an CASIA-SUB (no-rotation subset of CASIAFPV5-FULL), which means the measurement of displacement and orientation should be based on the prerequisite that no presence of the systematic rotation in the database. The proposed ORI which measures the rotation is also does not have fair performance, also because the orientation for the highest value cannot be determined, i.e., there is no great most sample possess the same orientation depicted in fig. B.4 due to the large-

scale rotation. As a result, it is not meaningful to analyse the experimental results of SP localization-based method for CASIAFPV5.

Among these SP localization-based methods, for MCYT330DP and MCYT330PB, DIS possess the better performance than HDIS and VDIS, which means the displacement on both x and y direction interfere the sample quality for these databases. Furthermore, the vertical displacement has more significant effect than the horizontal one, as the vertical distance distribution has larger scale than the horizontal direction in fig. B.1 and fig. B.2 for MCYT330DP and MCYT330PB.

However for CASIAFPV5-SUB, HDIS possess the best performance whereas VDIS does not offer fair performance, because the height is larger than the width of the foreground depicted in fig. 8.6. DIS is worse than HDIS due to the negative effect of VIDS. Furthermore, all the ratio version of DIS, HDIS and VDIS provide the better performance, which indicated the foreground area should be considered when measuring the displacement.

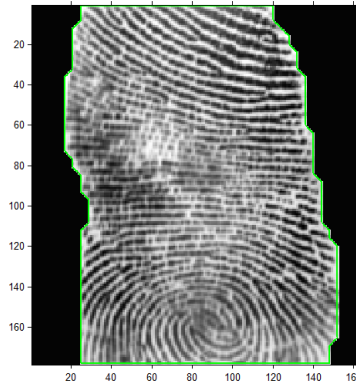


Figure 8.6: The height is larger than the width of the foreground, so that the effect of displacement in vertical direction is not as important as horizontal direction. The sample is taken from CASIAFPV5-SUB.

According to fig. B.1, fig. B.2 and fig. B.4, the ideal case can be determined where the fingertip points to the top of the image, and ORI can be used as a metric to measure the rotation of finger samples.

As a result of proposed SP localization-based QMAs, the displacement and orientation have the effect to the finger sample quality, i.e., large displacement and strong rotation does degenerate the finger sample quality.

Regarding to the proposed local QMAs, COH_x and CS_x has the satisfied

performance which is similar and even better than the reference methods for CASIAFPV5-FULL and CASIAFPV5-SUB. The performance of COH_x is similar with CS_x for MCYT330DP, whereas worth for MCYT330PB, and better for CASIAFPV5-FULL and CASIAFPV5-SUB. With regards to the size of x , the size 16×16 and 32×32 have almost the same performance.

8.3.2 Spearman correlation tables

Spearman correlation table can be used to observe whether two QMAs or QMA and utility scores give the same indication. The correlation with utility cannot fully reflect the scenario of QMA performance, because it is not significantly important to observe the correlation for the entire quality values. In practice at most 35% low quality samples are rejected, i.e., the correlation between high scores cannot indicate the performance of QMA. As a result, It is more interesting to observe the inter-QMA correlation by analysing if they are duplicated or complementary. The full correlation tables for MCYT330DP, MCYT330PB, CASIAFPV5-FULL and CASIAFPV5-SUB are illustrated in appendix E.

8.3.2.1 Inter-QMA correlation

It is reasonable that DIS, HDIS and VDIS are highly correlated with their ratio versions (DISR, HDISR and VDISR), as samples possess the similar foreground area in the same database. DIS is correlated with HDIS and VDIS (43% and 50% in CASIAFPV5-FULL) and HDIS and DIS are not correlated with each other. ORI does not correlated with any QMA. These SP localization-based QMAs are not correlated with the reference methods, which means these proposed metrics measure the quality using the new features.

Unsurprisingly the COH_x and its segmentation version CS_x are correlated, and for both methods $x = 16$ and $x = 32$ give highly similar indication. Furthermore, COH_x and CS_x are extremely correlated with the reference method OCL (98% for COH_32 and 80% for CS_32 in CASIAFPV5), as both give quality scores by measuring the reliability of ridgeline. COH_x and CS_x are also correlated with NIFQ and GABOR (both are 59% with COH_32 in CASIAFPV5-FULL).

8.3.2.2 Correlation with utility

Among all the three comparators, the computed utility scores by 63 are the highest correlated ones with SP localization-based QMAs (11%, 13%, 19% and 18% with DIS in MCYT330DP, MCYT330PB, CASIAFPV5-FULL and CASIAFPV5-SUB) except the ORI, which means the comparison algorithm 63 is the most position-sensitive.

In general, COH_x and CS_x are correlated with utility (44% and 31% between COH_x and utility 28 and CS_x and utility 28 in CASIAFPV5-FULL).

8.3.3 Utility heatmaps

The heatmap is generated according to the position of core point and utility scores as described in section 7.4.5. The full collections for MCYT330DP, MCYT330BP, CASIAFPV5-FULL and CASIAFPV5-SUB are depicted in appendix F.

Take MCYT330PB as an example in fig. 8.7, where each block is 10×10 block. The utility scores for comparator 63 are moderately decreased along with the increase of the displacement both in x and y direction, which means the comparison algorithm 63 is sensitive to the displacement. The utility scores for comparator 83 are slightly decreased especially the core position shifts to the left and bottom side. The high value around the boundary should be ignored because only extremely limited number of samples are computed as the mean of the utility scores, which cannot reflect the average utility score. It seems that the comparator 28 is not displacement-sensitive.

However, the utility map does not offer the same scenario for the CASIAFPV5-FULL, but CASIAFPV5-SUB does, which means the utility scores are interfered not only the displacement but also the rotation. Furthermore, it is reasonable that in CASIAFPV5-SUB, the average scores by comparator 28 and 83 are decreased starting from the coordinate $(0, 50)$ approximately, instead of the foreground centre $(0, 0)$, because as mentioned the height of foreground is larger than the width and thus most of the core points are on the bottom, depicted in fig. 8.8. As a result, the fingerprint in vertical direction is over complete, so that the displacement in horizontal direction is more important than the vertical direction. This point of view verifies the conclusion that HDIS offers the better performance by ERC in section 8.3 in CASIAFPV5-SUB.

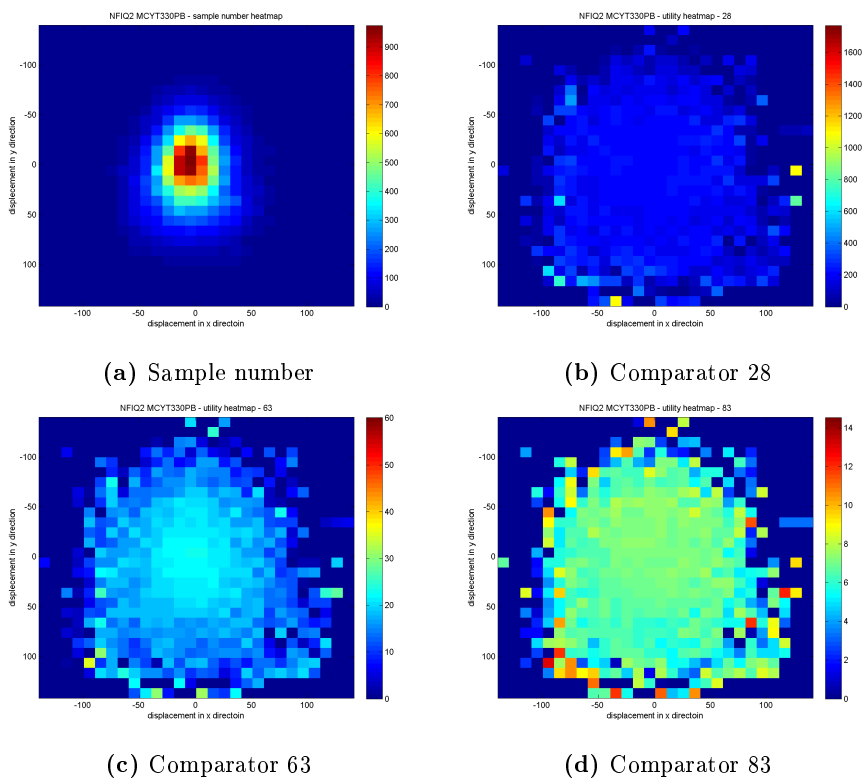


Figure 8.7: Number of samples and utility maps for MCYT330PB. Each block is 10×10 pixels, and the value of each block is the mean of the utility scores.

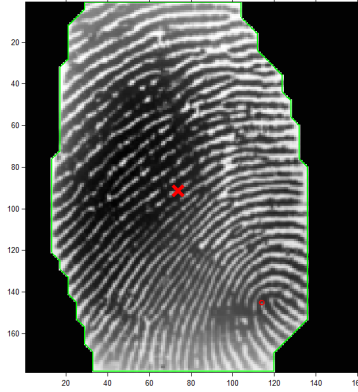


Figure 8.8: The core position of sample, which is lower than the centre of the foreground. The cross and circle refer to the centre of foreground and detected core. The sample is taken from CASIAFPV5-SUB.

8.3.4 Timing

The execution time for proposed QMAs are listed in table 8.6.

QMA	Execution time
NFIQ	0.16
OCL	0.08
FDA	0.18
GABOR	0.22
PS	0.06
SP localization-based	0.66
COH_16	0.02
COH_32	0.01
CS_16	0.12
CS_32	0.04

Table 8.6: Execution time for proposed QMAs (in s), where the quality measurement results of DIS, DISR, HDIS, HDISR, VDIS, VDISR and ORI can be obtained at once in SP localization-based approach.

Although the SP localization-based QMAs takes 0.66s which is higher than the reference methods, seven results of QMAs for measuring the distance and orientation of SP can be obtained. On the other hand, the COH_x and CS_x possess the much less execution time than the reference methods.

8.3.5 Summary

Foremost the SP localization-based QMAs are interfered by presence of large-scale systematic rotation. In the other words, the measurement of displacement and rotation is meaningful when they have similar orientation.

It is reasonable that the performance of SP localization-based QMAs provide slightly worse performance than the reference methods because each metric only measure one global property via one or two SPs, which hardly offer sufficient information for measuring the quality of fingerprints comprehensively. By contrast, most QMAs measure fine level characteristics (e.g., ridgeline, frequency and minutiae).

However, the slightly worth performance cannot be a reason to reject the measurement of property (displacement and orientation) of SPs because they are complementary to the reference methods with low correlation values.

In accordance with correlation tables with utility and utility heatmaps, the performance among different comparators are obtained that comparator 63 is sensitive to displacement and 28 is not. Although comparator 28 is not sensitive to displacement, the large dislocation degenerated the performance of comparison algorithm by the results of ERC.

As for COH_x and CS_x, the window size 32×32 pixels can be selected because almost the same result is obtained. Furthermore, theoretically it make more sense to measure the coherence when there are at least two ridges existed and less execution time is required. COH_x and CS_x offer extremely similar indication with the reference method OCL, and thus they can be considered to substitute OCL due the the less execution time.

It leaves an open question whether segmentation should be applied, because the contradicted results are obtained between the different databases. Hence, segmentation is recommended to the reference methods and the performance for more databases are expected to be observed.

Conclusion

The first task of this thesis is to propose a systematic singular point localization approach. Plenty of approaches are investigated for orientation field (OF) estimation and singular point (SP) extraction. The OF is estimated in pixel-wise for downsized finger sample, furthermore the SPs are extracted using Green's theorem-based approach. Most spurious SPs can be eliminated by the proposed segmentation algorithm. In addition, the five proposed pattern-based filters improve the correctness effectively.

Based on the proposed SP localization approach with the accepted error rate, the second task is to propose Quality Measurement Algorithm (QMA) to analyse the importance of SPs, which is possibly to be considered as Fingerprint Image Quality (NFIQ2.0) features [NIS12] and incorporated in ISO/IEC TR 29794-4 [ISO12c].

Because of the better performance of detection and the characters, the core point are used as a landmark to measure the displacement and orientation of fingerprints. Seven SP localization-based global QMAs are proposed to verify the significance of SP.

The QMA experiment is based on the large-scale databases and evaluated by Error versus Reject Curves (ERC) and Spearman correlation table. The conclusion is obtained that the large displacement and strong rotation does degenerate

the biometric performance, although it is not as profoundly important as influence of the other fine features such as ridgeline, frequency and minutiae. The low correlation with the reference QMAs means these SP-localization QMAs are complementary by measuring different features. Furthermore the quality measurements by these metrics are meaningful without presence of the large systematic rotation.

Additional conclusion is obtained that among the three comparators (28, 63 and 83), comparator 83 is the most position-sensitive, i.e., the biometric performance is degenerated along with the increase of the dislocation from the foreground centre. Even though for the least sensitive comparator 28, ERC indicates the biometric performance still suffers from the large displacement and large rotation. The two research goals are achieved as described in .

Beside the research goals, two local QMAs, coherence (COH) and coherence segmentation (CS) are proposed by analysing the coherence of the ridgeline. COH and CS have the slightly better performance with the reference QMAs in NFIQ 2.0 and much less execution time.

In summary, the measurement for the displacement and orientation of finger sample are suggested to be applied in case of the presence of large dislocation and strong rotation. Moreover, practically the proper placement can be easily achieved by the capture device which can offer the exact slot to guarantee the mentioned properties.

9.1 Future work

The pattern-based filters eliminate spurious SPs based on the assumption the certainty of detected SPs are uniform distributed from the centre of foreground to the boundary. The methods are suggested to be proposed for determining the reliability of the extracted SPs by measuring the features of detected singular regions. Moreover, the alignment or classification can be applied before the SP localization in order to apply more constraints, such as the position of core should not be much lower than the delta for the aligned finger sample and there are at most one core and one delta in the loop fingerprint.

In this thesis the importance of SP in biometric system is investigated. However, the significance in each procedure of comparison (e.g., alignment and classification) is not indicated due to the close-source of the comparator. This unknown factors allows to specified further to observe how does SP have the influence to the biometric performance.

It is ambiguous whether the segmentation in QMAs can improve the performance of quality prediction. The segmentation can be applied to the existing approach in NFIQ 2.0 and the result for more databases are suggested to be observed. Meanwhile, the area and degree of the noises also might be considered.

APPENDIX A

Effect of Displacement to Comparison Scores

Effects of displacement to the genuine comparison scores is illustrated using comparison algorithm 28, 63 and 83. The value of each block is the mean of the comparison scores within 10×10 pixels.

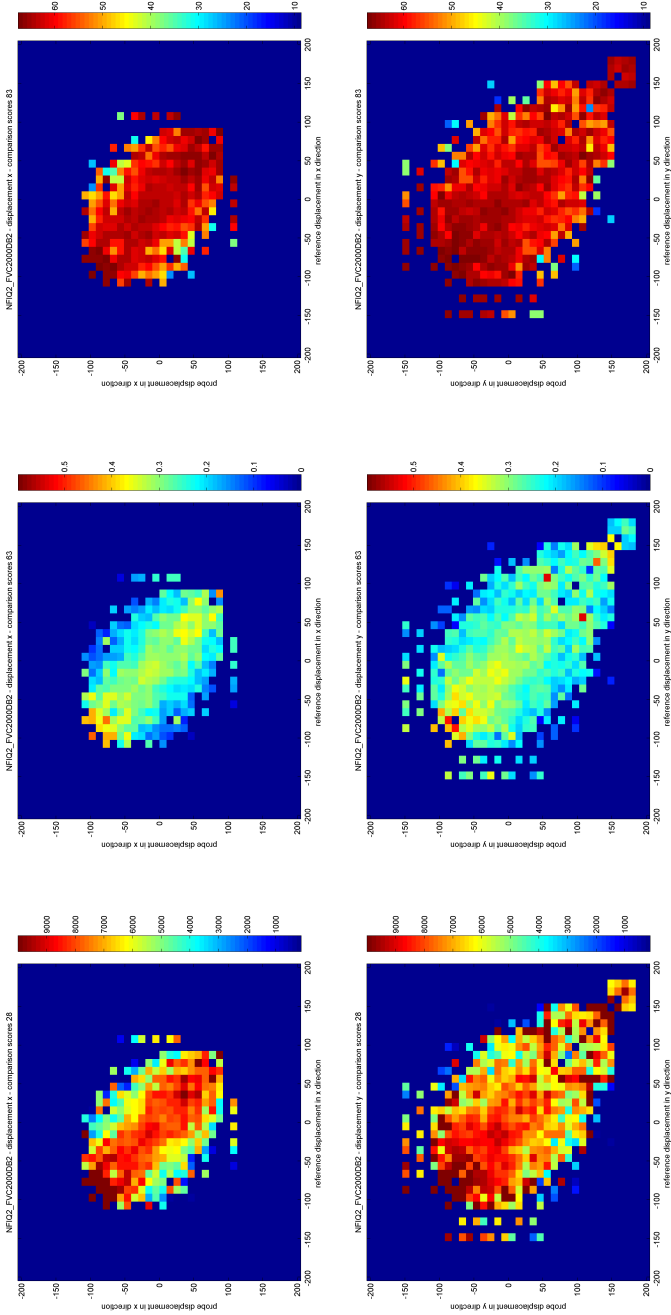


Figure A.1: The effect of displacement to FVC2000DB2 in x direction (top) and y direction (bottom) by comparator 28, 63, 83 (left to right).

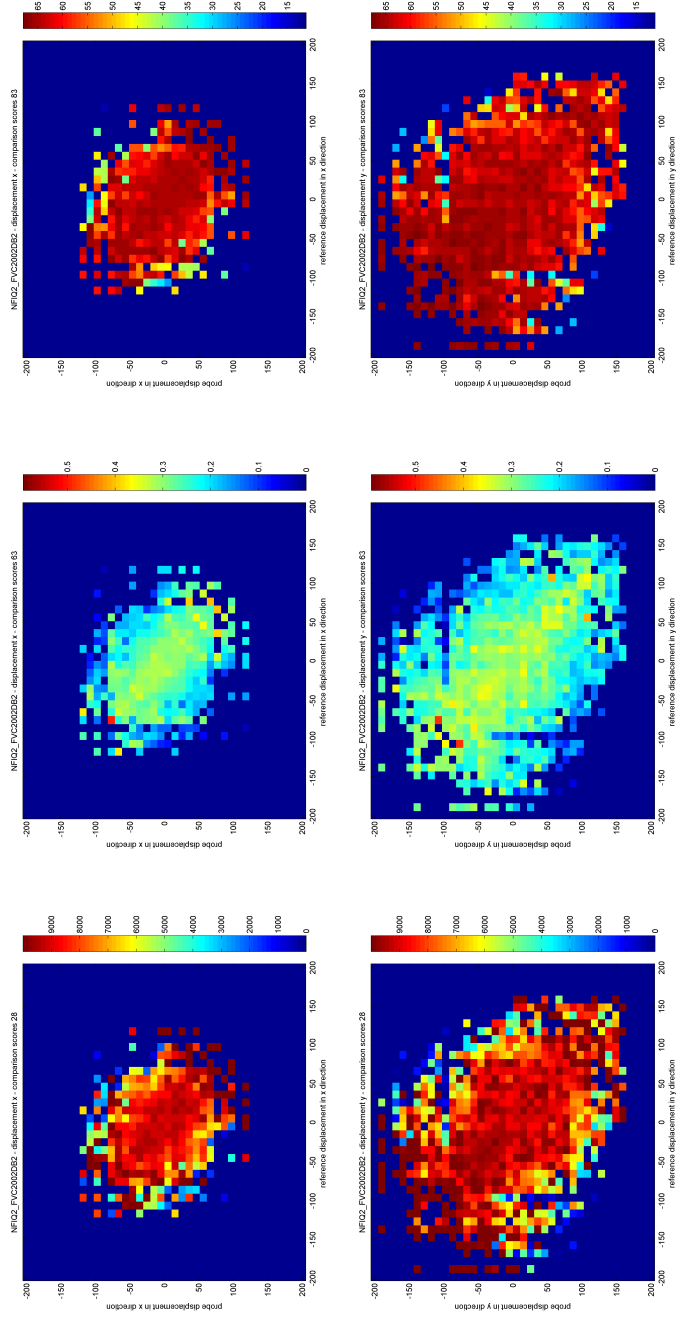
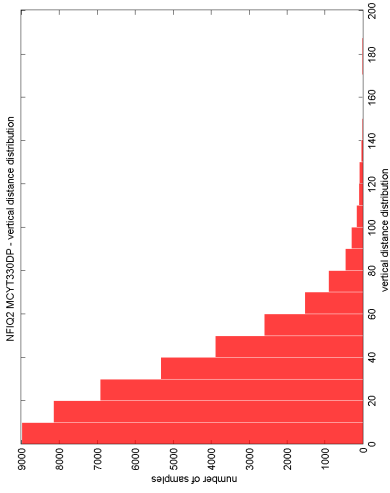


Figure A.2: The effect of displacement to FVC2002DB2 in x direction (top) and y direction (bottom) by comparator 28, 63, 83 (left to right).

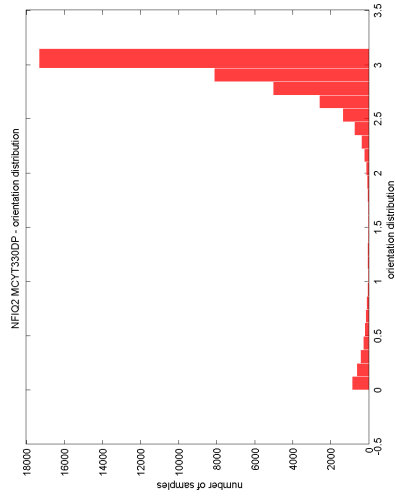
APPENDIX B

Distance and Orientation Distributions

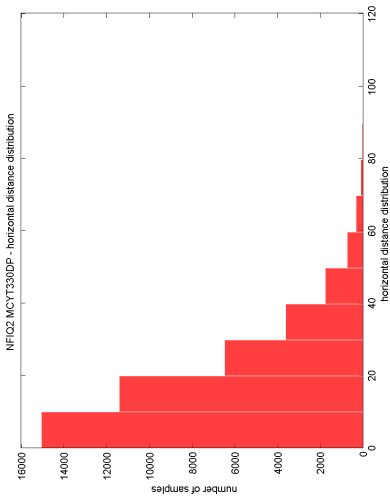
The distance and orientation distribution for MCYT330DP, MCYT330PB, CASIAFPV5-FULL and CASIAFPV5-SUB. In orientation distribution, π and 0 refer to the fingertip points to the top and bottom of images.



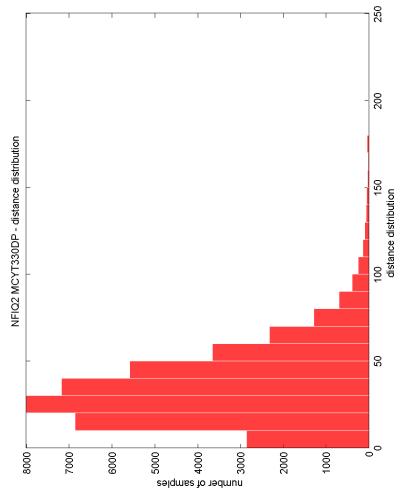
(b) Vertical



(d) Orientation

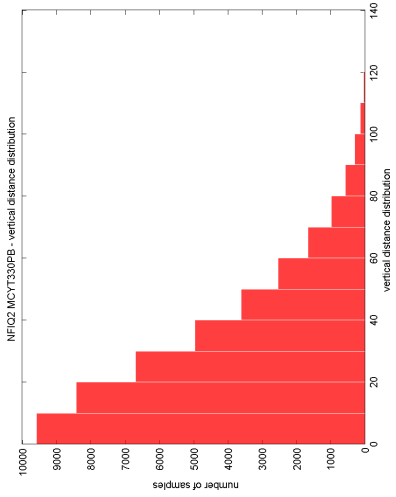


(a) Horizontal

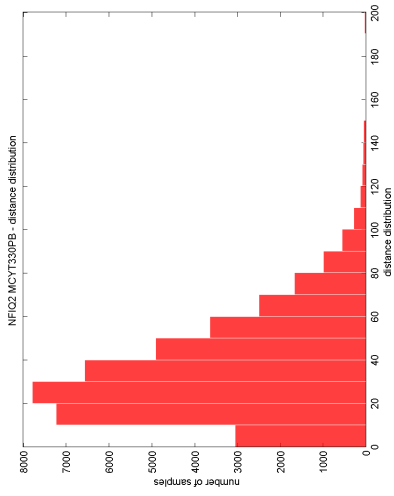


(c) Euclidean

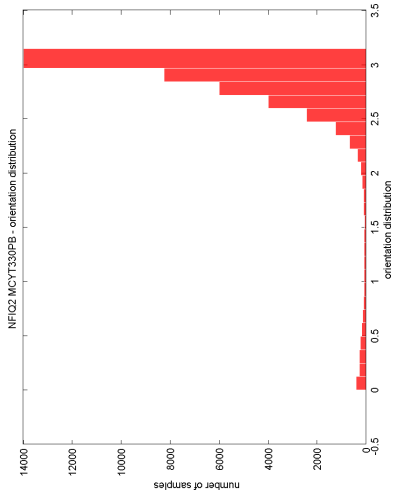
Figure B.1: Distance and orientation distributions for MCYT330DP.



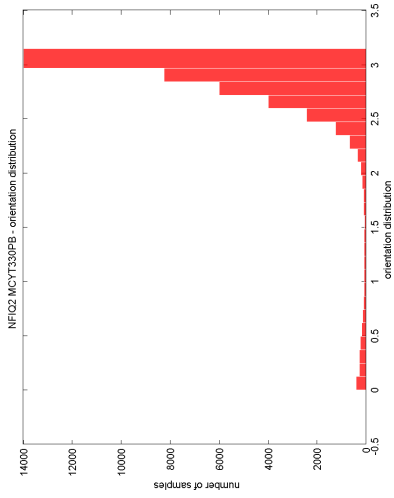
(a) Horizontal



(b) Vertical

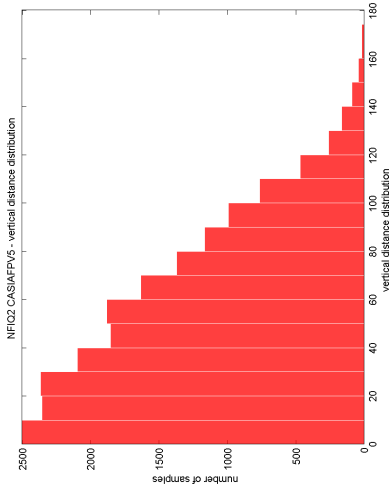


(c) Euclidean

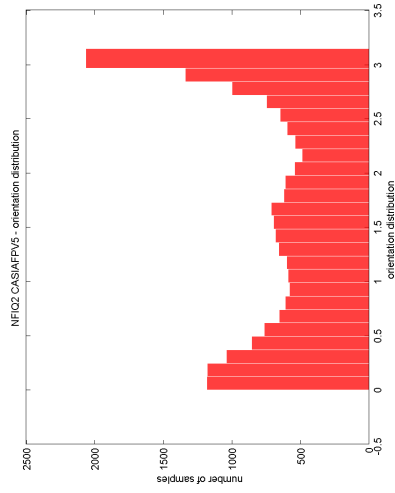


(d) Orientation

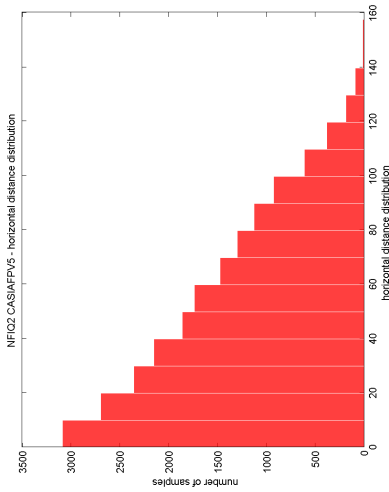
Figure B.2: Distance and orientation distributions for MCYT330PB.



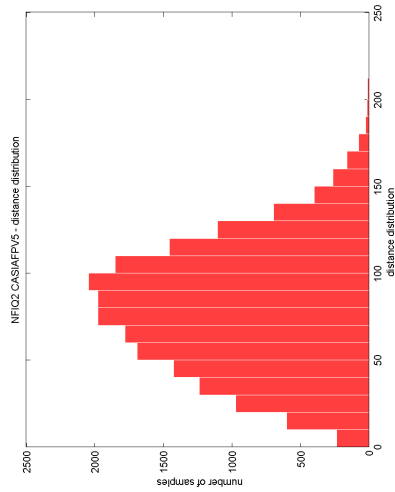
(b) Vertical



(d) Orientation

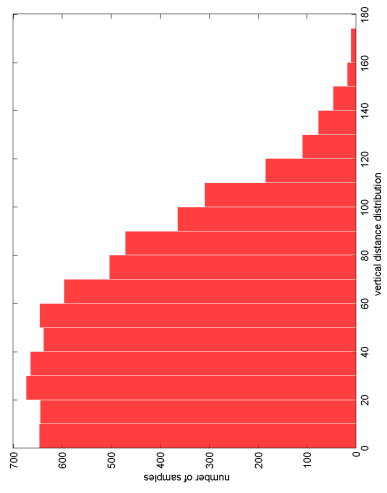


(a) Horizontal

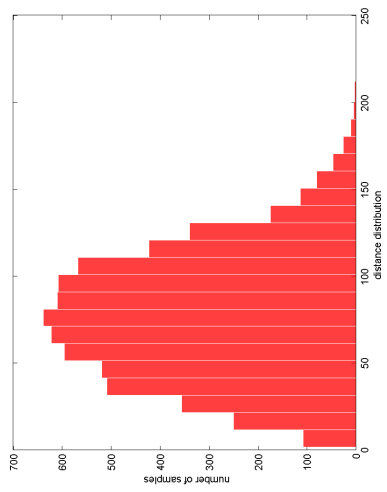


(c) Euclidean

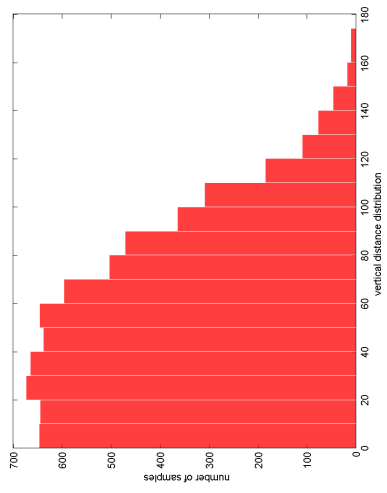
Figure B.3: Distance and orientation distributions for CASIAFPV5-FULL.



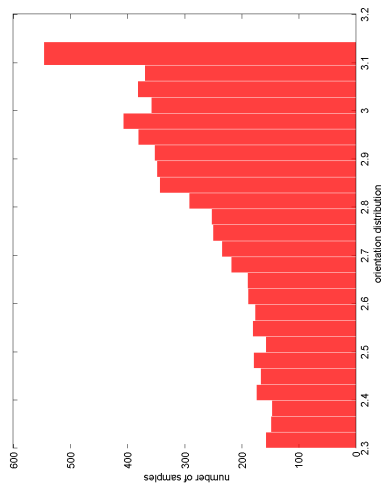
(a) Horizontal



(c) Euclidean



(b) Vertical



(d) Orientation

Figure B.4: Distance and orientation distributions for CASIAFPV5-SUB.

APPENDIX C

Comparison Scores Distribution

Genuine and imposter comparison scores distribution for MCYT330DP, MCYT330PB, CASIAFPV5-FULL and CASIAFPV5-SUB by comparator 28, 63 and 83.

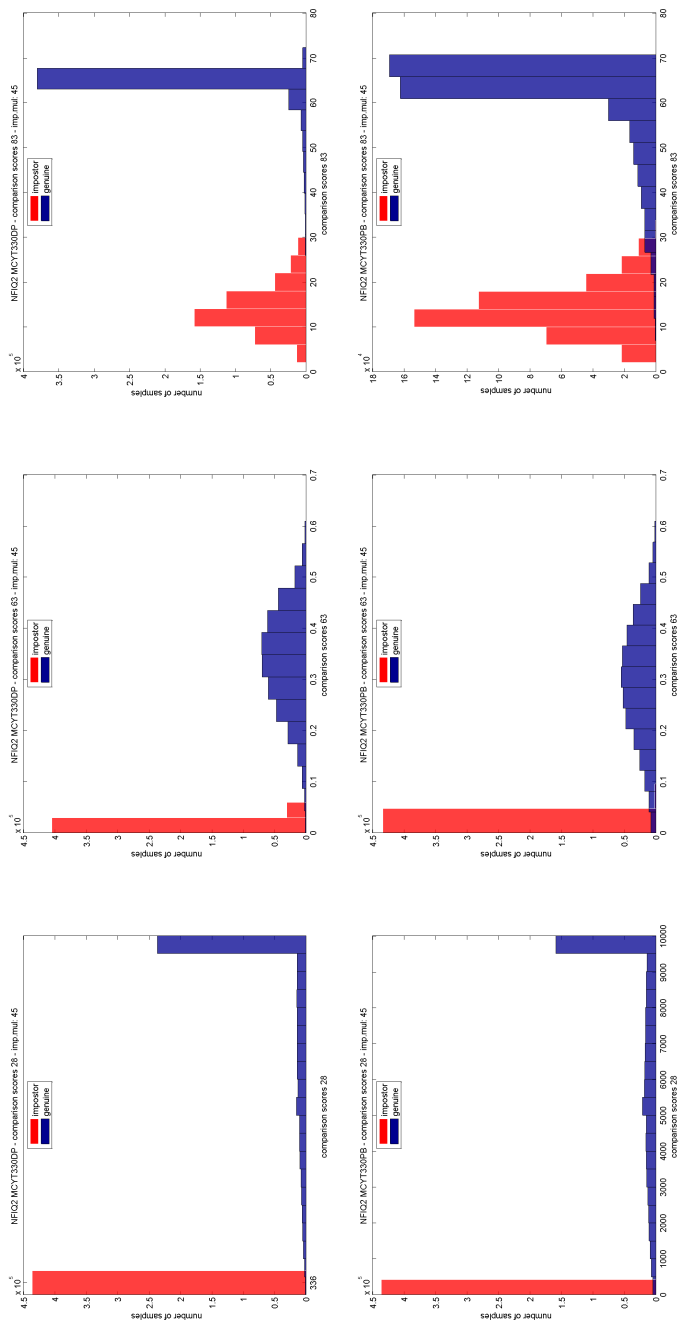


Figure C.1: Comparison scores for MCYT330DP (top) and MCYT330PB (bottom) computed by comparator 28, 63, 83 (left to right).

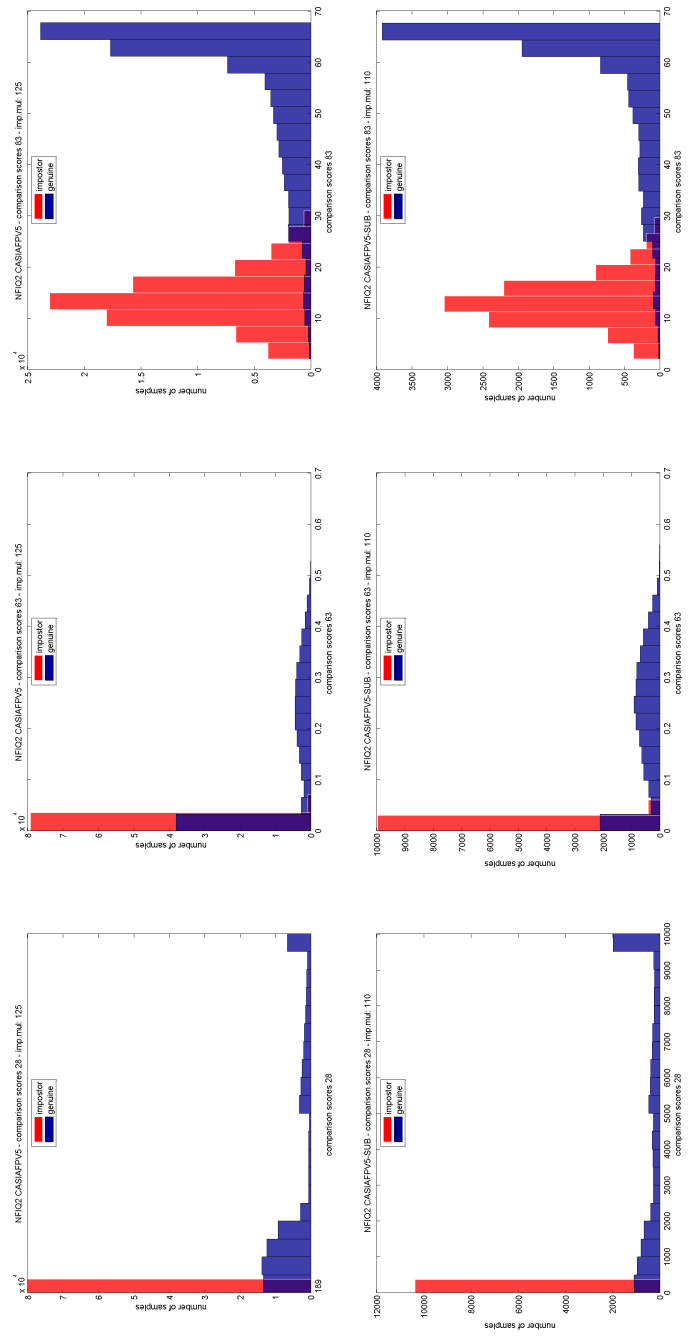


Figure C.2: Comparison scores for CASIAFPV5-FULL (top) and CASIAFPV5-SUB (bottom) computed by comparator 28, 63, 83 (left to right).

APPENDIX D

Error versus Reject Curves

ERC for the references QMAs (NFIQ, OCL, FDA, GABOR, PS) and Proposed QMAs (DIS, DISR, HDIS, HDISR, VDIS, VDISR, ORI, COH_16, COH_32, CS_16, CS_32) and utility (utility_28, utility_63, utility_83) in MCYT330DP, MCYT330PB, CASISFPV5-FULL and CASIAFPV5-SUB by comparator 28, 63, 83

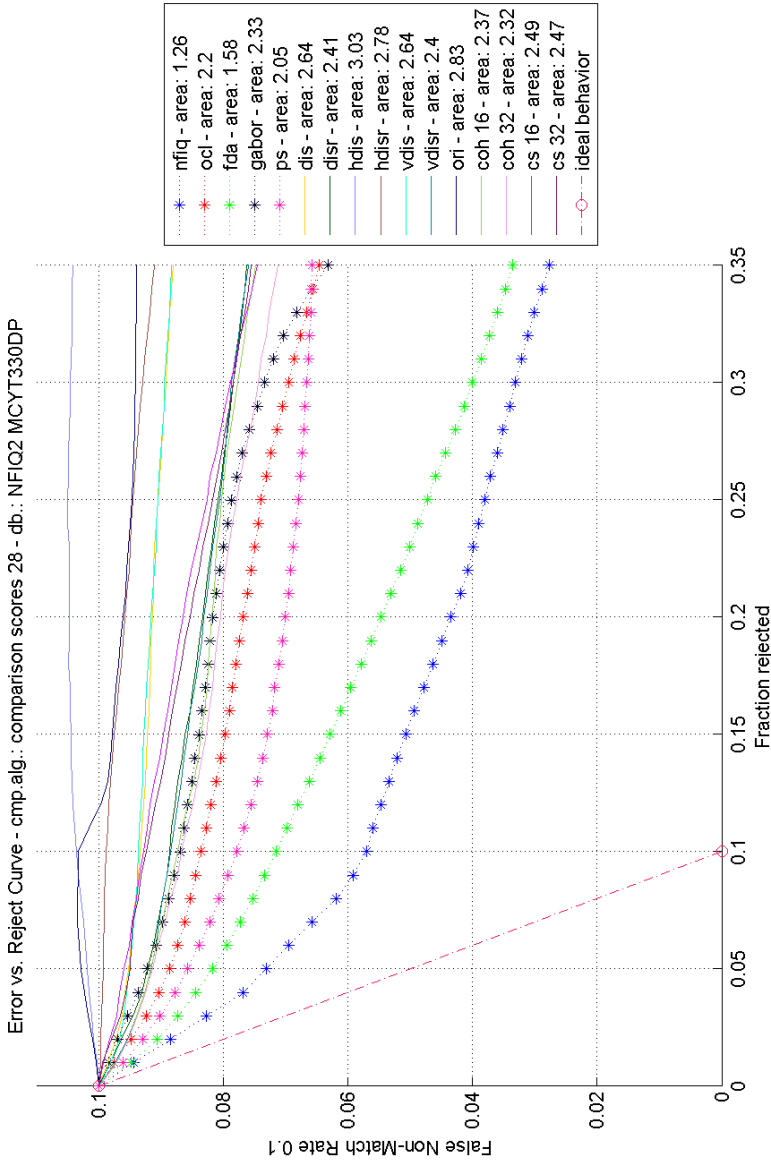


Figure D.1: ERC for MCYT330DP by comparator 28

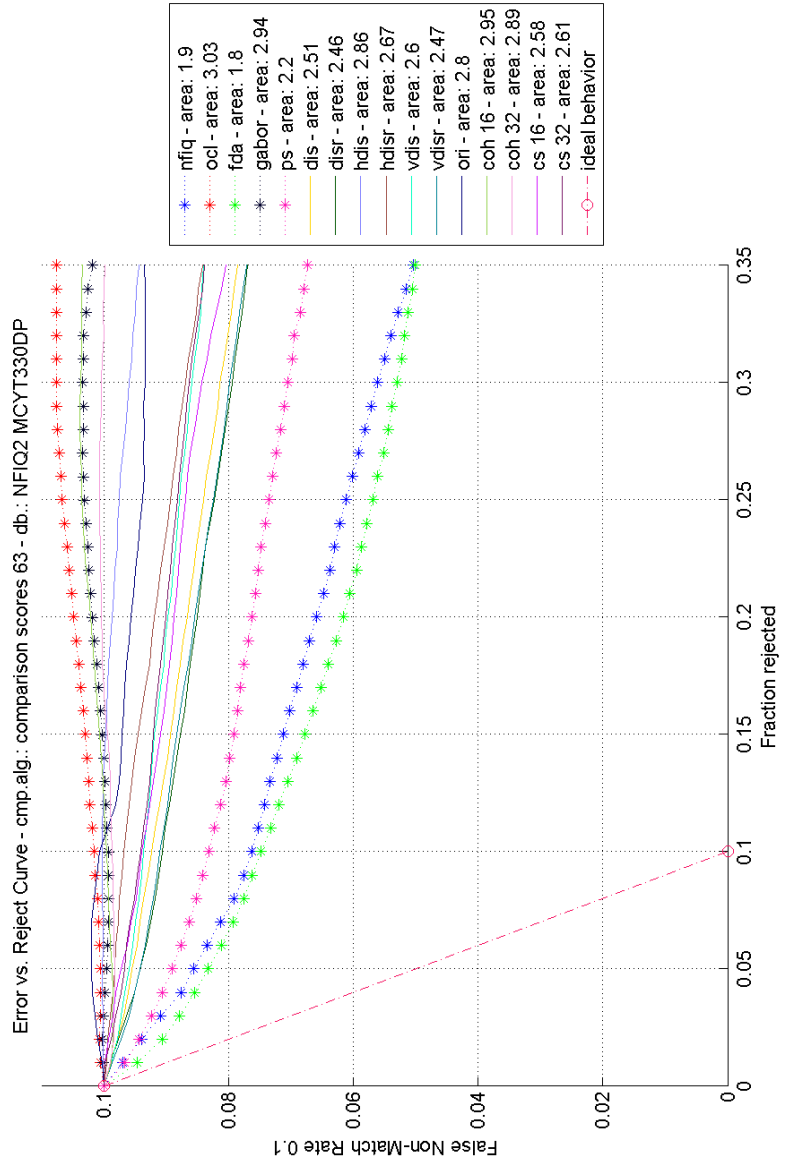


Figure D.2: ERC for MCYT330DP by comparator 63

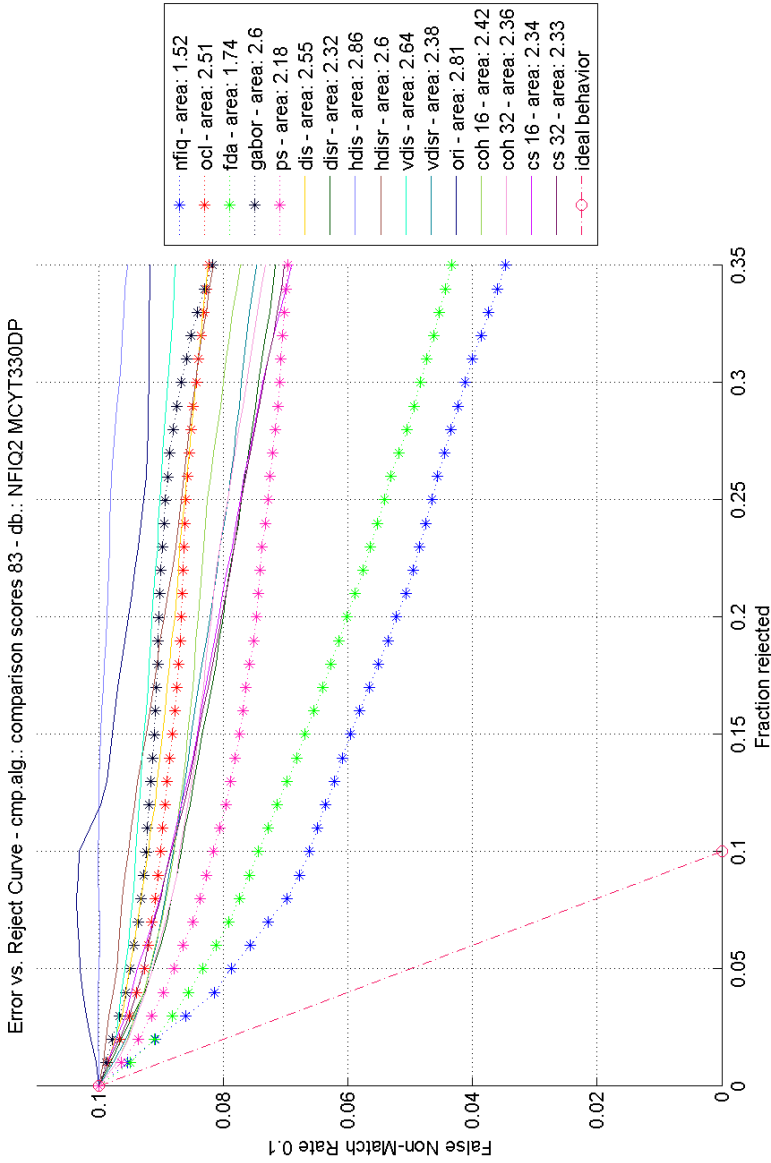


Figure D.3: ERC for MCYT330DP by comparator 83

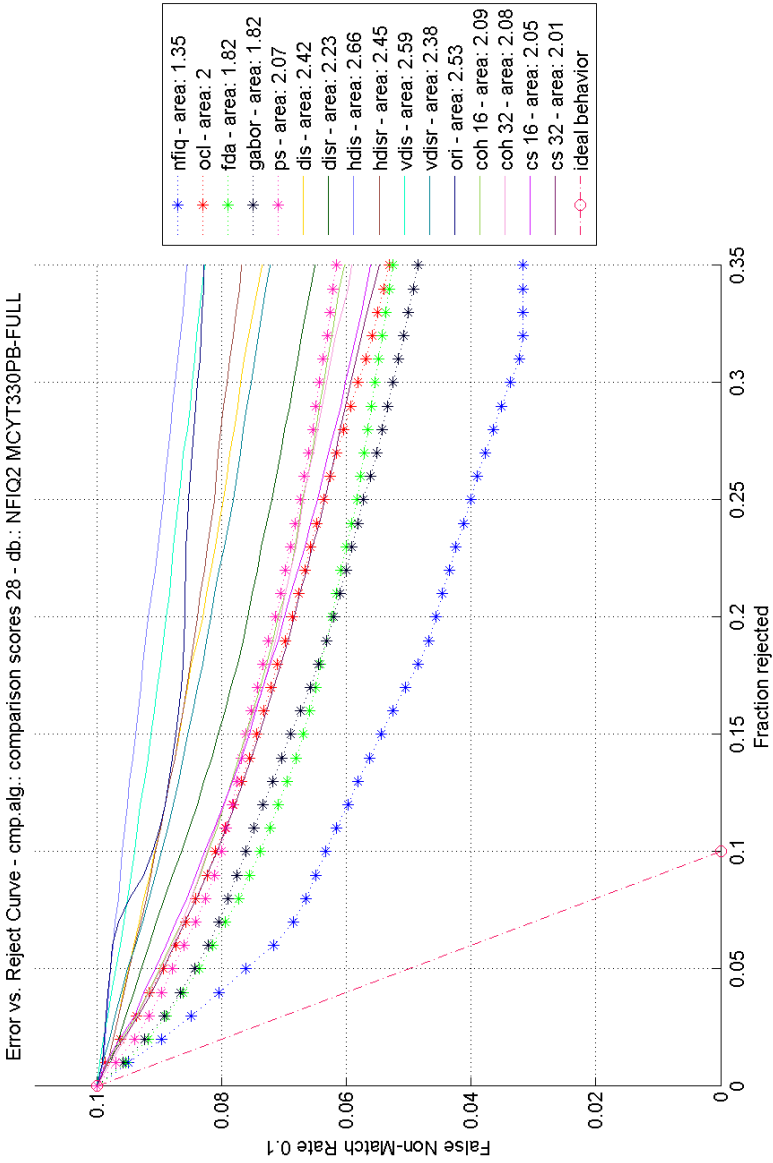


Figure D.4: ERC for MCYT330PB by comparator 28

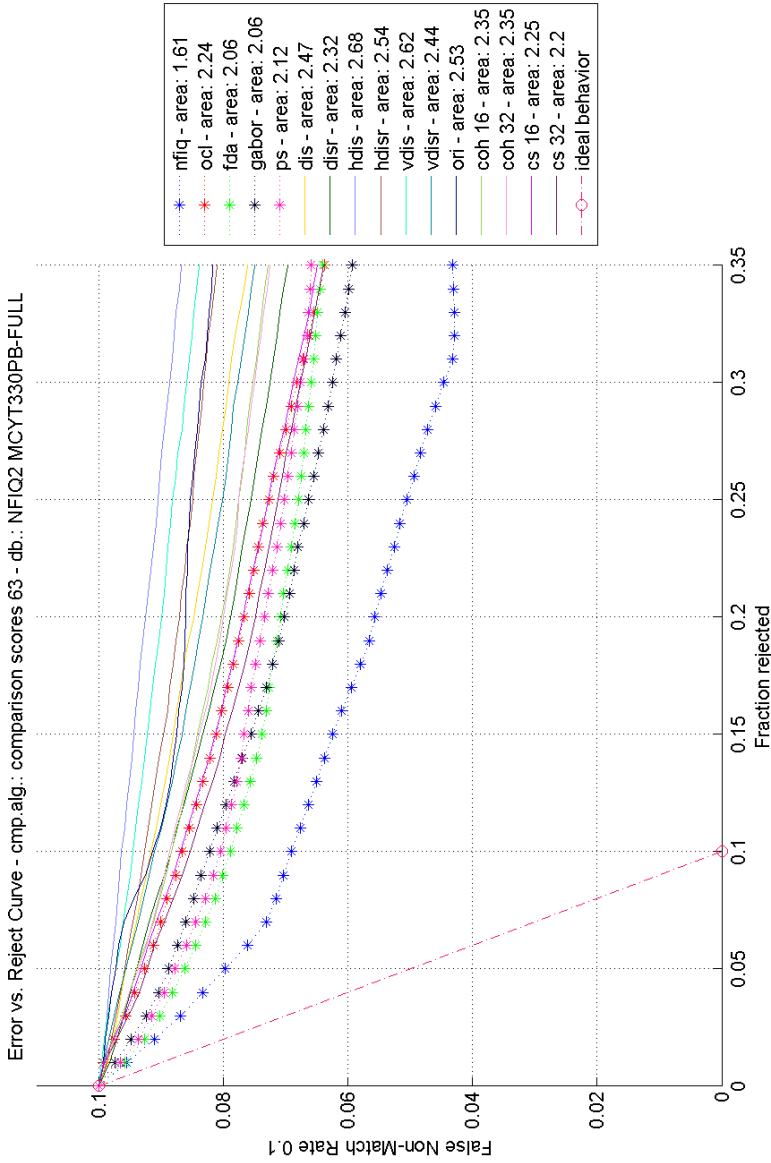


Figure D.5: ERC for MCYT330PB by comparator 63

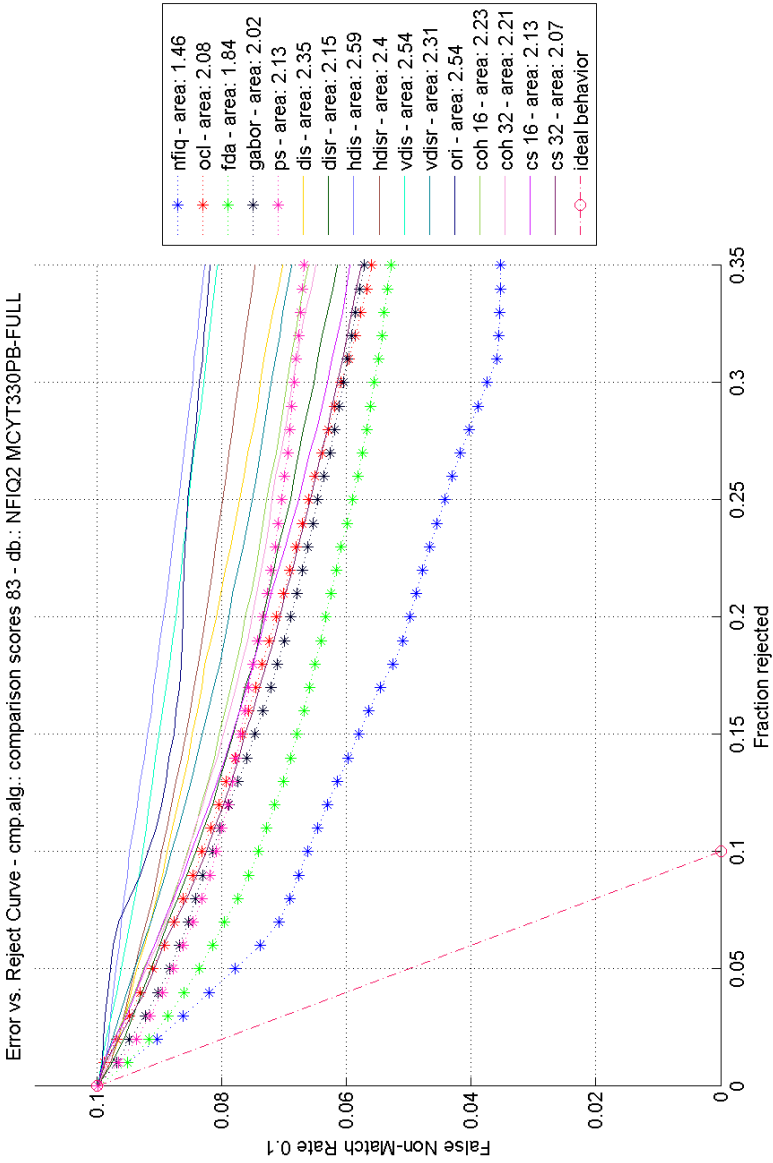


Figure D.6: ERC for MCYT330PB by comparator 83

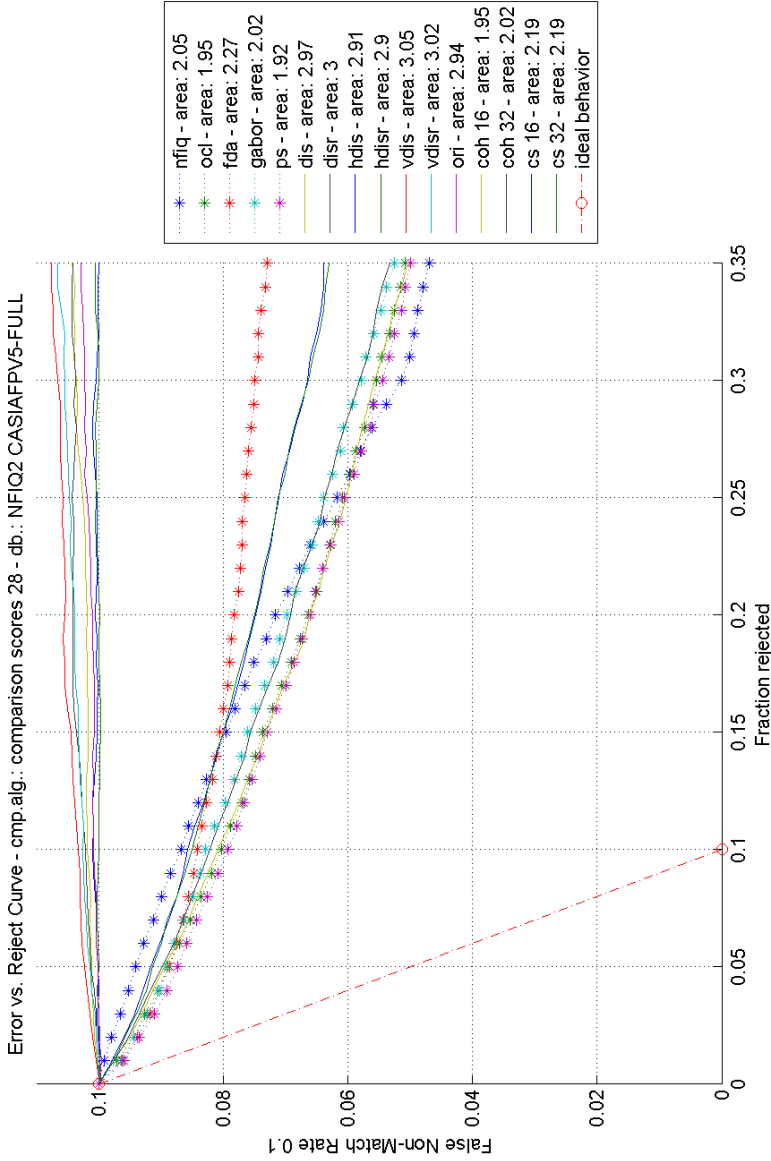


Figure D.7: ERC for CASIAFPV5-FULL by comparator 28

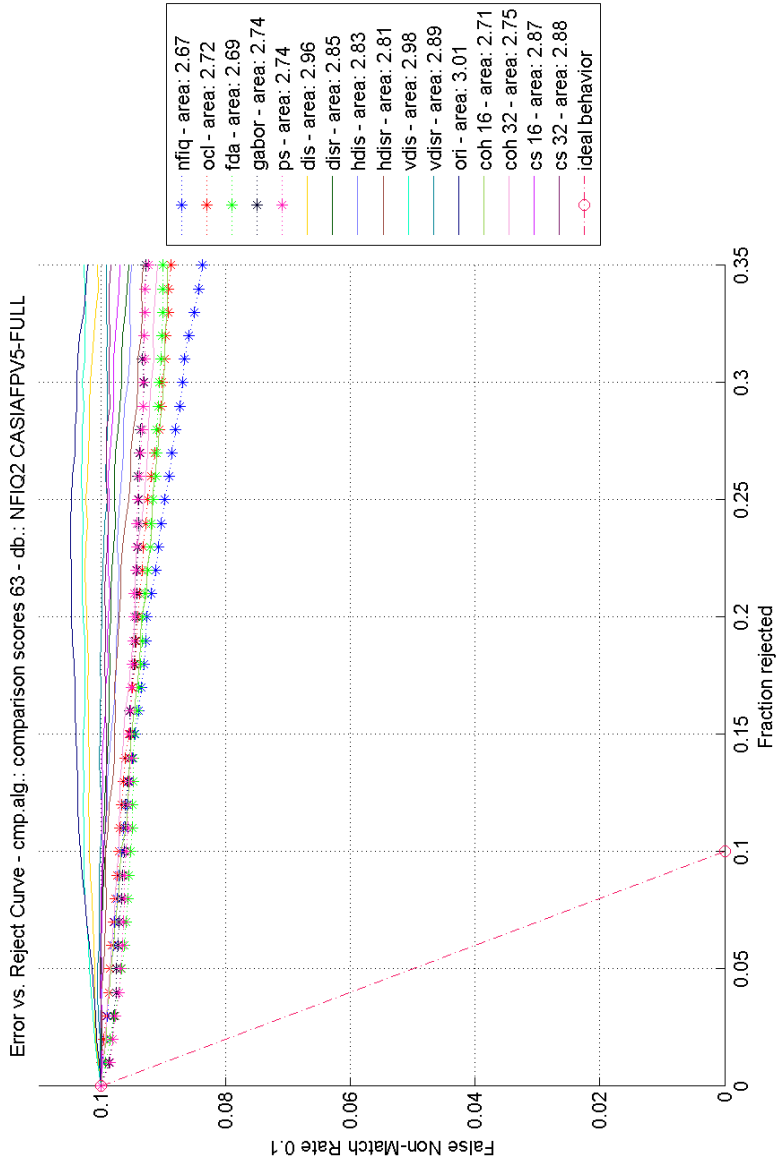


Figure D.8: ERC for CASIAFPV5-FULL by comparator 63

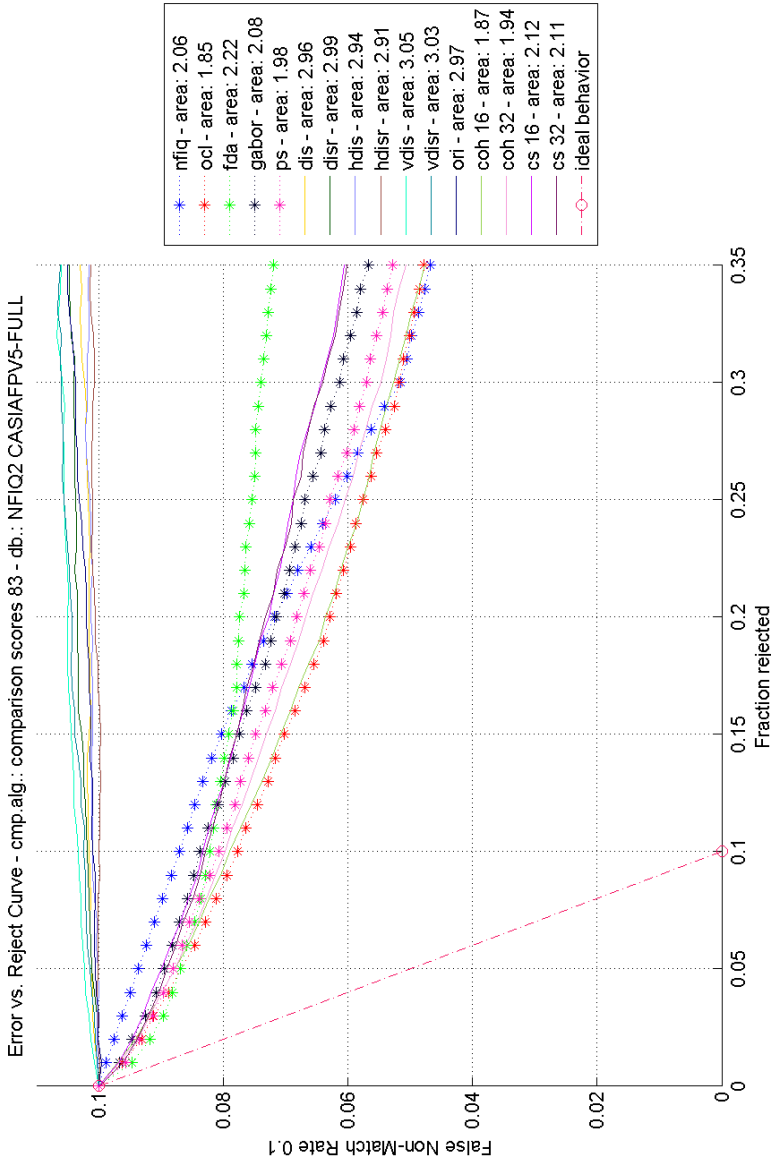


Figure D.9: ERC for CASIAFPV5-FULL by comparator 83

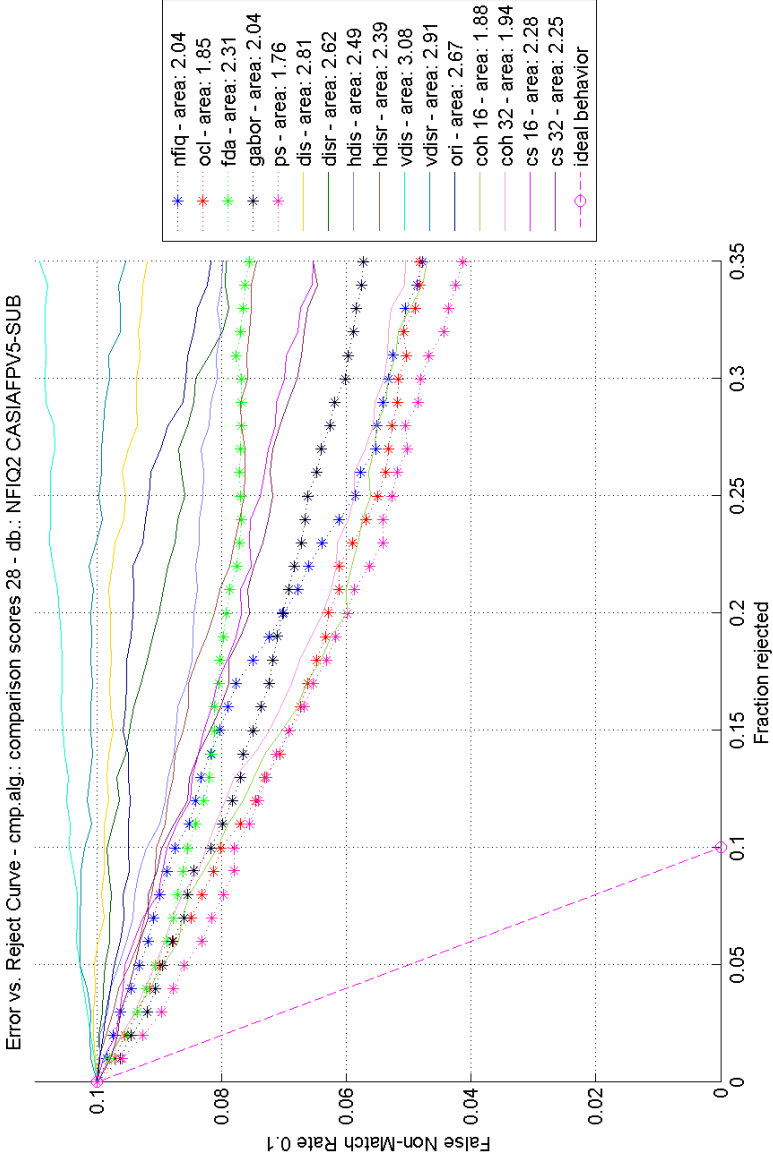


Figure D.10: ERC for CASIAFPV5-SUB by comparator 28

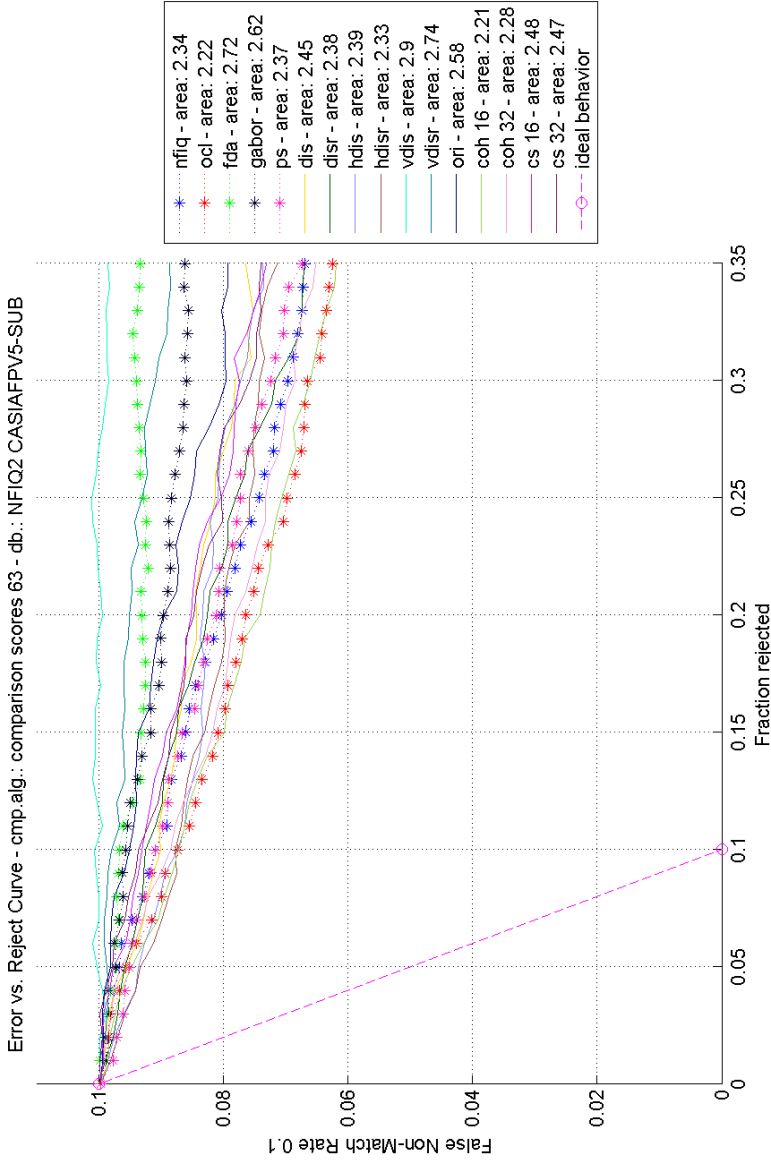


Figure D.11: ERC for CASIAFPV5-SUB by comparator 63

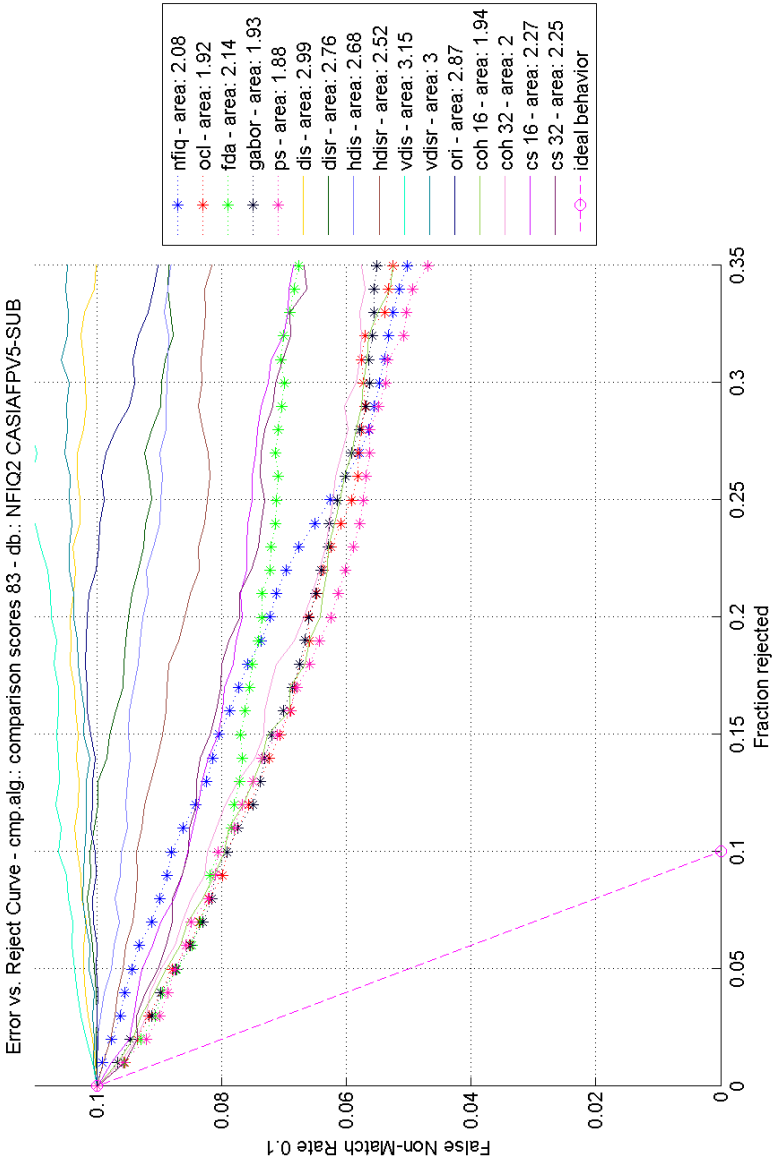


Figure D.12: ERC for CASIAFPV5-SUB by comparator 83

APPENDIX E

Spearman Correlation Tables

Spearman correlation tables for MCYT330DP, MCYT330PB, CASIAFPV5-FULL and CASIAFPV5-SUB using the references QMA_s (NFIQ, OCL, FDA, GABOR, PS) and Proposed QMA_s (DIS, DISR, HDIS, HDISR, VDIS, VDISR, ORI, COH_16, COH_32, CS_16, CS_32) and utility (utility_28, utility_63, utility_83).

nfiq	100	25	46	26	20	1	5	5	-6	-1	5	7	7	-1	32	34	34	35	34	34	29	9
oci	25	100	14	79	-34	-13	7	-3	3	3	-12	1	7	77	75	48	30	26	30	48	-14	31
feda	46	14	100	26	38	1	2	-10	-4	8	8	8	-10	22	25	24	22	22	24	40	40	13
gabor	26	79	26	100	-3	-14	3	-7	0	-11	0	0	-2	60	59	16	11	11	16	46	-8	29
ps	20	-34	38	-3	100	4	-3	-9	-6	10	5	5	-16	-38	-32	-9	-9	-9	-11	9	32	1
dis	1	-13	1	-14	4	100	96	43	42	82	80	-2	-2	-9	-8	5	7	7	5	-4	13	-10
disr	5	7	2	3	-3	96	100	43	44	77	81	1	9	9	9	9	10	10	9	3	8	-5
hdis	-6	-3	-10	-7	-9	43	43	100	99	1	2	2	5	0	0	5	5	5	5	-12	-1	-11
hdisr	-1	3	-4	0	-6	42	44	99	100	1	2	3	3	6	7	5	5	5	5	-8	0	-9
vdls	5	-12	8	-11	10	82	77	1	1	100	98	-5	-5	-11	-10	5	3	5	3	3	16	-5
vdlsr	7	1	8	0	5	80	81	2	2	98	100	-3	-3	2	2	7	6	7	6	8	12	-1
ori	-1	7	-10	-2	-16	-2	1	5	3	-5	-3	100	11	11	11	13	14	13	14	-4	-10	-1
coh_16	32	77	22	60	-38	-9	9	0	6	-11	2	2	11	100	99	62	67	62	67	27	-13	13
coh_32	34	75	25	59	-32	-8	9	0	7	-10	2	11	11	99	100	65	70	65	70	26	-11	11
cs_16	35	26	22	11	-9	7	10	5	5	5	7	13	13	62	65	100	96	100	96	9	7	-3
cs_32	34	30	24	16	-11	5	9	5	5	3	6	14	14	67	70	96	100	96	100	9	3	-3
utility_28	34	48	40	46	9	-4	3	-12	-8	3	8	-4	-4	27	26	9	9	9	9	100	45	66
utility_63	29	-14	40	-8	32	13	8	-1	0	16	12	-10	-10	-13	-11	7	3	7	3	45	100	32
utility_83	9	31	13	29	1	-10	-5	-11	-9	-1	-1	-1	-1	13	11	-3	-3	-3	-3	66	32	100

Figure E.1: Spearman correlation table for MCYT330DP

ntfq	100	53	53	39	31	12	13	8	10	9	9	6	49	51	49	51	39	48	28
ocl	53	100	41	48	31	10	11	8	10	6	7	7	84	86	95	92	29	30	17
fda	53	41	100	38	33	9	9	6	7	6	6	5	38	40	34	40	36	32	23
gabob	39	48	38	100	87	-2	1	-4	0	1	2	-3	63	63	50	55	47	30	29
ps	31	31	33	87	100	0	1	-2	1	2	2	-2	50	48	35	42	34	24	17
dis	12	10	9	-2	0	100	99	55	54	81	80	4	2	3	8	8	6	19	5
disr	13	11	9	1	1	99	100	54	54	80	81	3	6	6	9	9	7	20	6
hdis	8	8	6	-4	-2	55	54	100	99	14	14	7	1	2	7	7	2	13	2
hdisr	10	10	7	0	1	54	54	99	100	14	14	5	5	6	8	8	3	13	3
vdls	9	6	6	1	2	81	80	14	14	100	100	0	2	2	5	5	5	14	4
vdlsr	9	7	6	2	2	80	81	14	14	100	100	0	4	4	6	6	6	14	5
ori	6	7	5	-3	-2	4	3	7	5	0	0	100	3	3	7	6	-1	6	-1
coh_16	49	84	38	63	50	2	6	1	5	2	4	3	100	99	87	90	28	23	15
coh_32	51	86	40	63	48	3	6	2	6	2	4	3	99	100	87	91	28	23	15
cs_16	49	95	34	50	35	8	9	7	8	5	6	7	87	87	100	97	29	29	17
cs_32	51	92	40	55	42	8	9	7	8	5	6	6	90	91	97	100	30	29	16
utility_28	39	29	36	47	34	6	7	2	3	5	6	-1	28	28	29	30	100	72	72
utility_63	48	30	32	30	24	19	20	13	13	14	14	6	23	23	29	29	72	100	62
utility_83	28	17	23	29	17	5	6	2	3	4	5	-1	15	15	17	16	72	62	100

Figure E.2: Spearman correlation table for MCYT330PB

nflq	100	63	40	61	49	49	-2	1	3	3	-6	-2	62	59	39	42	50	16	39
oci	63	100	33	62	48	48	6	4	2	2	-2	0	98	98	78	80	48	14	39
fda	40	33	100	53	36	36	-23	-9	-5	-5	-12	2	33	29	5	8	32	10	21
gabor	61	62	53	100	75	75	-17	-10	-2	-2	-14	-1	63	59	38	41	51	8	34
ps	49	48	36	75	100	100	3	9	6	8	-10	-1	48	43	25	27	49	12	33
dis	-2	6	-23	-17	3	3	100	91	43	41	50	48	6	6	12	11	4	9	5
disr	1	4	-9	-10	9	9	91	100	46	48	41	47	3	2	-2	-2	8	14	6
hdis	3	4	-9	-4	6	6	43	46	100	99	-10	6	3	3	0	0	5	11	2
hdisr	3	2	-5	-2	8	8	41	48	99	100	-10	5	1	0	-5	-4	6	11	2
vdls	-9	-2	-19	-18	-10	-10	50	41	-10	-10	100	-2	-2	0	9	8	-5	1	0
vdlsr	-6	-2	-12	-14	-6	-6	48	47	-7	-6	97	-1	-2	-1	2	2	-2	5	1
ori	-2	0	2	-1	-1	-1	0	0	6	5	-2	-1	100	1	0	0	3	8	-1
coh_16	62	98	33	63	48	48	6	3	3	1	-2	1	100	98	83	84	48	14	38
coh_32	59	98	29	59	43	43	6	2	3	0	0	1	98	100	85	86	44	12	37
cs_16	39	78	5	38	25	25	12	-2	0	-5	9	2	83	85	100	99	29	1	28
cs_32	42	80	8	41	27	27	11	-2	0	-4	8	2	84	86	99	100	31	2	29
utility_28	50	48	32	51	49	49	4	8	5	6	-5	-2	48	44	29	31	100	45	74
utility_63	16	14	10	8	12	12	9	14	11	11	1	5	14	12	1	2	45	100	27
utility_83	39	39	21	34	33	33	5	6	2	2	0	1	38	37	28	29	74	27	100

Figure E.3: Spearman correlation table for CASIAFPV5-FULL

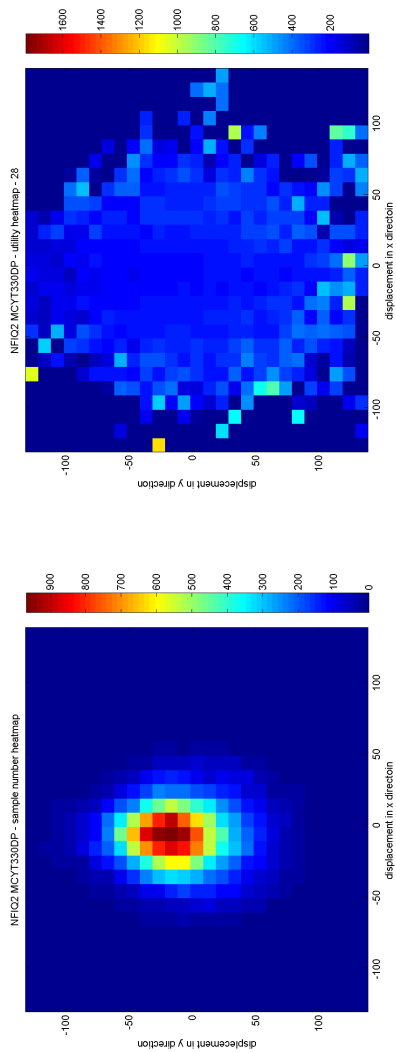
ntfq	100	63	42	59	47	4	4	4	4	5	64	60	41	44	45	18	39
ocl	63	100	36	61	47	7	8	6	6	9	98	98	78	80	45	17	37
fda	42	36	100	56	40	-22	-7	-4	-4	-6	36	32	6	10	30	8	21
gabpr	59	61	56	100	76	-17	-8	0	-3	1	63	58	36	39	46	9	33
ps	47	47	40	76	100	4	13	11	13	10	48	43	23	24	45	15	32
dis	-1	7	-22	-17	4	100	92	34	31	15	6	7	13	11	7	16	5
disr	4	8	-7	-8	13	92	100	32	34	14	7	5	1	0	14	21	8
hdis	4	8	-9	-3	11	34	32	100	99	13	8	7	8	7	9	12	7
hdisr	4	6	-4	0	13	31	34	99	100	12	6	5	2	2	10	13	7
vdls	-9	-5	-18	-19	-11	62	58	-6	-7	100	97	2	2	1	-3	7	-3
vdlsr	-4	-2	-11	-13	-4	59	64	-5	-4	100	4	-3	-3	-3	3	11	0
ori	5	9	-6	1	10	15	14	13	12	2	100	9	10	9	6	5	7
coh_16	64	98	36	63	48	6	7	8	6	9	100	98	82	83	45	17	37
coh_32	60	98	32	58	43	7	5	7	5	9	98	100	85	86	41	14	34
cs_16	41	78	6	36	23	13	1	8	2	10	82	85	100	99	24	2	25
cs_32	44	80	10	39	24	11	0	7	2	9	83	86	99	100	26	4	26
utility_28	45	45	30	46	45	7	14	9	10	6	45	41	24	26	100	60	71
utility_63	18	17	8	9	15	16	21	12	13	5	17	14	2	4	60	100	31
utility_83	39	37	21	33	32	5	8	7	7	7	37	34	25	26	71	31	100

Figure E.4: Spearman correlation table for CASIAFPV5-SUB

APPENDIX F

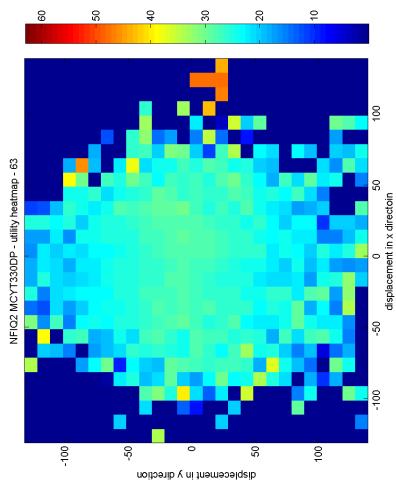
Utility Heatmaps

Utility heatmaps plotted by the position of cores and utility scores for MCYT330DP, MCYT330PB, CASIAFPV5-FULL and CASIAFPV5-SUB by comparator 28, 63, 83. The values in each 10×10 pixels block are computed by the mean of utility scores, and number of samples in each block are also plotted.

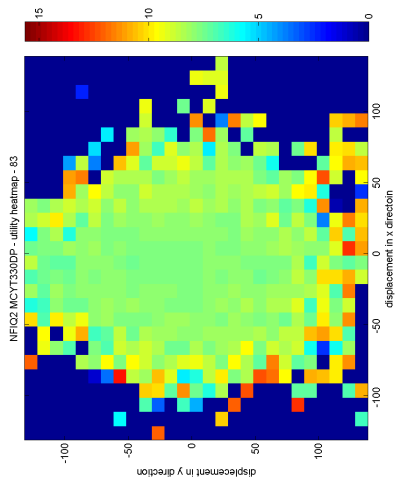


(a) Sample number

(b) Comparator 28

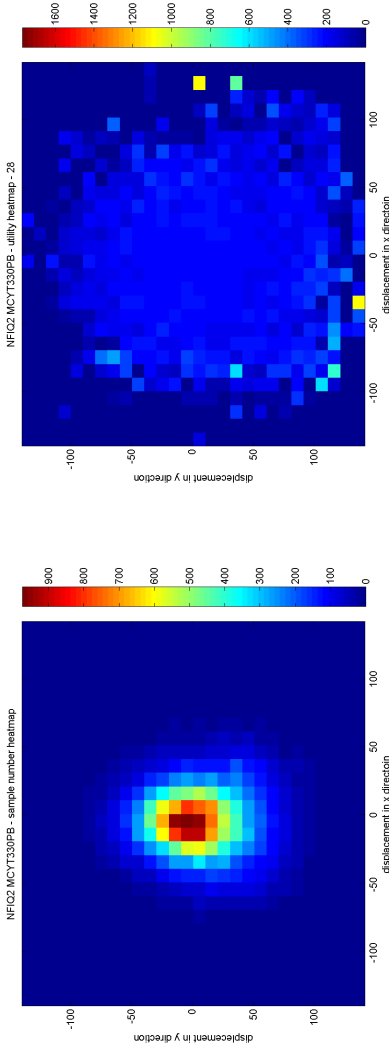


(c) Comparator 63



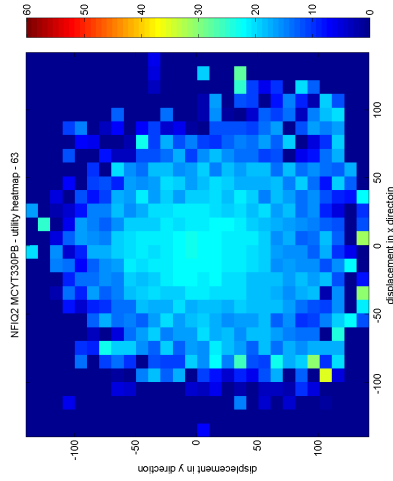
(d) Comparator 83

Figure F.1: Number of samples and utility maps for MCYT330DP.

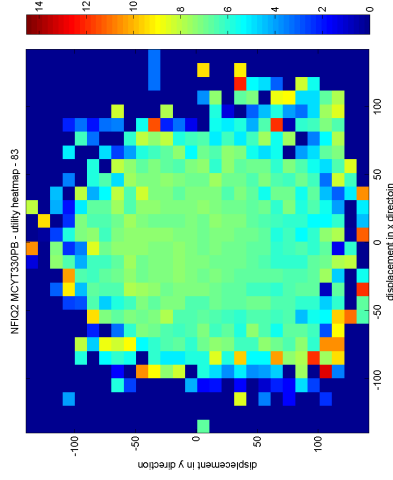


(a) Sample number

(b) Comparator 28

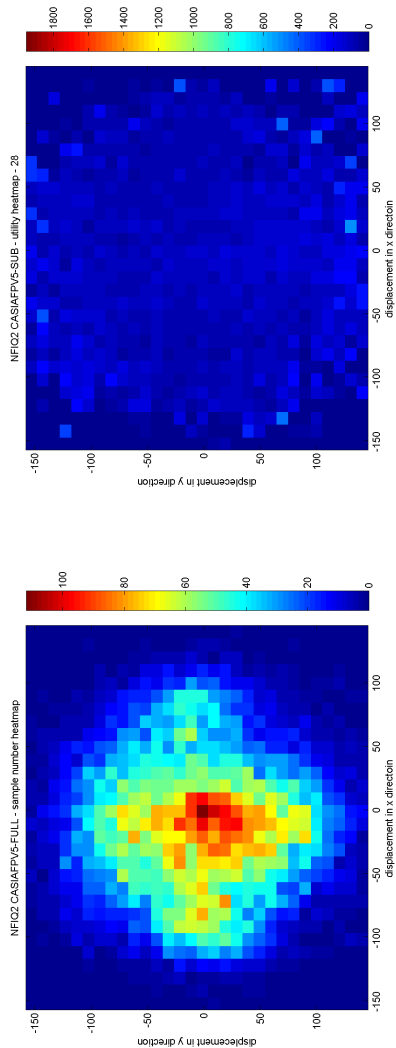


(c) Comparator 63



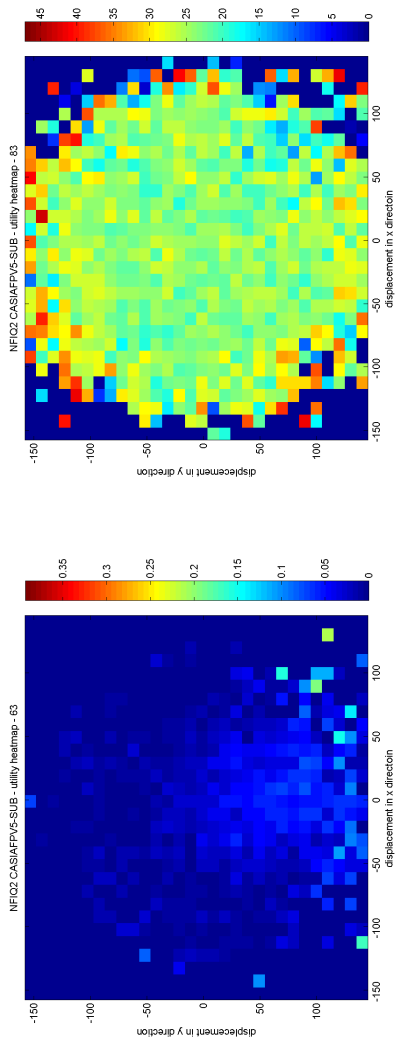
(d) Comparator 83

Figure F.2: Number of samples and utility maps for MCYT330PB.



(b) Comparator 28

(a) Sample number



(d) Comparator 83

(c) Comparator 63

Figure F.3: Number of samples and utility maps for CASIAFPV5-FULL.

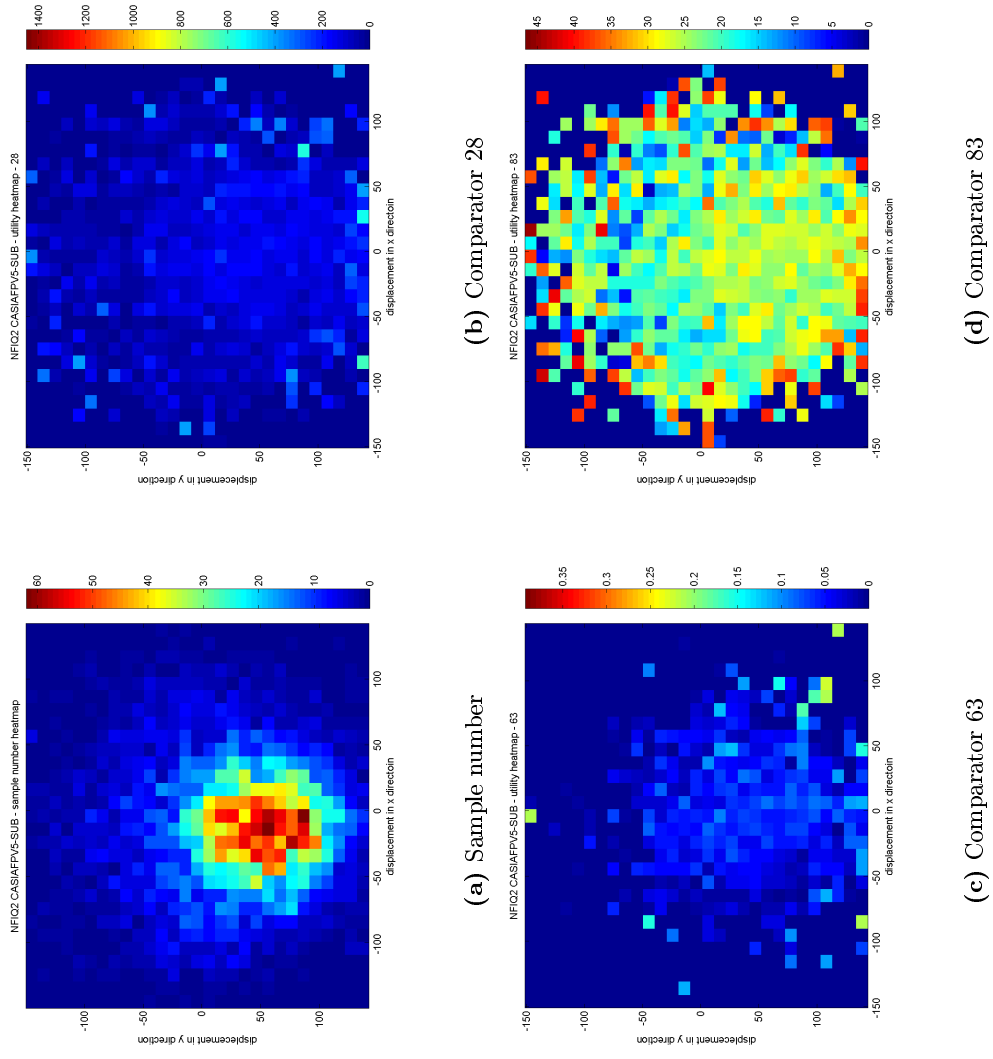


Figure F.4: Number of samples and utility maps for CASIAFPV5-SUB.

Bibliography

- [AFFOG⁺07] F. Alonso-Fernandez, J. Fierrez, J. Ortega-Garcia, J. Gonzalez-Rodriguez, H. Fronthaler, K. Kollreider, and J. Bigun. A comparative study of fingerprint image-quality estimation methods. *Information Forensics and Security, IEEE Transactions on*, 2(4):734–743, 2007.
- [BG02] A. M. Bazen and S. H. Gerez. Systematic methods for the computation of the directional fields and singular points of fingerprints. *IEEE Trans. Pattern Anal. Mach. Intell.*, 24(7):905–919, July 2002.
- [Bus09] C. Busch. Biometric systems. January 2009.
- [CDJ05] Y. Chen, S. Dass, and A. K. Jain. Fingerprint quality indices for predicting authentication performance. In *In: Proc. AVBPA, Springer LNCS-3546*, pages 160–170, 2005.
- [CLMM99] R. Cappelli, A. Lumini, D. Maio, and D. Maltoni. Fingerprint classification by directional image partitioning. *Pattern Analysis and Machine Intelligence, IEEE Transactions on*, 21(5):402–421, 1999.
- [Com] European Commission. Visa information system. http://ec.europa.eu/dgs/home-affairs/what-we-do/policies/borders-and-visas/visa-information-system/index_en.htm. [Online; accessed 25-June-2013].
- [fSoP] Institute for Systems and Computer Engineering of Porto. Competition spd2010 - fingerprint singular points detection.

- <http://www2.inescporto.pt/ip-en/news-events/events/spd2010-fingerprint-singular-points-detection/>. [Online; accessed 25-June-2013].
- [Gal92] Francis Galton. *Finger prints*. Macmillan and Company, London, 1892.
- [GMM09] C. Gottschlich, P. Mihailescu, and A. Munk. Robust orientation field estimation and extrapolation using semilocal line sensors. *Information Forensics and Security, IEEE Transactions on*, 4(4):802–811, 2009.
- [Gra69] A. Grasselli. On the automatic classification of fingerprints. *Methodologies of Pattern Recognition*, 1969.
- [GT07] P. Grother and E. Tabassi. Performance of biometric quality measures. *IEEE Trans. Pattern Anal. Mach. Intell*, pages 531–543, 2007.
- [HA91] R. A. Haddad and A. N. Akansu. A class of fast gaussian binomial filters for speech and image processing. *Signal Processing, IEEE Transactions on*, 39(3):723–727, 1991.
- [Has08] B. Hastings. An integrated representation of fingerprint patterns. In *16th School of Computer Science & Software Engineering Research Conference, Yanchep, Western Australia*, 2008.
- [HJ04] L. Hong and A. K. Jain. Fingerprint enhancement. In *Automatic Fingerprint Recognition Systems*, pages 127–143. Springer, 2004.
- [HUW+98] Y. Hamamoto, S. Uchimura, M. Watanabe, T. Yasuda, Y. Mitani, and S. Tomita. A gabor filter-based method for recognizing handwritten numerals. *Pattern Recognition*, 31(4):395–400, 1998.
- [ISO11] ISO. ISO/IEC 19794-1:2011 information technology – biometric data interchange formats – part 1: Framework. July 2011.
- [ISO12a] ISO. ISO/IEC 2382-37:2012 information technology – vocabulary – part 37: Biometrics. December 2012.
- [ISO12b] ISO. ISO/IEC 29794-1:2009 information technology – biometric sample quality – part 1: Framework. September 2012.
- [ISO12c] ISO. ISO/IEC TR 29794-4:2010 information technology – biometric sample quality – part 4: Finger image data. September 2012.
- [Jai89] A. K. Jain. *Fundamentals of digital image processing*, volume 3. prentice-Hall Englewood Cliffs, 1989.

- [JK10] C. Jin and H. Kim. Pixel-level singular point detection from multi-scale gaussian filtered orientation field. *Pattern Recogn.*, 43(11):3879–3890, November 2010.
- [JPH99] A. K. Jain, S. Prabhakar, and L. Hong. A multichannel approach to fingerprint classification. *Pattern Analysis and Machine Intelligence, IEEE Transactions on*, 21:348–359, 1999.
- [JPHP00] A. K. Jain, S. Prabhakar, L. Hong, and S. Pankanti. Filterbank-based fingerprint matching. *Trans. Img. Proc.*, 9(5):846–859, May 2000.
- [Kov] P. D. Kovesi. MATLAB and Octave functions for computer vision and image processing. Centre for Exploration Targeting, School of Earth and Environment, The University of Western Australia. [Online; accessed 25-June-2013].
- [KT84] M. Kawagoe and A. Tojo. Fingerprint pattern classification. *Pattern Recogn.*, 17(3):295–303, June 1984.
- [KW87] M. Kass and A. Witkin. Analyzing oriented patterns. *Computer vision, graphics, and image processing*, 37(3):362–385, 1987.
- [LG10] H. C. Lee and R. E. Gaensslen. *Advances in Fingerprint Technology, Second Edition*. Forensic and Police Science Series. Taylor & Francis, 2010.
- [Lin93] T. Lindeberg. *Scale-space theory in computer vision*. Kluwer Academic Print on Demand, 1993.
- [Lin98] T. Lindeberg. Feature detection with automatic scale selection. *International journal of computer vision*, 30(2):79–116, 1998.
- [LJY02] E. Lim, X. Jiang, and W. Yau. Fingerprint quality and validity analysis. In *Image Processing. 2002. Proceedings. 2002 International Conference on*, volume 1, pages I–469. IEEE, 2002.
- [LS72] G. Levi and F. Sirovich. Structural descriptions of fingerprint images. *Inf. Sci.*, 4(3-4):327–355, January 1972.
- [LTS⁺04] E. Lim, K.-A. Toh, P. N. Suganthan, X. Jiang, and W.-Y. Yau. Fingerprint image quality analysis. In *Image Processing, 2004. ICIP'04. 2004 International Conference on*, volume 2, pages 1241–1244. IEEE, 2004.
- [LZH06] T. Liu, C. Zhang, and P. Hao. Fingerprint reference point detection based on local axial symmetry. In *Pattern Recognition, 2006. ICPR 2006. 18th International Conference on*, volume 1, pages 1050–1053. IEEE, 2006.

- [MDK⁺97] A. F. Martin, G. R. Doddington, T. Kamm, M. Ordowski, and M. A. Przybocki. The det curve in assessment of detection task performance. Technical report, DTIC Document, 1997.
- [Meh93] B. M. Mehre. Fingerprint image analysis for automatic identification. *Machine Vision and Applications*, 6(2-3):124–139, 1993.
- [MMC⁺02] D. Maio, D. Maltoni, R. Cappelli, J. L. Wayman, and A. K. Jain. FVC2002: Second fingerprint verification competition. In *Proceedings of the 16th International Conference on Pattern Recognition (ICPR '02) Volume 3 - Volume 3*, ICPR '02, pages 30811–, Washington, DC, USA, 2002. IEEE Computer Society.
- [MMC⁺04] D. Maio, D. Maltoni, R. Cappelli, J. L. Wayman, and A. K. Jain. FVC2004: Third fingerprint verification competition. In *Proceedings of the First International Conference on Biometric Authentication*, pages 1–7, 2004.
- [MMJP09] D. Maltoni, D. Maio, A. K. Jain, and S. Prabhakar. *Handbook of Fingerprint Recognition*. Springer Professional Computing. Springer, 2009.
- [MMWJ02] D. Maio, D. Maltoni, J. L. Wayman, and A. K. Jain. FVC2000: Fingerprint verification competition. *IEEE Transactions on Pattern Analysis and Machine Intelligence*, 24:402–412, 2002.
- [Moe71] A. A. Moenssens. *Fingerprint techniques*. Inbau law enforcement series. Chilton Book Company, 1971.
- [NIS12] NIST. Development of nfiq 2.0 - evaluation of potential image features for quality assessment. June 2012.
- [Nyk] D. Q. Nykamp. The idea behind green's theorem. http://mathinsight.org/greens_theorem_idea. [Online; accessed 25-June-2013].
- [OGFAS⁺03] J. Ortega-Garcia, J. Fierrez-Aguilar, D. Simon, J. Gonzalez, M.s Faundez-Zanuy, V. Espinosa, A. Satue, I. Hernaez, J-J. Igarza, C. Vivaracho, D. Escudero, and Q.-I. Moro. Mcyt baseline corpus: a bimodal biometric database. *IEEE Proceedings-Vision, Image and Signal Processing*, 150(6):395–401, 2003.
- [oHS] U.S.A. Department of Homeland Security. Office of biometric identity management. <http://www.dhs.gov/obim>. [Online; accessed 25-June-2013].
- [OLBC10] F. W. J. Olver, D. W. Lozier, R. F. Boisvert, and C. W. Clark. *NIST handbook of mathematical functions*. Cambridge University Press, 2010.

- [oSIoA] Chinese Academy of Sciences' Institute of Automation. Casia fingerprint image database version 5.0. <http://biometrics.idealtest.org/>. [Online; accessed 25-June-2013].
- [OXB12] M. A. Olsen, H. Xu, and C. Busch. Gabor filters as candidate quality measure for nfiq 2.0. In *ICB*, pages 158–163, 2012.
- [Pea01] K. Pearson. On lines and planes of closest fit to systems of points in space. *Philosophical Magazine*, 2:559–572, 1901.
- [PR96] J. K. Patel and C. B. Read. *Handbook of the Normal Distribution*. Statistics: A Series of Textbooks and Monographs. MARCEL DEKKER Incorporated, 1996.
- [RN88] J. L. Rodgers and W. A. Nicewander. Thirteen ways to look at the correlation coefficient. *The American Statistician*, 42(1):pp. 59–66, 1988.
- [SKK01] L. Shen, A. Kot, and W. Koo. Quality measures of fingerprint images. In *Audio-and Video-based Biometric Person Authentication*, pages 266–271. Springer, 2001.
- [SM92] V.S. Srinivasan and N.N. Murthy. Detection of singular points in fingerprint images. *Pattern Recognition*, 25(2):139–153, 1992.
- [SM93] B. G. Sherlock and D. M. Monro. A model for interpreting fingerprint topology. *Pattern Recognition*, 26(7), 1993.
- [Smi97] S. W. Smith. *The scientist and engineer's guide to digital signal processing*. California Technical Pub., first edition, 1997.
- [Spe87] C. Spearman. The proof and measurement of association between two things. by c. spearman, 1904. *The American journal of psychology*, 100(3-4):441–471, 1987.
- [TG09] E. Tabassi and P. Grother. Fingerprint image quality. In *Encyclopedia of Biometrics*, pages 482–490. 2009.
- [TW05] E. Tabassi and C. L. Wilson. A novel approach to fingerprint image quality. In *ICIP (2)*, pages 37–40, 2005.
- [UPPJ04] U. Uludag, S. Pankanti, S. Prabhakar, and A. K. Jain. Biometric cryptosystems: issues and challenges. *Proceedings of the IEEE*, 92(6):948–960, 2004.
- [USKV07] K. Upendra, S. Singh, V. Kumar, and H. K. Verma. Online fingerprint verification. *Journal of Medical Engineering & Technology*, 31(1):36–45, 2007.

- [VG96] P. R. Vizcaya and L. A. Gerhardt. A nonlinear orientation model for global description of fingerprints. *Pattern Recognition*, 29(7):1221–1231, 1996.
- [WBS12] L. Wang, N. Bhattacharjee, and B. Srinivasan. Fingerprint reference point detection based on local ridge orientation patterns of fingerprints. In *Neural Networks (IJCNN), The 2012 International Joint Conference on*, pages 1–8. IEEE, 2012.
- [WCW94] C.L. Wilson, G.T. Candela, and C.I. Watson. Neural network fingerprint classification. *Journal of Artificial Neural Networks*, 1(2):203–228, 1994.
- [Weg82] J. H. Wegstein. *An automated fingerprint identification system*. US Department of Commerce, National Bureau of Standards, 1982.
- [WHH07] Y. Wang, J. Hu, and F. Han. Enhanced gradient-based algorithm for the estimation of fingerprint orientation fields. *Applied Mathematics and Computation*, 185(2):823–833, 2007.
- [WHS05] Y. Wang, J. Hu, and H. Schroder. A gradient based weighted averaging method for estimation of fingerprint orientation fields. In *Digital Image Computing: Techniques and Applications, 2005. DICTA '05. Proceedings 2005*, pages 29–29. IEEE, 2005.
- [WYY11] Dawei W., Yilong Y., and Dong Y. Singular points detection based on multi-resolution in fingerprint images. *Neurocomputing*, 74(17):3376 – 3388, 2011.
- [XYP⁺11] S. J. Xie, J. Yang, D. S. Park, S. Yoon, and J. Shin. Fingerprint quality analysis and estimation for fingerprint matching. *State of the art in Biometrics. Intech, Vienna. ISBN*, pages 978–953, 2011.
- [YA06] L. Yang and F. Albrechtsen. Fast and exact computation of moments using discrete green’s theorem. 2006.
- [Yam98] N. Yamaguchi. Advanced automated fingerprint identification system. In *Security Technology, 1998. Proceedings., 32nd Annual 1998 International Carnahan Conference on*, pages 154–157. IEEE, 1998.
- [YC06] E.-K. Yun and S. Cho. Adaptive fingerprint image enhancement with fingerprint image quality analysis. *Image and Vision Computing*, 24(1):101 – 110, 2006.

- [YE07] M. R. Young and S. J. Elliott. Image quality and performance based on henry classification and finger location. In *Automatic Identification Advanced Technologies, 2007 IEEE Workshop on*, pages 51–56. IEEE, 2007.
- [ZC93] M. H. Zweig and G. Campbell. Receiver-operating characteristic (roc) plots: a fundamental evaluation tool in clinical medicine. *Clinical chemistry*, 39(4):561–577, 1993.
- [ZG04] J. Zhou and Ji. Gu. A model-based method for the computation of fingerprints’ orientation field. *Image Processing, IEEE Transactions on*, 13(6):821–835, 2004.
- [ZYHZ06] E. Zhu, J. Yin, C. Hu, and G. Zhang. A systematic method for fingerprint ridge orientation estimation and image segmentation. *Pattern Recognition*, 39(8):1452–1472, 2006.